Digital Mix Design for Performance Optimization of Asphalt Mixture

Ying Li

Dissertation submitted to the faculty of

Virginia Polytechnic Institute and State University

in partial fulfillment of the requirements for the degree of

Doctor of Science

In

Civil Engineering

Wang, Linbing

Abbas, Montasir Mahgoub

Dove, Joseph E

Hajj, Muhammad R

Easterling, William S

November 21, 2014

Blacksburg, Virginia

Keywords: Discrete Element Method, Aggregate Gradation, Asphalt Content, Visco-elastic Model, Binder Film, X-Ray Tomography, Compaction Temperature, Pore Water Pressure

Digital Mix Design for Performance Optimization of Asphalt Mixture

Ying Li

(ABSTRACT)

Asphalt mix design includes the determination of a gradation, asphalt content, other volumetric properties, the evaluation of mechanical properties and moisture damage potentials. In this study, a computational method is developed to aid mix design. Discrete element method (DEM) was used to simulate the formation of skeleton and voids structures of asphalt concrete of different gradations of aggregates. The optimum gradation could be determined by manipulating the particle locations and orientations and placing smaller particles in the voids among larger particles. This method aims at an optimum gradation, which has been achieved through experimental methods. However, this method takes the mechanical properties or performance of the mixture into consideration, such as inter-aggregate contacts and local stability. A simple visco-elastic model was applied to model the contacts between asphalt binder and aggregates. The surface texture of an aggregate particle can be taken into consideration in the inter-particle contact model. The void content before compactions was used to judge the relative merits of a gradation. Once a gradation is selected, the Voids in Mineral Aggregate (VMA) can be determined. For a certain air void content, the mastics volume or the binder volume or the asphalt content can be determined via a digital compression test. The surface area of all the aggregates and the film thickness can be then calculated. The asphalt content can also be determined using an alternative approach that is based on modeling the inter-particle contact with

an asphalt binder layer. In this study, considering the necessity of preservation of the compaction temperature, the effect of various temperatures on Hot Mix Asphalt (HMA) samples properties has been evaluated. As well, to evaluate the effect of this parameter on different grading, two different grading have been used and samples were compacted at various temperatures. Air voids also influence pore water pressure and shrinkage of asphalt binder and mixture significantly. The shrinkage is measured on a digital model that represents beams in a steel mold and is defined as the linear autogenous deformation at horizontal direction.

ACKNOWLEDGEMENT

I would like to gratefully and sincerely thank Dr. Linbing Wang for his guidance, understanding, patience, and most importantly, his friendship during my graduate studies at Virginia Tech. His mentorship was paramount in providing a well-rounded experience consistent my long-term career goals. He encouraged me to not only grow as an experimentalist and an engineer but also as an instructor and an independent thinker. I am not sure many graduate students are given the opportunity to develop their own individuality and self-sufficiency by being allowed to work with such independence. For everything you've done for me, Dr. Wang, I thank you. I would also like to thank all of the members of Dr. Wang's research group. These friends and co-workers provided for some much needed humor and entertainment in what could have otherwise been a somewhat stressful laboratory environment.

I would like to thank the Department of Civil Engineering at Virginia Tech, especially those members of my doctoral committee for their input, valuable discussions and accessibility.

Finally, and most importantly, I would like to thank my parents Yuan Li and Li Wang. I thank my parents, for their faith in me and allowing me to be as ambitious as I wanted. It was under their watchful eye that I gained so much drive and an ability to tackle challenges head on.

Table of Contents

LIST OF FIGURES

LIST OF TABLES

1. INTRODUCTION

Asphalt concrete is a composite material consisting of aggregates, asphalt binder and air voids. The constitutive behavior of the material depends largely on the interaction between aggregates and asphalt binder. The aggregate skeleton determines the load carrying mechanism and the asphalt binder serves as an adherent, which enables the mixture to hold tensile and shear stresses (*1*). Discrete Element Method (DEM) can be used to analyze the individual characteristic effects of each component in the asphalt mixture, such as the influence of asphalt content, gradation and relative slippage among aggregate particles. Given the proper internal structure and constitutive contact models, the simulation could avoid a huge amount of sample preparation work in lab and provide preliminary assessment of the behavior of asphalt mixtures, aiding the mix design by providing fundamental understanding of the behavior.

DEM was developed by Cundall and Strack for simulating movement and interaction of assemblies of rigid particles (*2*). In their original BALL model, the movement and interaction of unbound assemblies of rigid spherical particles subjected to external stress was simulated. Later developments of this approach were implemented in software PFC3d (Itasca Consulting Group Inc. 2003). In PFC3d, a gradation of three-dimensional (3D) particles are assembled together to form a skeleton structure, and inter-particle contacts can be assessed.

Major works presented in this study include: packing aggregates and determining of the optimal gradation through DEM simulation; determining the optimal asphalt content by simulating compression tests on asphalt mixtures via a computational method; and estimating

the film thickness based on determined gradation and asphalt content. In order to represent visco- elastic properties of asphalt binder, a simple visco-elastic model and parallel bonds were applied to the contacts between aggregates and asphalt binder in PFC3d.

DEM was used to simulate the formation of the skeleton and the void structures in asphalt concrete for different gradations of aggregates before compaction. The particle surface texture can be included in the inter-aggregate contact model. The void content before compactions may be used to judge the relative merits of a gradation. It is assumed that an optimum gradation can be achieved, and the structure is most stable if the number of inter-aggregate contacts of coarse aggregate reaches the maximum value. The optimum gradation could be determined by manipulating the particle locations and orientations and placing smaller particles in the voids among larger particles. For the same type of aggregates, one criterion of judging the rationality of computational simulation method is whether the computational method could yield the same gradation as obtained in the traditional mix design. The computational method can take the mechanical properties or performance of the mixture into consideration, such as inter-aggregate contacts and local stability.

Once a gradation is selected, the Voids in Mineral Aggregate (VMA) can be determined. For a certain target air void content, the asphalt content can be determined. If the asphalt content is known, then the average binder film thickness, which is related to the total surface area of both aggregates and filler, can be conveniently determined. As the binder layer might affect the plastic/permanent deformation of particles in contact, this layer's thickness might be directly related to the rutting performance of the mixture. In addition, if the asphalt film thickness is too small, aging and wearing of the asphalt binder will reduce its fatigue life.

Therefore estimation of the film thickness is important and can be conveniently obtained via the computational method.

Mineral aggregate constitutes approximately 95% of hot-mix asphalt (HMA) by weight. The mineral aggregate is made up predominantly of coarse aggregate. Aggregate characteristics such as particle size, shape, and texture influence the performance and service ability of hot-mix asphalt pavement. Flat and elongated particles tend to break during mixing, compaction, and under traffic. Therefore, aggregate shape is one of the important properties that must be considered in the mix design of asphalt pavements to avoid premature pavement failure. In this study, DEM has been used to simulate standard particle index test and indirect tensile test in order to evaluate the effect of aggregate shape on the strength of asphalt mixtures.

Due to HMA's high durability, solid production, temperature control, moisture and quick provision for traffic crossing, it has still caught attention by many people. Determination of volumetric parameters of HMA samples is of vital importance for quality control of constructed roads. The compaction temperature is one of the major issues in HMA and also one of important criteria in the process of producing good quality hot mix asphalt. Also, the temperature is a key factor in the control of bitumen viscosity, which affects its ability to coat and provide adequate lubrication for the aggregates and slides with each other. In this study, compaction temperature changes from 120 ^{o}C to 165 ^{o}C. Changes of density, air voids, and flow of asphalt mixture which result from the increasing compaction temperature are evaluated.

Previous work has revealed that the pore water pressure (PWP) reduction of materials such as paste, mortar and concrete reflects rather well the stiffness evolution and volume change of such materials. Early PWP reductions are caused by two interacting mechanisms: Vacuum effect caused by thermal shrinkage and meniscus effect (capillary tension). Air voids will alter the early age PWP, and thus, the above mentioned properties, mainly because air voids act as buffer for both mechanisms. This is because they may grow as long as the stiffness of the asphalt concrete is low, which results in PWP release. The study presents and discusses some results from a DEM based test program of asphalt binder with and without air entraining admixture (AEM) as well as concretes with and without AEM, conducted in order to evaluate the influence of air voids on the mentioned properties, both from a fundamental and practical point of view.

2. DETERMINATION OF GRADATION OF AGGREGATE

Literature Review

Background of Particle Packing

The impact of aggregate gradation on the performance of asphalt mixtures has been extensively studied through the years. Several studies have shown that aggregate gradation affects the resistance of asphalt mixture to cracking, rutting, ageing and moisture damage (*1*). Furthermore, the way that aggregate particles, bitumen binder and air voids interact with each other influences how a mixture responds under different loading conditions (*3*). With a better understanding of these interactions, future mix design can be optimized by mixing the available materials in the best way.

Asphalt mixture microstructure depends mainly on their size distribution, shape and angularity. Bitumen binder flows around the particles, forming a film around them and binding all the components together. Aggregates´ mechanical properties, such as resistance to abrasion and strength, are dependent primarily on their mineral composition. However, good processing procedures can significantly improve the quality of the final aggregate by the elimination of weaker rock layers and crushing particles to reveal rough surfaces. Aggregate gradation is the distribution of particle sizes expressed as a percent of the total weight. Gradation can be determined by sieve analysis and expressed as total percent passing various sieve sizes.

Experimental studies on granular materials showed the existence of stress-transmitting paths enclosing virtually stress free regions. In particulate materials then, the load is

transferred through chains of particles and other smaller particles play the secondary role in preventing the main chain from buckling (*4*). Based on the observations mentioned above, two sub-structures within the aggregate particles have been defined: the Primary Structure, range of sizes which due to their volume fraction provides the load bearing capacity of the mixture; and the Secondary Structure, range of sizes smaller than the first one, which provides stability to the Primary Structure (*5*). Each substructure can be identified by the packing theory for spherical particles. Results from field and laboratory tests can be used to validate the relationship between the aggregate content of Primary Structure and rutting performance. The model also proposes a distribution system of the bitumen binder. Former researches show that the thickness of the film around both structures effects not only permanent deformation but also the resistance to moisture damage of asphalt mixtures. Early studies proposed that the best gradation for HMA is the one that gives the densest packing, increasing stability through increased inter-particle contact (*6*). Sufficient air void content is necessary for the durability and workability of the mixture, so there still are some air voids in the mixture to avoid bleeding or rutting.

The determination of the grading of an aggregate blend or stockpile is one of the oldest test procedures used in the hot mix asphalt (HMA) and aggregate industries. The control of aggregate grading by the HMA industry begins during aggregate production and ends when the grading of the finished HMA is determined. Sieve analyses are used in many different applications, some of which are the determination of aggregate grading for use in HMA mix design procedures (Marshall, Hveem, and Superpave), the process control of produced material, and the particle size control and monitoring of quarried materials. In the HMA

industry, sieve analyses are often performed on plant produced samples to determine the proximity of the produced aggregate blend to the job mix formula aggregate grading. The number of grading tests performed for a given project depends on many factors such as the number of stockpiles, type of HMA plant, tonnage of HMA produced, process control methods used, and acceptance procedures outlined by the owner. Furthermore, the grading of the aggregate blend in HMA can be considered one of the most important mix parameters since it affects, in varying degrees, the stiffness, stability, durability, permeability, workability, fatigue resistance, frictional resistance, moisture susceptibility, and volumetric properties of the produced mixture. Therefore, it is very critical that the grading analysis of the produced material be done in a timely and accurate manner, so as to yield the true result, and to allow for the adjustment of the aggregate grading, if necessary, to ensure a quality product. Although aggregate grading analysis is one of the oldest test procedures, it remains a very time consuming and labor intensive task.

There is a need today within the HMA industry for a rapid, automated method to determine aggregate grading. This automated method should reduce the time required to perform a grading test as well as reduce the amount of technician time required. The need to reduce the test time arises from the fact that grading testing of aggregate samples is used for process control during the production of HMA and requires a significant amount of time for an HMA project. A typical project may require from 5-10 grading tests per day depending on the specification requirements, number of aggregates, and plant production rate. If the test time for grading testing can be reduced by 50 percent (approximately 15 minutes), several hours of total test time per day can be saved.

Today, the most widely accepted and accurate method for aggregate grading determination is through a washed or wet sieve analysis, as outlined in ASTM C117 (*7*) and ASTM C136 (*8*). The main reason for performing a wet sieve analysis is to obtain a more accurate indication of the true grading, primarily on the material passing the 0.075 mm sieve. As one might expect, when the amount of material passing the 0.075 mm sieve is low, the washed and the dry sieving procedures often yield very comparable results; however, when the percent passing is high the results can vary considerably.

A method of determining the gradation of an aggregate blend in a more efficient manner is greatly needed in the HMA and aggregate industries. By increasing the efficiency of the grading analysis, there is a potential for greater control to be obtained over the produced product by the increased ability to perform more grading analysis throughout production.

Besides aggregate stockpile grading, the grading of the finished HMA mixture must also be determined for control and acceptance purposes. To obtain the aggregate grading either the aggregate must be recovered from the HMA or a belt sample be taken and analyzed. The technician time involved is approximately one-half to one hour for each test. Add this to the time required to determine stockpile grading and several hours of technician time can easily be expended on a relatively small amount of process control. The need to automate the testing procedure is evident.

If grading testing can be automated, the resulting reduction in time requirements would allow the producer to choose one of two options. With the increase in available technician time, more testing could be performed to allow for better process control. Or if desired, fewer technicians would be needed to perform the same level of process control.

Current Technology Review

In reviewing current technologies for possible application to aggregate grading testing, many possibilities were investigated. Several industries make use of grading tests for manufacturing and/or quality control of products. For example, both the food and drug industries make wide use of grading testing to assist them during production. In addition, the in-line measurement of particle size is used by heavy industries such as power generation and steel manufacturing to help control plant emissions.

The HMA and aggregate production industries have continued to pursue new technology aimed at increasing the accuracy of grading testing while decreasing the time required. Air separation techniques are now being used at aggregate production facilities to "air wash" aggregates. Washing of the coarse aggregate in this manner creates less waste and reduces environmental concerns.

In the preparation of this report, all of these technologies were carefully reviewed. Each of these was judged against the four criteria of reduced test time, reduced technician time, affordability, and the ability to obtain an accurate grading. The methods reviewed are discussed individually in the following paragraphs.

Gradex 2000

The Gradex 2000 Particle Size Analyzer, manufactured by Rotex, Inc., located in Cincinnati, Ohio, has been used for a number of years in many industries, such as the pharmaceutical, ceramic, food products, etc. (*9*). However, its application in the hot mix

asphalt and aggregate industries as a means of determining the grading of an aggregate blend has only recently been evaluated.

The automatic grading device, shown in FIGURE 2.1, accomplishes grading analysis by automating the conventional sieve analysis procedure which has been used for many years with good results. The grading device consists of a set of standard 203 mm diameter round U.S. sieves, an automatic feeding/loading assembly (optional), a collection pan, and a 0.1 gram resolution electronic balance. The device, as first built, was capable of holding six full-height sieves or nine half-height sieves, or any combination thereof.

FIGURE 2.1 Gradex 2000 Particle Size Analyzer (*9*)

A computer system, completed with operational software for the grading device, is

interfaced with the device to allow for operator control and retrieval of grading analysis data. Operation of the device is very simple and requires a minimum amount of labor. Firstly the operator completes all of the sample information using the provided computer software. This information includes items such as the operator's name, test specimen identification, sieving time, etc. Next, a sample is loaded into the top of the device, either manually through the feed chute, or by the automatic feeding/loading assembly, which is sold as an attachment. Once the sample is loaded, the operator initiates the grading analysis by the touch of a key. The device then sieves the material for the specified sieving time (approximately 10 minutes) in a rotary or tapping motion, which is currently used by many mechanical sifters or shakers in operation today. After sieving is complete, the sieves are emptied, as shown in FIGURE 2.2, into the collection pan, which rests upon the electronic balance. This process begins with the pan and proceeds through the sieves from fine to coarse, until the last sieve is emptied. After each individual sieve is emptied into the collection pan, a brush, shown in FIGURE 2.3, operated through air pressure, cleans the inside of the sieve to remove any particles which may have become lodged during the sieving process. After the individual sieve has been cleaned, it is returned to its appropriate location in the sieve stack. Following the completion of the sieving, weighing, and cleaning procedures, the results of the grading analysis can be viewed on the computer screen or saved to a data file. A sample of the product file information is shown in FIGURE 2.4. As is shown, information such as sample identification, sieves used for analysis, and tabular results showing the percent retained and percent passing are provided for the user.

FIGURE 2.2 Gradex 2000 Sieve Configuration (*9*)

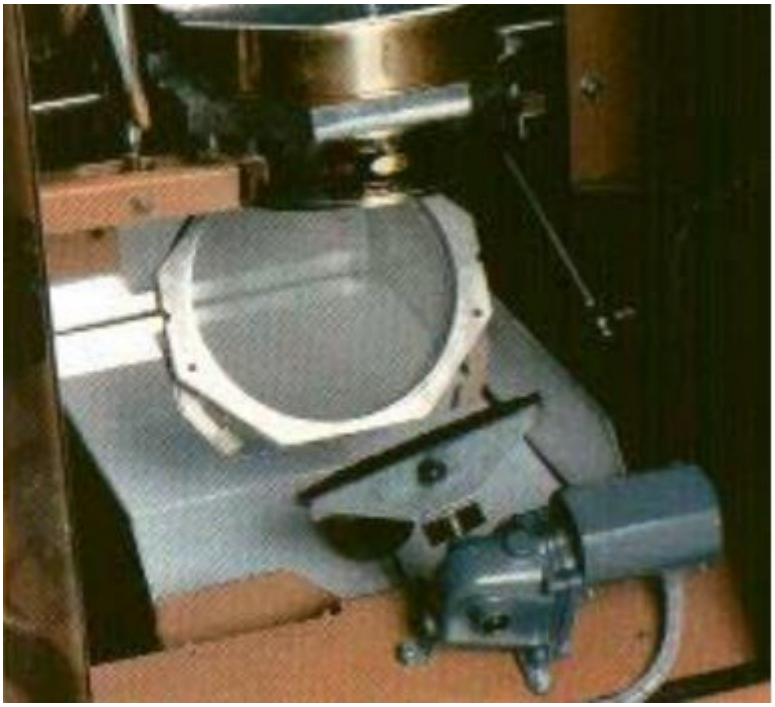

FIGURE 2.3 Gradex 2000 Brush Cleaning Attachment (*9*)

In order to determine accuracy of the Gradex 2000 to determine the grading of aggregate

samples, two blended aggregate mixes were prepared and tested in the device. The results of this preliminary testing with the Gradex 2000 are shown in TABLE 2.1. None of the results shown in TABLE 2.1 include sample washing prior to the grading determination. The results indicate that the Gradex 2000 is accurate at determining the percent passing for most sieves, but it has a tendency to underestimate the percent passing the 0.075 mm sieve. However, some of the underestimating on the 0.075 mm sieve is believed to have been caused by sieve blinding, a problem that can be remedied. Note also that the Gradex 2000 is limited in the number of sieves that it can hold. The sieve stack can consist of either six full height sieves or nine half height sieves. Mixture 1 was tested using a stack of six full height sieves. Mixture 2 was tested using a stack of nine half height sieves. The ninth sieve in this stack was a "placeholder" (a sieve frame with no wire). Placeholder sieves can be used to make the Gradex 2000 even more flexible. A placeholder sieve was therefore inserted into the stack as the ninth sieve. The placeholder does not measure an aggregate fraction size, but simply allows the Gradex 2000 to hold the stack properly.

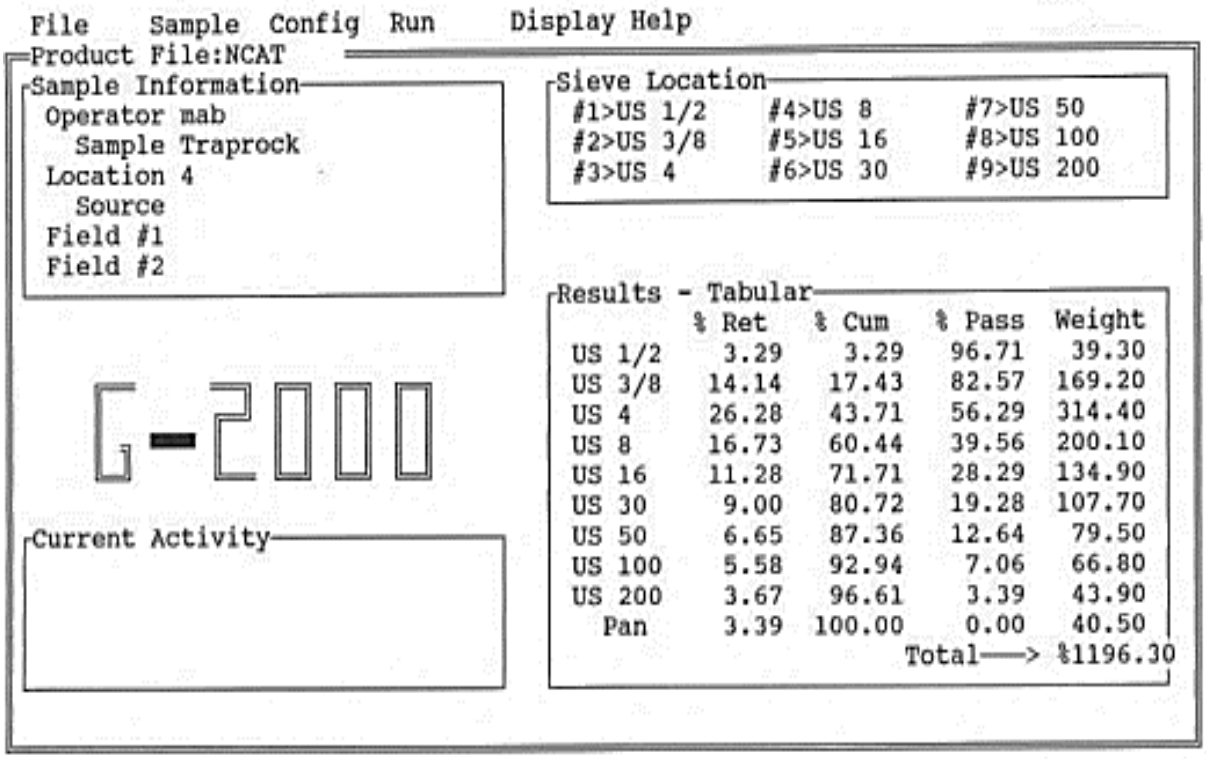

FIGURE 2.4 Product File Information from Gradex 2000 (*9*)

TABLE 2.1 Grading Results vs. Standard Dry Sieve Analysis with Gradex 2000 (*9*)

Sieve size (mm)	Percent Passing			
	Mixture 1		Mixture 2	
	Standard Test	Gradex 2000	Standard Test	Gradex 2000
25.0	100.0	100.0	100.0	100.0
19.0	100.0	99.8	100.0	99.7
12.5	78.8	78.9	89.2	89.9
9.5	24.7	24.1	49.0	49.1
4.75	1.1	0.5	25.6	25.3
2.36	1.0	-	20.3	20.2
1.18	1.0	-	17.3	-
0.600	0.9	0.4	14.5	14.1
0.300	0.9	-	13.5	-
0.150	0.8	-	10.8	-
0.075	0.5	0.1	5.0	1.2

A shorter testing time is possible if the sample is not washed prior to testing. If an accurate measure of the percent finer than the 0.075 mm sieve is required, the sample can be

washed prior to using the Gradex 2000. However, in certain instances, an apparent reduction in both test time and required technician time can be realized while obtaining an accurate measure of the percent passing the 0.075 mm sieve. This arises from the ability to automatically test several samples in sequential order. Therefore, if a technician has several aggregate gradations to perform, all of the preliminary work such as washing the sample (or extracting the asphalt binder) could be performed during the working day and the resulting aggregate samples could be set to sequentially test during the night. When the technician returned the next day, the computer would have all of the grading testing completed. In this scenario an accurate measure of the percent passing the 0.075 mm sieve is achieved, the technician time involved is reduced (he/she doesn't have to empty and weigh the contents of each sieve), and the grading testing time is removed from the normal work day. At the time of this study the cost for the Gradex 2000 varies, depending upon equipment configuration, from $17,000 to $25,000.

VDG-40 Video Grader

The VDG-40 Video Grader was developed by the Laboratoire Central des Ponts et Chaussèes (the French Public Works Laboratory) and is currently marketed in North America by a Canadian Company. It has recently become the standard French test method for the determination of aggregate grading as well as percent flat and elongated particles. The equipment consists of a chute through which the aggregate is fed, a vibrator and rotating drum for separating particles, a light source, and a bank of photosensitive cells (*10*). A schematic of the machine is shown in FIGURE 2.5. A personal computer is used to collect and analyze the data. The VDG-40 can be used to continuously monitor the grading of an

aggregate stream. Cost for the standard VDG-40 Video Grader is approximately $50,000.

Prior to sample testing, the VDG-40 must be calibrated. This is done by preparing two blended aggregate samples, one corresponding to the minimum grading specification and the second to the maximum grading specification. These samples are tested in the machine individually to allow it to establish the grading envelope. Once the grading envelope has been determined for the given aggregate blend, testing of samples can begin (*11*).

Firstly, all particles that smaller than 1.0 mm must be removed from the sample when you try to test a sample using VDG-40. This is due to the limits of the machine. It is capable of testing aggregate sizes ranging from 1.0 to 50.0 mm although it can be adapted to handle particles up to 63.0 mm. The separation of particles smaller than 1.0 mm involves washing and “scalping” the sample with a 1- mm sieve. The total weight of the sample, the weight of the sample portion finer than the 1- mm sieve, and the weight of the sample portion coarser than the 1- mm sieve must all be entered into the computer by the operator. The fraction of the sample larger than the 1-mm sieve can then be introduced into the machine. The particles are fed through the chute and onto the vibrator which helps to separate the particles. The particles then pass over the drum and fall through the light curtain established by the light source and light-sensitive cells. The resolution of the light sensitive cells is 0.2 mm horizontally and 0.4 mm vertically. When the aggregate particles pass through the light, the computer determines a two-dimensional shape for the particles. The computer software can then determine a three-dimensional shape for the aggregate particles using the principle of an ellipsoid of revolution. In addition, the computer also determines flat and elongated characteristics. A sample takes approximately eight minutes to be tested once it has been

introduced into the VDG-40 (*10*).

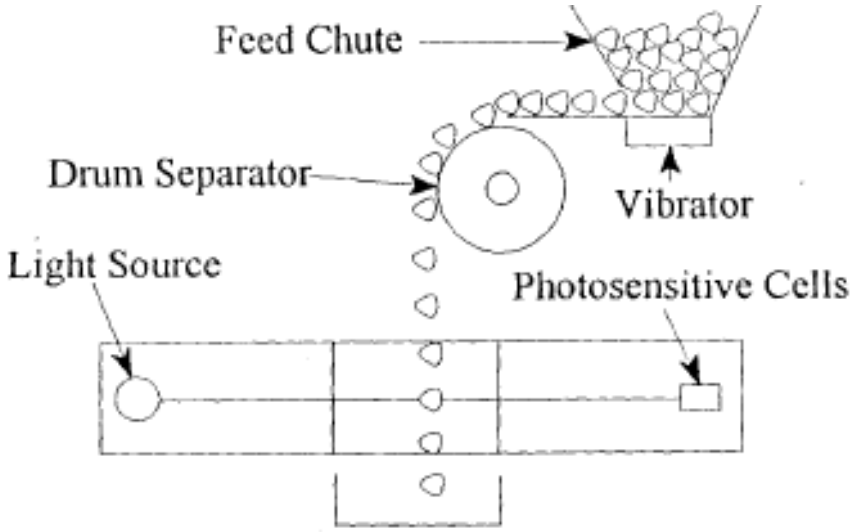

FIGURE 2.5 Schematic of the VDG-40 Video Grader (*10*)

The VDG-40 is automated, but suffers from lack of ability to test particles smaller than 1.0 mm. In addition, the washing and scalping needed prior to testing increases the overall test and technician time involved, thus increasing the cost for testing.

Full-Scale Particle Size Analyzer

In 1972, a report was completed at the University of Texas-Austin describing a full-scale particle size analyzer (*12*). The analyzer, based on sedimentation theory, consisted of an inner and outer ring. The outer ring was 6.1 m tall and 90 cm in diameter. The basic purpose for the outer ring was to hold the water and to provide structural support for the inner ring. The inner ring was 5.2 m tall and had an outside diameter of 76 cm. Two gates, one at the top and one at the bottom were used to hold the sample until introduction into the column and to collect it once it had settled in the column. The inner ring was suspended in the water by a scale linkage connecting it to the outer ring. This scale linkage served as means of transferring the

force applied to either the upper or lower gate to load a cell. This mechanism allowed for the sample mass to be determined on the upper gate prior to its introduction. It also allowed for the mass of the sample to be recorded as a function of time as it settled onto the bottom gate. No cost estimate was included in the report, but any such estimate would certainly be outdated. Indeed the ideas used for this full-scale particle size analyzer could benefit from technology developed since 1972.

Operation of the full-scale analyzer involved tarring the mass of the inner column and water, introducing the sample onto the top gate and recording its mass, opening the top gate to introduce the aggregate sample into the water column, and recording the mass of the sample particles as a function of time as they settled onto the bottom gate. The report concluded that a particle size ranging from 0.43-37.5 mm could be separated and analyzed (*12*).

Comparison of this method against the criteria outlined earlier is difficult. It appears that a version of this equipment making use of current technology would be automated and reduces both test time and technician time requirements. The cost for the system is unknown, but would most certainly be relatively expensive. It also has limits on particle sizes that can be analyzed and it will not produce an accurate measure of the percent passing the 0.075 mm sieve. Although the aggregate is washed in the water column, the 0.075 mm particles cannot be detected by the system because of their small sizes.

Fractionating Water Column

This method was evaluated at the University of Waterloo (*13*) and is a smaller, modified version of the full-scale particle size analyzer previously discussed. It consists of a 1.5 m long

by 77 mm inner diameter Plexiglas tube that is filled with water. Near the bottom of the tube a constant intensity light shines through the water column and impinges on a bank of light-sensitive photocells. The photocells are connected to a computer via electrical circuitry and an analog to digital (A/D) converter board. When the intensity of the light shining on the photocells changes, the photocells respond by changing their voltage output. This changing voltage is registered and converted by the A/D board and then recorded by the computer. Estimated cost for the equipment including the computer is $5,000-$10,000.

To determine the grading of an aggregate sample, the sample is put into the column at the top. The particles descend in the water according to their sizes as modeled by Stoke's law. As the particles pass through the light curtain established by the light source and photocells, the light intensity is altered and the varying voltages are recorded by the computer. By recording the voltage as a function of time, the computer can calculate the grading of the aggregate sample. This method has been shown to produce fairly good results when compared with standard sieve analysis. The method does have a tendency to slightly underestimate the coarse fraction and overestimate the fine fraction.

This method is automated and takes approximately three minutes to test a sample. It therefore meets the criteria for reduced test time and technician involvement. The method is also simple and the equipment relatively inexpensive. The disadvantage of this system is that it is currently limited in the particle sizes that can be accommodated. The system is designed to determine the grading of particles ranging from 2.38 mm to 0.075 mm. This limitation means that the grading of the coarse aggregate fraction is not determined, nor is an accurate measure of the percent finer than the 0.075 mm obtained. The researchers do offer

alternatives for solving these problems. The retained 2.38 mm fraction could firstly be separated out and its grading determined by some other method (conventional sieve analysis for example) while the minus 2.38-mm, retained 0.075 mm fraction grading could be determined by the Fractionating Water Column. This would lengthen the test time. Aljassar and Haas (*13*) also suggest that the minus 0.075 mm fraction could possibly be handled by the water column with some modifications to the current technology. The size limitations of this method make it unattractive at present, but research on this method is ongoing and should be monitored for significant progress towards solving the problem.

Laboratory Particle Size Analyzers

Another method that can be used to determine particle size uses laser diffraction/Mie scattering theory. Machines based on this method consist of an optical bench which contains the lasers, mirrors, and other optical equipment, a sample chamber, and a computer for control, data acquisition, and displaying results. The cost varies according to machine capability and manufacturer, but is approximately $40,000.

To use a particle size analyzer the sample is firstly put into suspension in a fluid, normally water and then placed in the sample chamber. The analysis is done by shining laser light through the suspended sample and measuring the intensity of the scattered light as a function of the scattering angle. The resulting light intensity function is then analyzed by the software to determine what distribution of particle sizes would scatter the light in a similar pattern (*14*). The operator only needs to aid the computer in properly calibrating the system, and to supply the proper information to the computer for sample identification. When the analysis is complete, the computer displays the results in any one of the various formats

selected by the user.

Particle size analyzers are automated and can typically analyze a sample in under 10 minutes with a minimal amount of technician time required. The test does provide an accurate measure of the percent passing the 0.075 mm sieve. However, the equipment is expensive and limited to the measurement of only small particle sizes. Typical equipment can measure particles ranging in size from 0.1 to 2000 μm. This inability to handle larger particles makes these systems unsuitable for determining the grading of complete aggregate samples. However, this type of system could accurately determine the grading of the finer portion of an aggregate grading.

Imaging Analysis

Imaging analysis to determine aggregate grading is now in the early stages of development and holds promise for the future. Several different projects are under way to develop the equipment and methods.

The imaging analysis process involves using a camera to "look" at the aggregate and determine its grading. This process can be broken into five separate components: Image generation and capture, and image coding, image reconstruction, image enhancement, and image analysis. Image generation and capture is the process of creating the image with the camera. This can sometimes be difficult because some information may be lost in the process due to shadows, particle overlap, and other uncontrollable conditions. Image coding refers to the techniques for storing the image. For example, most systems store the image such that each screen element (pixel) is associated with an x-y coordinate system and brightness. Image reconstruction is used to correct problems in the image such as distortion. Image

enhancement is used to make the digitized image clearer. For example, enhancement of the image is used to separate particles that overlap. Image analysis is when the computer actually determines the parameters sought. In this step, the two-dimensional shape of the particles is determined (*15*).

In a practical sense, grading analysis by imaging techniques uses a photographic image in a digitized form. The computer software uses the digitized photograph and chooses the boundary lines for each aggregate particle according to the given algorithms. Having identified the boundaries of each of the particles, the computer then determines the two-dimensional shape of each particle from which it estimates the three-dimensional shape. This projection of two dimensions into three is again dependent of software algorithms. Once the number of particles and their sizes have been determined, the computer calculates the grading of the sample in question.

Laboratory work in imaging analysis has been performed at Purdue University where the techniques were used to differentiate siliceous and calcareous sands (*15*). Work has also been performed at the University of Arkansas-Little Rock (UALR) on techniques to identify aggregate shape and grading using imaging analysis. This work could hold promise for future laboratory aggregate testing methods. The cost of a system similar to this is highly variable with estimates ranging from $15,000 to $50,000.

One full-scale imaging analysis study worth noting is being field tested by Felix Alba, Associates of Murray, Utah (*16, 17*). The study involves the real-time determination of aggregate grading. Each of the cold feed bins is instrumented so that the grading from each is constantly monitored using imaging analysis techniques. When the information is sent to the

control computer, it checks to make sure that the current blend of aggregates being used by the plant will meet the job-mix-formula. If not, the computer can alter the feeding rate of any of the cold feed bins in order to alter the total aggregate blend. In this fashion, the aggregate blend being fed to the plant can be kept in constant control. The system has shown remarkable promise and is expected to cost between $70,000 and $100,000. This process offers obvious advantages. However, it is unable to determine the amount of dust present in the aggregate.

Image analysis is a fully automated system that holds potential for determining aggregate grading in a short period of time or on a continuous basis and all but eliminates the need for a technician. However, the current cost is high and no accurate measure of the percent passing the 0.075 mm sieve is possible. A considerable amount of work remains to be done before this method can be used in practice.

Summary of Current Technologies

TABLE 2.2 shows a summary of the methods reviewed along with approximate costs and availability. Each of the methods has advantages and disadvantages when compared to the others. None of them can be employed immediately to accurately determine a complete grading from the coarsest sieves through the 0.075 mm sieve.

TABLE 2.2 Summary of Current Technology

Technology	Estimates Availability (Years)	Estimates Cost
Gradex 2000	Immediate	$17,000-25,000
VDG-40 Video Grader	Immediate	$50,000
Full-Scale Particle Size Analyzer	Unknown	Unknown

Fractionating Water Column	1-2	$5,000-10,000
Laboratory Particle Size Analyzer	Immediate	$40,000
Laboratory Image Analysis	5-10	$15,000-50,000
Full Scale Imaging Analysis	1-5	$70,000-100,000

In reviewing the current technologies available for adaptability to grading testing, it is obvious that none technology currently exists to fulfill the criteria of reducing test time, reducing technician involvement, providing an accurate measure of the grading, including the percent passing the 0.075 mm sieve, and being affordable. TABLE 2.3 lists each of the methods reviewed and how well they meet the first three criteria. While several of the systems are automated and reduce both the testing time and required technician time, they suffer from the inability to measure the range of particle sizes used in HMA mixes. Some technologies can measure larger particles while others measure the smaller sizes. None of the systems currently offers adequate means for accurately determining the amount of material passing the 0.075 mm sieve present in an aggregate sample.

TABLE 2.3 Capability Summary of the Technologies Reviewed

Technology	**Reduced Test Time**	**Reduced Technician Time**	**Accurate Measure of % Passing 0.075 mm Sieve**
Gradex 2000	Maybe	Yes	No
VDG-40 Video Grader	No	No	No
Full-Scale Particle Size Analyzer	Yes	Yes	No
Fractionating Water Column	Yes	Yes	No
Laboratory Particle Size Analyzer	Yes	Yes	No
Laboratory Image Analysis	Yes	Yes	No
Full Scale Imaging Analysis	Yes	Yes	No

Gradex 2000

The main problem with developing an automated grading analysis system seems to be in determining how to get an accurate measure of the percent passing the 0.075 mm sieve within the time allotted. If this requirement is waived, then the Gradex 2000 can quickly be adapted for use. Contractors and laboratories could use the same sieves they currently employ and the only added expense would be the Gradex 2000 and computer. If an accurate measure of the percent passing the 0.075 mm sieve is required, the Gradex 2000 still presents the best alternative. Although the actual testing time involved would not be reduced, the automation makes it possible to reduce the technician time required.

VDG-40 Video Grader

The VDG-40 Video Grader is one of the only two technologies reviewed that offers the potential ability to obtain an accurate measure of the percent passing the 0.075 mm sieve. However, if the percent passing the 0.075 mm sieve is coating the coarser aggregate particles, the ability of accurately determining the percent passing the 0.075 mm sieve material is reduced. Additionally, this method does not reduce test time or technician time requirements and is expensive.

Full-Scale Particle Size Analyzer

This method does have the potential to reduce test time and technician involvement, but its cost is estimated to be high and it does not offer an accurate measure of the percent passing the 0.075 mm sieve. In addition, it is limited in the particle size that can be evaluated.

Fractionating Water Column

At the present time, the method lacks the ability to produce an accurate measure of the percent passing the 0.075 mm sieve. In addition, it is limited in the particle size that can be evaluated.

Laboratory Particle Size Analyzer

At present the equipment is relatively expensive. This method is also limited in the particle size that can be evaluated. Additionally, the equipment does not physically measure the grading, but rather statistically estimates the grading. This equipment is also somewhat sensitive and requires a clean, stable environment that may not be available in some HMA production laboratories.

Imaging Analysis

Both laboratory and full-scale imaging analysis are in their infant states for grading applications. The equipment is expensive and cannot offer an accurate measure of the percent passing the 0.075 mm sieve. Research efforts are ongoing and should be closely monitored for improvements.

Simulation of Aggregates Packing Process in PFC3d

Because different sizes and distributions of aggregate particles have different sensitivities to the changes of VMA, their effects on volumetric properties should be analyzed separately. For this analysis two assumptions are made:

1) All particles are assumed spherical.

2) The aggregate particles are uniformly distributed within the total volume.

The evaluation of aggregate packing begins with the comparison of two different states of aggregate structures: State (I), a compacted structure of Aggregate 1 (Primary Structure), and State (II), a compacted structure using both Aggregate 1 and Aggregate 2 (Secondary Structure). For the purpose of simplicity, it's assumed that newly added Aggregate 2 has the size equal to or smaller than that of Aggregate 1. In the State (I) structure, the following volumetric relation holds:

$$V_1=V_{a1}+V_{v1} \quad (1)$$

$$P_1=V_{v1}/V_1 = (V_1-V_{a1})/V_1 \quad (2)$$

$$V_1=V_{a1}/(1-P_1) \quad (3)$$

Where V_1 = total volume at state (I); V_{a1} = total aggregate volume at State (I); V_{v1} = total air void volume at State (I); and P_1 = aggregate porosity or VMA at State (I).

In this study a gradation weighing factor f_v was defined as the percentage of void change by volume because of the addition of unit aggregate (Equation (4)), which is an indication of the resulting volumetric impact when smaller aggregates are added into the structure (*7*).

$$f_v=(V_{v2}-V_{v1})/V_{a2} \quad (4)$$

$$V_{v1}=V_1P_1 \quad (5)$$

$$V_{v2}=V_2P_2 \quad (6)$$

Where V_2 = total volume at State (II); V_{a2} = the added aggregate volume at State (II) compared with State (I); V_{v2} = total air void volume at State (II); and P_2 = aggregate porosity or VMA at State (II).

The development of the f_v parameter provides a straightforward method to estimate the VMA of an aggregate structure. This method includes an iterative process starting from an

aggregate structure with only one size of aggregates. When smaller size aggregates are added in, the porosity of the new structure can be determined as

$$P_2 = V_{v2}/V_2 = (f_v V_{a2} + V_{v1}) / [V_1 + (1+f_v)V_{a2}] \quad (7)$$

Repeating the same procedure, smaller size aggregates are added into the mixed aggregate structure and the corresponding f_v values are determined. Once all f_v values for each sieve size are determined, Equation (8) will be used to predict the VMA (or porosity) of the HMA mixtures:

$$P = \frac{\sum_{i=1}^{n} f_{vi} V_{ai}}{\sum_{i=1}^{n} (1+f_{vi}) V_{ai}} \quad (8)$$

Where f_{vi} = f_v value for the i^{th} sieve size of the gradation; V_{ai} = percentage of aggregate retained on the i^{th} sieve size; and P = porosity or VMA of the aggregate structure.

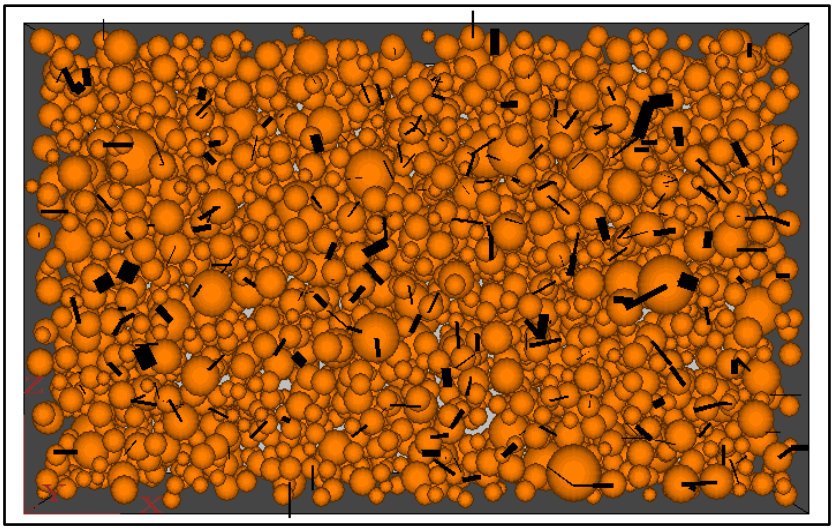

FIGURE 2.6(a) Mixture Contains Aggregate Larger Than 4.75mm (State I).

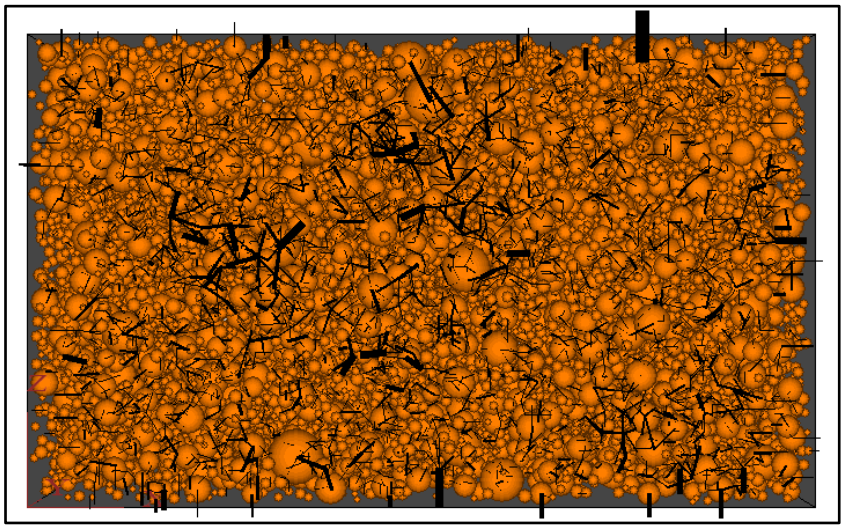

FIGURE 2.6(b) Mixture Contains Aggregate Larger Than 2.36 mm (State II).

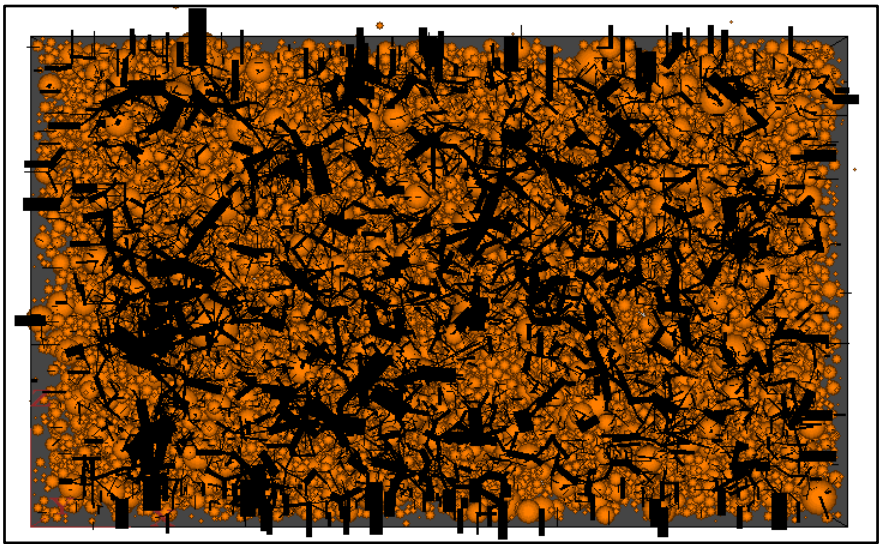

FIGURE 2.6(c) Mixture Contains Aggregate Larger Than 1.18 mm (State III).

The determination of f_v values in the DEM simulation follows an iteration process as follows:

1. Generate a basic model with only large aggregates, and calculate the volume and porosity of this structure. The basic model, which includes aggregates retained on 4.75 mm sieve size, is shown in FIGURE 2.6(a). The mixture reaches equilibrium after gravity and loading cycles are applied. The contact force and unbalanced force are recorded at equilibrium state.

2. Add an appropriate amount of finer aggregates into the structure, mix and compact the structure to equilibrium state, and calculate the volume and porosity of the new structure. FIGURE 2.6(b) and FIGURE 2.6(c) present the aggregate structures when particles of sizes 2.36–4.75 mm and 1.18–2.36 mm are added into the system consecutively.
3. Use Equation (8) to calculate the f_v value for this portion of aggregate.

Determination of Optimal Gradation

In this session, five aggregate gradations tabulated in TABLE 2.4, are adopted for the evaluation. Consequently, there are five models conducted in PFC3d for different gradations. Based on evaluation and calculation method described above, the value of f_v and VMA are calculated, shown in TABLE 2.5. As we can see, Model 1 with the smallest porosity has the largest density. While largest density as sole criterion may not be rational, it is widely used in experimental approaches, and therefore adopted for the computational method. Nevertheless, other criteria will be identified and used for future work.

TABLE 2.4 Gradation of Five Models

ID	Percentage passing (%)									
	19 mm	12.5 mm	9.5 mm	4.75 mm	2.36 mm	1.18 mm	0.6 mm	0.3 mm	0.15 mm	0.075 mm
1	100	93	80	49	32	23	17	12	8	5.2
2	100	93	83	55	35	24	18	13	7	5.4
3	100	98	85	53	32	20	14	10	8	6.1
4	100	99	87	51	29	20	14	10	6	4.6
5	100	97	82	52	30	17	11	8	6	5.1

TABLE 2.5 Calculated f_v and Porosity of Five Models

fv / ID	Sieve size (mm)										Porosity
	19	12.5	9.5	4.75	2.36	1.18	0.6	0.3	0.15	0.075	(%)
1	0.426	0.426	0.426	0.426	0.194	-0.396	-0.396	-0.419	-0.600	-1.000	16.3
2	0.432	0.432	0.432	0.432	0.198	-0.404	-0.404	-0.421	-0.600	-1.000	16.7
3	0.420	0.420	0.420	0.420	0.190	-0.388	-0.388	-0.417	-0.566	-1.000	16.5
4	0.441	0.441	0.441	0.441	0.199	-0.396	-0.396	-0.416	-0.600	-1.000	17.0
5	0.462	0.462	0.462	0.462	0.208	-0.404	-0.404	-0.415	-0.634	-1.000	17.7

The FHWA Advisory suggests using the 0.45 power curve to evaluate and adjust aggregate gradations. The most convenient way to evaluate gradation is to plot the combined gradation on a plot on which the FHWA 0.45 power gradation line has been graphed, shown in FIGURE 2.7. Maximum density line is also plotted in FIGURE 2.7. Based on Goode and Lufsey's recommendation (*6*), this maximum density line is considered to be the most realistic one for 3/4 inch nominal maximum aggregate size (NMAS). It's very important to have consensus among designers on this issue. A gradation in close proximity to the maximum density line generally gives low VMA, resulting in a less durable mix that is more sensitive to slight variations in asphalt content during production. To avoid these difficulties, gradations are usually shifted away from the maximum density line. It's clearly shown in FIGURE 2.7 that gradation of Model 1 satisfies this criterion. To sum up, gradation of Model 1 has the lowest porosity and is adequately away from the maximum density line, so Model 1 is considered as the optimal gradation (Gradation 1).

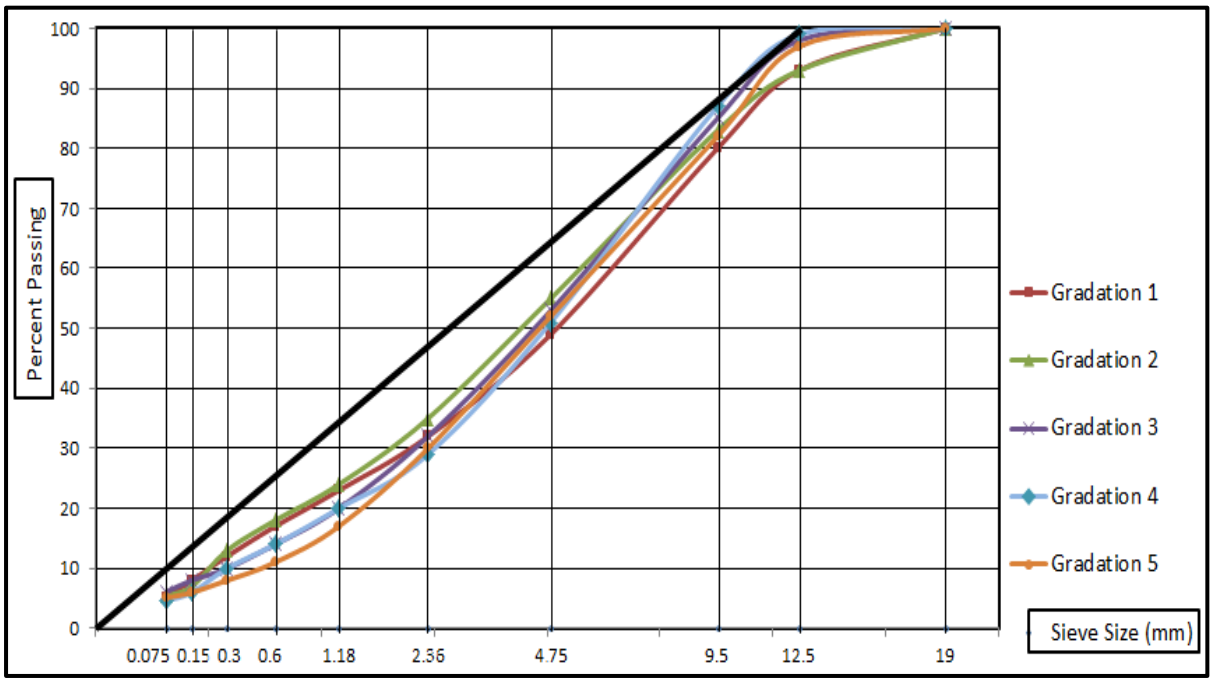

FIGURE 2.7 Five Gradation Curve VS. Maximum Density Line.

The following asphalt mixture is based on selected gradation (Model 1). The gradation has a NMAS of 3/4 inch and a primary control sieve size of 2.36 mm, and belongs to coarse-graded group. As shown in FIGURE 2.8(a), orange balls represent aggregates and smaller yellow balls represent asphalt binder. A complete consideration of fine particles in DEM is almost impossible, because it not only significantly increase the computational time and cost but also affects the system's capability to reach equilibrium. Assuming that smaller particles mainly fill in the voids created by coarse aggregates, only the particles retained on 1.18 mm sieve were simulated in a cylinder (rad = 40 mm, height = 160 mm) under a unidirectional gravitational force. Then, balls are compacted by the assigned gravitational force to their stable position. An equilibrium state is reached when the unbalanced force reaches 1% of the maximum contact force. Maximum contact force = 9.837×10^{8} Newton, is shown in FIGURE 2.8(b), mean unbalanced force = 9.468×10^{6}Newton. The equilibrium state

is reached in FIGURE 2.8(b) since unbalanced force/ maximum contact force = 0.009625 ≈ 0.01.

Based on findings by Shen and Yu (*18*), the contact stiffness *kn* of 30 GN/m, the rigid wall stiffness of 300 GN/m, and the inter-aggregate contact friction coefficient of μ=0.5 are calibrated parameters that can reasonably simulate the volumetric properties of the aggregate structure using the spherical DEM model. While these parameters are varying with different types of aggregate, it is acceptable for this qualitative evaluation (mix design for a selected aggregates).

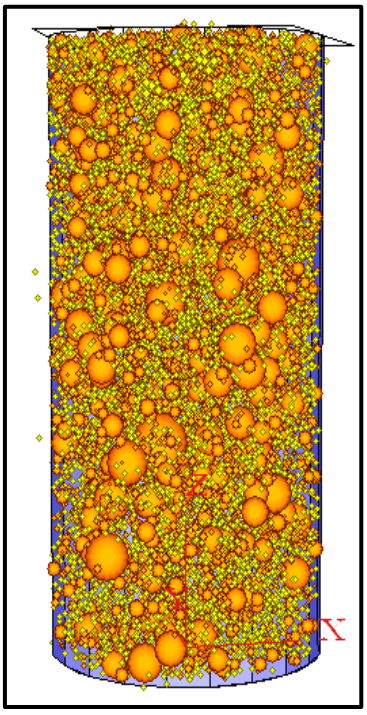

FIGURE 2.8(a) Mixture Model with Selected Gradation Aggregates and Asphalt Binder.

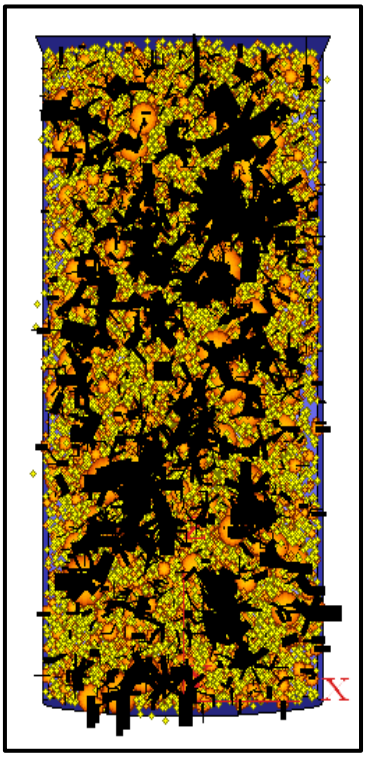

Maximum Contact Force
= 9.837×10^{8} N

FIGURE 2.8(b) View of Contact Force of the Mixture at Equilibrium State.

Summary

Gradation is determined based on a simulated packing process. The evaluation of aggregate packing begins with the comparison of two different states of aggregate structures. We assume the newly added aggregates are always equal in size to or smaller than aggregates in former state. After gravity and loading cycles are applied, the contact force and unbalanced force were recorded. Then finer aggregates were added into the structure. After mixing and compacting the structure into equilibrium, volume and porosity of the new structure were calculated. By comparing five digital models, an optimal model which has the lowest porosity was selected.

3 DETERMINATION OF ASPHALT CONTENT

Literature Review

The binder content in an asphalt mixture is one of the critical factors determining the quality of the mixture. Using a mixture with too much binder can lead to pavement rutting and bleeding, whereas having a mixture with too little binder can lead to pavement durability problems, including raveling and cracking. The Virginia Department of Transportation (VDOT) now accepts hot mix asphalts (HMA) based on their volumetric properties (voids in the mineral aggregate (VMA) and percent air voids) and binder content (the mass of binder expressed as a percentage of the total mass of the mix), so accurate determination of the binder content is essential. Historically, the binder content of a mixture has most commonly been determined by one of several extraction methods in which a solvent is used to remove binder from a known mass of HMA. The main advantages of these methods are as follows: (a) no calibration factor needs to be determined and (b) the properties of the binder and aggregate recovered from the HMA may be tested after extraction. The main limitations associated with solvent extraction methods are related to the length of the test time, possible alteration of binder properties and the hazardous nature of the solvents. The ignition oven is one alternate to solvent extraction. This oven uses high temperature to burn the asphalt off the aggregate. The procedure terminates when the weight of the sample stabilizes, indicating that there is no more binder to ignite. In 1999, VDOT began using the ignition oven on a few trial projects; usage increased substantially after that because of the advantages of the method. Those advantages include the relatively fast test time and avoidance of the use of hazardous chemicals.

The ignition method has generally worked well on HMAs, except those containing dolomitic aggregates and some limestone sources containing pyrite. These types of aggregates, however, are prevalent in some areas of the state, especially dolomites. With these "problematic aggregates," the high temperatures experienced during ignition cause chemical changes within the aggregates, which result in variable mass loss. In some cases, the sample weight does not stabilize at or below the threshold level, and the ignition test continues for excessive periods of time. This variability in the aggregate mass loss causes difficulties in determining a consistently accurate calibration (or correction) factor and in obtaining consistent and repeatable test results from multiple samples of the same material. Because of this problem, ignition ovens are not used at all in some parts of the state or are only used for those mixes that do not contain dolomite.

Binder Content Determination Methods

Historically, the binder content has most commonly been determined by one of the several extraction methods in which a solvent is used to remove the binder from a known mass of HMA. The solvents used were typically chlorinated solvents such as methylene chloride, trichloroethylene or trichloroethane. The main advantages of these methods are: (a) no calibration factor needs to be determined and (b) the properties of the binder and aggregate extracted from the HMA may be tested after extraction.

Another method for binder content determination is the nuclear gauge method. The nuclear gauge uses radiation to detect the presence of hydrogen in the binder. While relatively quick and easy to conduct, this test does not offer the possibility of testing the binder and

aggregate since they are not separated in the process. Another disadvantage of using the nuclear gauge is the requirement for obtaining a Nuclear Regulatory Commission license. The nuclear asphalt content gauge requires calibration for each mixture tested, which can be time consuming.

In the 1980s, the conventionally used chlorinated solvents for asphalt extractions began to fall into disfavor. Due to concerns over potential carcinogenicity and environmental impacts, some solvents became difficult to obtain and dispose of after use. Costs also increased greatly. The asphalt industry, which relied heavily on solvent extractions to determine binder contents, needed to find alternatives to chlorinated solvents. In 1990, the National Center for Asphalt Technology (NCAT) began development of an ignition oven to burn off the asphalt from a sample of hot mix. Eventually, this effort led to the development of the NCAT ignition oven (*19*). This developmental effort built on work from the late 1960s by Antrim and Busching showed that the asphalt cement in a mixture could be completely combusted by heating to 843^{o}C (1550^{o}F) with an excess of oxygen. At this high temperature, some aggregate mass was also lost; more mass loss occurred with limestone than with gneiss in the early work.

NCAT built upon this earlier work, but substituted a muffle furnace for the special furnace Antrim and Busching had used. NCAT also used a lower burn temperature (593^{o}C or 1100^{o}F) to reduce the aggregate mass loss. NCAT was motivated to reduce the test time, so they experimented with different ignition temperatures and burn times to optimize the two factors (*19*).

Since the method does not use potentially hazardous solvents, it has become quite

popular across the country. The oven also does not require nuclear regulatory licensing, so it is easier to implement than the nuclear asphalt content gauge. In addition, the aggregate remaining after ignition is generally (but not always) suitable for gradation analysis, which cannot be conducted with the nuclear gauge. At least one study (*20*) has demonstrated that the ignition oven is potentially far less expensive to operate than the nuclear gauge or various solvent extractions. Many states have adopted the oven for use and find it similar to or fewer variables than alternate binder content determination methods. (*21, 22, 23, 24, 25, 26*)

Currently, the ignition oven test is described in both AASHTO and ASTM standards. The ignition oven uses high temperature to burn the asphalt off the aggregate; the typical test is conducted at 538^{o}C or 1000^{o}F. (ASTM specifies a test temperature of 540°C or 1000°F in keeping with their policy of using rationalized unit conversion, so-called "hard conversions.") During a typical ignition test, the sample is heated continuously until three consecutive readings of the mass of the sample, taken at one minute intervals, do not change by more than a specified threshold level, typically 0.01%. To facilitate this determination, many ovens have internal balances to provide continuous readout of the sample weight. All calculations of the asphalt content must account for the calibration factor, which is the difference between the known binder content and ignition oven test result. The calibration factor should be determined independently for each mix. The results of two properly conducted tests by the same operator on the same size samples of HMA should not differ by more than 0.196 %.

If the calibration factor is higher than 1.0%, as is the case for some high mass-loss aggregates, the test temperature should be lowered to 482^{o}C (900^{o}F). The calibration factors for most limestone aggregates are typically less than 0.2%. For some dolomitic aggregates,

however, the factor can be over 2%. (According to AASHTO T308 (*27*), a correction factor greater than 1.0% is considered unusually high.) The correction factor has been observed to decrease when the ignition temperature was decreased from 538ºC (1000ºF) to 482ºC (900ºF). (*28, 29, 30*)

In a conventional ignition oven, the furnace chamber is heated with a radiant heat source. However, there is an alternate type of ignition oven, called the infrared oven. In this oven, an infrared heating element is used to heat the sample. Hurley, Prowell (*31*) and Prowell (*32*) compared the results obtained using both types of ovens. They found the correction factor due to aggregate weight loss for the infrared oven to be generally smaller than that for the conventional oven. They reported the results from the infrared and conventional oven were not statistically different. Research conducted by Williams and Hall (*33*) reached a similar conclusion that the accuracy of both types of ovens is statistically similar. However, they did not observe that infrared heating limited the over-heating of the aggregate. They discovered that the peak temperature recorded by the infrared oven was often greater than the peak temperature recorded by the conventional oven for the same type and size of sample.

Changes in aggregate properties resulting from binder ignition were observed by Mallick et al. (*34*). During a study involving different types of aggregate (granite, limerock, gravel and traprock), the authors found that for the same duration of test, the ignition process has a greater effect on the properties of aggregate when an asphalt - aggregate mix (rather than an unbound aggregate sample) is placed in a preheated ignition oven.

Similar research was conducted by Prowell and Carter (*35*). In their study, the impact of the ignition test on the aggregate properties was evaluated. In six of ten cases, they noticed

significant differences between the bulk specific gravity before and after the test. They also noted that aggregate recovered using the ignition furnace appears to be unsuitable for sand equivalency testing. The results of fine aggregate angularity testing were significantly different between the virgin and burnt samples in three of ten cases. They also observed that accurate results may be obtained for gradation analysis and flat and elongated particle measurements performed on aggregates recovered from the ignition oven test.

During a typical ignition test, the pre-set oven temperature is often exceeded due to the binder ignition. Rogers et al. (*36*) conducted a study with a modified ignition oven, where a thermo-kinetics infrared thermometer was placed in the oven door. The temperature of the flame created during the ignition process was measured. They noticed up to a 200ºC difference between the flame and oven temperatures. Temperatures above 565ºC were consistently measured in the oven, but in no case did the temperature exceed 750ºC. In addition, differences in flame temperature due to differences in binder content were observed.

Ignition Method Test Procedures

Currently, the ASTM D6307 "Standard test method for asphalt content of hot mix asphalt by the ignition method" (*37*), and the "Virginia test method for determination of asphalt content from asphalt paving mixtures by the ignition method" (*30*) are the two widely known test procedures of ignition tests. In both procedures, the test temperature is specified at 538 ºC for HMA and 578 ºC for aggregate only calibration, and the sample size is determined by the nominal maximum size (defined as one size smaller than the: first sieve that retains aggregate) of the aggregate according to TABLE 3.1.

In the ASTM procedure, two samples are required per calibration, no specific guideline of the calibration of RAP mixes is provided. In the VDOT procedure, a total of six samples (two at design asphalt content, two at 0.5 percent below, arid two at 0.5 percent above the design asphalt content) are required for mixture calibration. Four samples are required for aggregate only calibration. The method provides a guideline for the calibration of RAP mixtures.

TABLE 3.1 Minimum Sample Weight

Nominal maximum aggregate size (mm)	Minimum sample weight (g)
4.75 (No.4)	1200
9.5 (3/8 in.)	1200
12.5 (1/2 in.)	1500
19.0 (3/4 in.)	2000
25.0 (1 in.)	3000
37.5 (1 ½ in.)	4000

Procedure of Determination of Asphalt Content Using DEM

In addition to gradation, the content of asphalt is another important factor in the design of asphalt concrete. Ten sample mixtures were prepared with same gradation but different asphalt content, as summarized in TABLE 3.2 and TABLE 3.3. The asphalt content ranges from 3.9% to 5.9%. In a common sense, the asphalt mixture that reaches highest peak strength is the strongest. As compressive load is applied, mixtures become weaker, and cracks initiate and propagate.

Here the contacts between aggregates and asphalt binder are considered as the evaluation factor to determine whether the mixture is damaged because of cracking. A simple

visco-elastic model and parallel bonds were applied on these contacts. The type of asphalt binder used in the simulations is PG 64-28. In order to simulate the properties of this type of asphalt, some important parameters were selected and shown in TABLE 3.4. The following procedures were followed to determine the exact optimal asphalt content value based on DEM method.

1. Calculate gradation and surface area. Since aggregates in simulations are represented by balls with regular shape and sizes, gradation and surface area of the mixture could be easily calculated.
2. Record contact number between aggregates and asphalt binder. TABLE 3.3 shows contact information in ten mixtures at initial state and after load applied, respectively. The information could be used to determine whether the mixture is cracked. It is assumed that the mixture will stop working due to cracking when the contact number decreases to 50%~60% of that at the initial state.
3. Compare peak strengths when the mixtures cracked. The model with the highest strength was considered as the optimum mix design.

TABLE 3.2 Gradation Information

Sieve size (mm)	19	12.5	9.5	4.75	2.36	1.18	0.6	0.3	0.15	0.075
Percentage passing (%)	100	93	80	49	32	23	17	12	8	5.2

TABLE 3.3 Asphalt Content and Contact Information

Mixture ID	Number of Contacts at initial state	Number of Contacts after compression	Asphalt content	Peak strength
1	19746	11774	5.3%	84.81 MPa
2	18400	10428	4.6%	47.82 MPa
3	17632	9628	3.9%	30.87 MPa

4	19156	11034	5.0%	72.01 MPa
5	17980	10019	4.3%	39.55 MPa
6	20246	12037	5.7%	58.36 MPa
7	20499	11558	5.9%	38.97 MPa
8	20371	11476	5.8%	40.01 MPa
9	20135	11377	5.6%	69.82 MPa
10	19960	11292	5.5%	79.44 MPa

TABLE 3.4 Contact Properties Applied in Simulations

Properties for parallel bonds:	**Properties for viscoelastic contact model:**
Normal stiffness = $30*10^{15}$ Nm^{-3}; Shear stiffness = $30*10^{15}$ Nm^{-3};	Viscoelastic normal stiffness = $0.36*10^{6}$ N/m
Normal strength = 190 MPa; Shear strength = 190MPa;	Viscoelastic shear stiffness = $0.12*10^{6}$ N/m
Radius multiplier = real parallel bond radius/radius = $30x10^{-9}$	Shear viscosity = $0.414*10^{6}$ N/m

Results and Analysis

Peak strengths were recorded in TABLE 3.3. From TABLE 3.3, Mixture 1 which has asphalt content equal to 5.3% is the optimal one. The Stress-Strain figure of Mixture 1 is shown in FIGURE 3.1. A relationship between the asphalt content and the peak strengths of ten mixtures is shown in FIGURE 3.2; Mixture 1 with the asphalt content of 5.3% locates at the turning point on the curve.

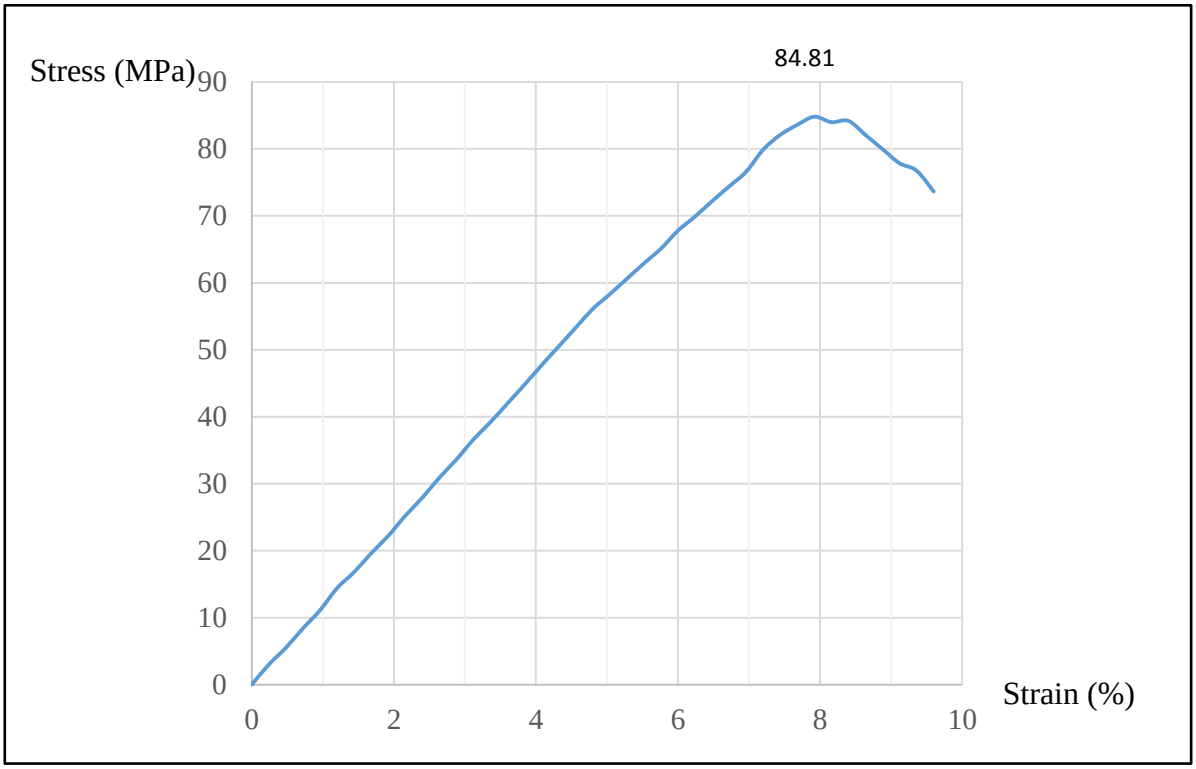

FIGURE 3.1 Stress VS. Strain of Mixture 1

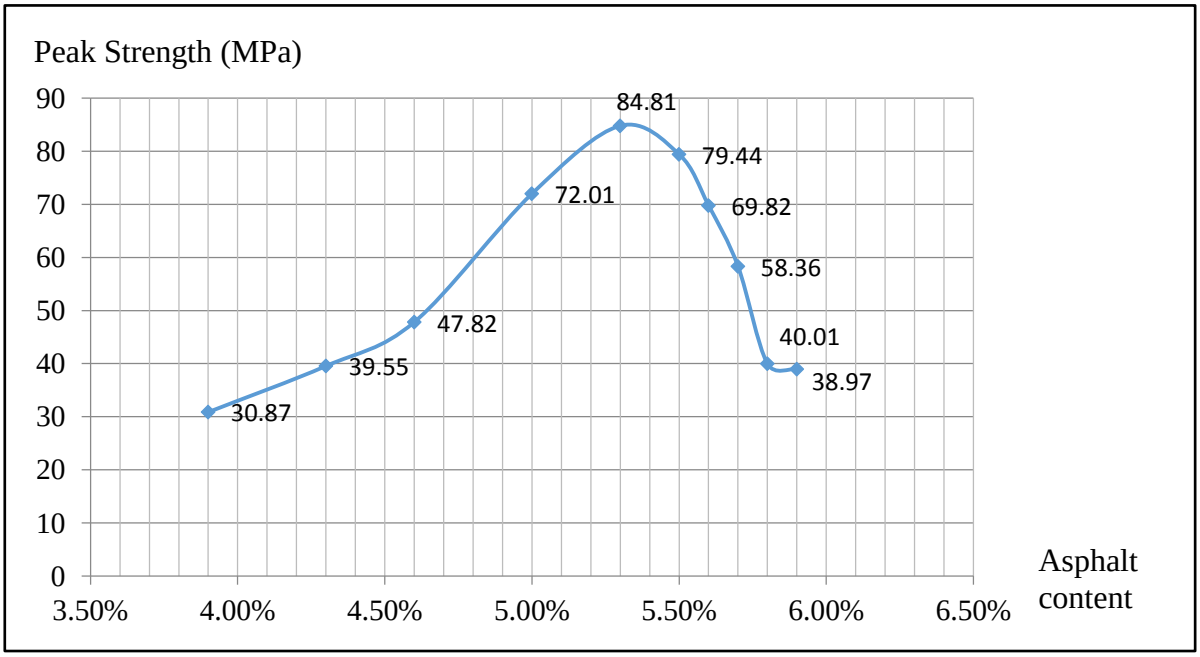

FIGURE 3.2 Asphalt Content VS. Peak Strength.

Calculation of Film Thickness by Using Selected Gradation and Asphalt Content

Calculation of Specific Surface Area Factor.

The Hveem–Edwards's method (*38*) is used to estimate surface area. The specific surface area of aggregate is determined from sieve analysis based on the total percentage passing a stipulated group of sieves as

$$SA = 0.01 SPP_i \text{ x } CP_i \quad (9)$$

where SA = specific surface area of the aggregate in m^2/kg (ft^2/lb); SPP_i = percent of aggregate by weight passing the i^{th} sieve; CP_i = surface area factor (a coefficient for "passing") in m^2/kg (ft^2/lb); i = sieve index (i = 0,1…N); N = 9 for the standard set (ASTM C136-06) with the following diameters: D_0=19.0 mm, D_1=12.5 mm, D_2 = 9.50 mm, D_3 = 4.75 mm, D_4 = 2.36 mm, D_5 = 1.18 mm, D_6 = 0.600 mm, D_7 = 0.300 mm, D_8= 0.150 mm, and D_9 = 0.075 mm.

The surface area factors CP_i have been tabulated but the background research data on them are not available. To derive them, one can start from specific surface of aggregate fraction that passed the $(i\text{ -}1)^{th}$ sieve and retained in the i^{th} sieve. By definition, the specific surface is a surface-to-weight ratio. The specific surface of particles contained in the i^{th} sieve can be expressed as the average specific surface of the endpoints of the sieve range:

$$CR_i = 3 / (g_i\text{-}1\ D_{i\text{-}1}) + 3 / (g_i\ D_i) \quad (10)$$

where CR_i = specific surface of the particles with diameter in the range (D_i, $D_{i\text{-}1}$), retained in the i^{th} sieve (a coefficient for "retained"), m^2/kg (ft^2/lb); g_i= effective density of aggregate in kg/m^3; G_{sbi} = bulk specific gravity of aggregates contained in the i^{th} sieve; g_w= density of

water; K_{sph} = sphericity coefficient = (surface area of spherical shape / surface area of irregular shape): 1 for sphere, 0.806 for cube, 0.874 for cylinder (h=d), etc. Sphericity values relate the surface area of the non-spherical shape to a spherical shape based on the assumption that both particles have the same volume.

Once the relationship between the specific surface of particles retained in the sieve and the sieve diameter is established, the specific surface area of the aggregate based on the percentage retained in a group of sieves can be expressed as

$$SA = 0.01 SPR_i \text{ x } CR_i \quad (11)$$

Where PR_i = percent of aggregate by weight retained in the i^{th} sieve; i = sieve index (i = 1, 2…N+1); N = 9 for the same standard set of ASTM sieves.

Since the percent of aggregate retained in the i^{th} sieve, PR_i, is related to the percent passing the $(i\text{-}1)^{th}$ and i^{th} sieves by:

$$PR_i = PP_{i\text{-}1} - PP_i \quad (12)$$

Equation (11) can be rewritten as:

$$SA = 0.01[(PP_0 - PP_1)\ CR_1 + (PP_1 - PP_2)\ CR_2 + \ldots\ (PP_N - PP_{N+1})\ CR_{N+1}] \quad (13)$$

Which is same as:

$$SA = 0.01[PP_0\ CR_1 + PP_1\ (CR_2 - CR_1) + PP_2\ (CR_3 - CR_2) + \ldots PP_N\ (CR_{N+1} - CR_N)] \quad (14)$$

Then the unknown surface area factors for the percentage passing the sieves (CP_i), can be related with specific surface of particles retained (CR_i), as:

$$CP_0 = CR_1\ CP_i = CR_{i+1} - CR_i\ (i = 1, 2\ldots N), \quad (15)$$

Substituting Equation (10), we finally get the presumable equation for conventional surface area factors:

$CP_0 = 3 / (g_0 D_0) + 3 / (g_1 D_1)$ $CP_i = 3 / (g_{i+1} D_{i+1}) - 3 / (g_{i-1} D_{i-1})$, ($i$ = 1, 2...N) (16)

TABLE 3.5 lists the surface area factors calculated using Equation (16). These results can be used to calculate film thickness. Combine with gradation listed in TABLE 3.2, the specific surface area has been calculated to be 5.92 m^2/kg.

TABLE 3.5 Calculated and Surface Area Factors

Sieve index, i	Sieve size (mm), D_i	Effective density of aggregate retained, x 1000 kg/m^3	Calculated surface area factor, m^2/kg
0	19	2.34	0.410
1	12.5	2.34	0.410
2	9.5	2.34	0.415
3	4.75	2.34	0.418
4	2.36	2.34	0.827
5	1.18	2.34	1.694
6	0.6	2.34	3.012
7	0.3	2.44	6.160
8	0.15	2.44	12.295
9	0.075	2.44	32.787

Calculation of Film Thickness

The asphalt binder specific gravity is 1.03 g/mL, selected asphalt content is 5.3%, and the bulk density of the mixture is 2.340 g/mL. Film thickness can be calculated by Equation (17).

$$T_F = 1000 \times V_{asp} / (SA \times W) \quad (17)$$

Where,

T_F = Average film thickness (micrometer);

V_{asp} = Effective volume of asphalt binder (liters);

SA = Surface area of the aggregate (m^2 per kg of aggregate);

W = Weight of aggregate (kg).

Let's take a one liter sample as example:

Total volume of asphalt binder = total weight × asphalt content / asphalt binder specific gravity = 2340 g×0.053/1.03 = 120.4 mL

If we ignore absorbed asphalt, V_{asp} = 120.4 mL = 0.1204 L.

W = (1-0.053) ×2340 = 2215.98 g = 2.21598 kg

T_F = 1000×0.1204 / (5.92×2.21598) = 9.2 micrometers

So the optimal film thickness calculated through determined gradation and asphalt content is 9.2 micrometers.

Summary

In this session, a computational method is developed to aid mix design, especially for determine the asphalt content. Discrete element method (DEM) was used to simulate the formation of skeleton and voids structures of asphalt concrete of different asphalt contents. This method takes the mechanical properties or performance of the mixture into consideration, such as inter-aggregate contacts and local stability. A simple visco-elastic model was applied to model the contacts between asphalt binder and aggregates. The surface texture of an aggregate particle can be taken into consideration in the inter-particle contact model. For a certain air void content, the mastics volume or the binder volume or the asphalt content can be determined via a digital compression test. The surface area of all the aggregates and the film thickness can be then calculated.

Ten digital mixtures were built in software PFC3d, and the asphalt content ranges from

3.9% to 5.9%. During compressive loading being applied, the number of contacts between aggregates and asphalt binder were recorded. This number was used as a judgment to tell whether the mixtures were damaged due to cracking. The mixture that reached the highest peak strength was considered as optimal. Therefore, optimal asphalt content determined by this process was 5.3%. The procedure described in this study helps to improve the experimental method to determine the optimum asphalt content by adding the capability of internal deformation mechanism (breaking of bonds and loss of contacts).

4 EFFECT OF FILM THICKNESS ON ASPHALT MIXTURE

Literature Review

Asphalt mixture is a composite material which consists of interspersed aggregates, asphalt binder and air voids. The constitutive behavior of the material depends largely on the interaction between the aggregates and asphalt binder. The aggregate skeleton determines the load carrying mechanism and the asphalt binder serves as an adherent which enables the mix to hold tensile and shear stresses. A comprehensive understanding of the mechanical behavior of aggregate-binder system is critical for research in the area of the deformation mechanism of asphalt mixtures. To study the constitutive behavior of an aggregate-binder system, the contact between aggregates coated with asphalt binder is the key problem to solve. A contact model which properly shows the relationship between the contact force and relative movement is needed. Combined with the mechanical model, numerical tools could be incorporated into the study, such as the Finite Element Method (FEM) and Discrete Element Method (DEM).

Both of the FEM and the DEM are utilized in the simulation of mechanical materials. The former is based on the continuum approach and has been successful in capturing the stress-strain distribution within the asphalt mixtures and its effect on the stiffness anisotropy. The latter based on the discrete approach could analyze the individual characteristic effects of each component in the mixture, such as the influence of shape, gradation and relative slippage of aggregates. The proper representation of the asphalt mixture internal structure is possible through the use of image analysis techniques. These techniques are utilized to accurately capture the actual microstructure of the asphalt mixture. Such images offer a

realistic representation of the internal structure of asphalt mixtures and could be used to analyze the deformation of the composite material. Given the proper internal structure and constitutive contact models, the simulation could avoid huge amount of sample preparation work in lab and provide reliable results in the research of the asphalt mixtures.

Contact Model

Asphalt mixture can be considered to be three-phase composites consisting of asphalt, aggregates and air voids. Because of the complex heterogeneous nature of the material, the macro load carrying behavior depends on many micro-phenomena that occur at the aggregate/binder level. Some important micro behaviors are related to binder properties including volume percentage, elastic moduli, time-dependent response, aging hardening, micro-cracking, and de-bonding from aggregates. Other microstructural features include aggregate size, shape, texture and packing geometry. Because of these issues it appears that a micromechanical model would be best suited to properly simulate such a material. Furthermore, micromechanics offer the possibility to more accurately predict asphalt performance and to relate such behavior to particular mix parameters such as binder properties, aggregate gradation, and sample compaction.

Van der Poel (1954) attempted to model the behavior of asphalt mixture by calculating the rigidity of a concentrated solution of elastic spheres in an elastic medium, using a method developed for dilute dispersions by Frohlich and Sack (*39*). The model was reported to give reasonable agreement with experimental measurements of dynamic mix stiffness up to a volume fraction of 60 % aggregate.

Hills (1973) attempted to develop theoretical models for the long time creep behavior of asphalt mixes (*40*). His modeling approach described the internal structure in terms of a characteristic asphalt thickness, and the evolution of this state variable as a function of the macroscopic straining of the material. The macroscopic strain of a mix was assumed to be accommodated, on a microscopic scale, by displacements of adjacent aggregate particles in both shear and compression. These displacements were assumed to be independent of each other. It was further postulated that the macroscopic strain of the mix was uniquely related to the shear displacements of adjacent aggregate particles. The microscopic shear resistance of the asphalt was considered to be controlled by the thickness of the asphalt. The effect of compression was taken into account by changing the thickness of the asphalt. The asphalt was modeled as an incompressible, linear viscous fluid. The general forms of the constitutive equations were given in terms of the 'stiffness' of asphalt, S_{bit}, in the region $S_{bit} < 5$ MPa. Hills' model was based on an empirical estimation of the evolution of film thickness under deformation rather than by analysis of the deformation of the film. The model depended on curve fitting to experimental data to obtain numerical data.

Cheuang at al (1997) used the isolated model for micromechanical modeling of the stage I sintering process, when the dominant mechanism of contact deformation is rate-independent plasticity or power law creep (*41*). A compatible strain rate field is assumed for describing the motion of individual particles. The constraints on the motion of each contact are determined by analysis of the corresponding deformation mechanism. Using kinematics bounds, the macroscopic deformation behavior can then be estimated by integrating the microscopic deformation behavior, assuming that individual contacts deform in isolation. They assumed

that all of the aggregate particles are separated by thin films of asphalt; the constraints on the relative motion of the particles will largely be determined by the deformation behavior of the bitumen films until they become so thin that their stiffness becomes comparable with the stiffness of the aggregate particles. They also assumed that asphalt existing in larger quantities of particles within the random aggregate skeleton will have only secondary effects on the deformation behavior of the mix. The assumption of isolated contacts means asphalt displaced by the deformation of each contact flows into an air void rather than into an adjacent contact. It is therefore necessary for the volume of asphalt displaced to be small compared with the volume of voids. Analysis based on the assumption of isolated contact behavior provides a theoretical limiting case solution regarding the macroscopic behavior of the idealized mix, corresponding to the case when microscopic deformation occurs at all distributed thin film bitumen contacts.

Uddin (1998) presented a micromechanical analysis method for calculating the creep compliance of asphaltic mixes on a microscopic level using laboratory viscoelastic characterization of the binder and elastic material properties of the aggregates at a given temperature (*42*). The micromechanical model is based upon the "method of cells" (MOC) developed to predict viscoelastic response of resin matrix composites. The properties of the aggregate are assumed to be linear elastic and can be described by the elastic constitutive relationship. A time-stepping algorithm was developed for a viscoelastic material with a Prony series representation of the time-dependent properties. And the micromechanical model was incorporated in a microcomputer program which calculates the viscoelastic response of the mix and predicts the mix stiffness. It is reported that reasonably good

agreement is found between the predicted modulus and measured modulus of the mix if proper percent air voids are considered in the micromechanical model.

Zhong and Chang (1999) applied a micromechanics approach to investigate the inter-particle behavior of two particles connected by binder (*43*). The model is based on the premises that the inter-particle binder initially contains micro-cracks. As a result of external loading, these micro-cracks propagate and grow. Thus, binders are weakened and fail. Theory of fracture mechanics was employed to model the propagation and growth of the micro-cracks. The contact law is then incorporated in the analysis for the overall damage behavior of material using a discrete element method. Using this model, the stress-strain behaviors under uniaxial and biaxial conditions were simulated. And it is reported that a reasonable agreement is found between the predictions and experimental results.

Levenberg and Uzan (2003) developed a triaxial cross-anisotropic viscoelastic-viscoplastic constitutive model for asphalt aggregate mixtures for the small-strain domain (*44*). The model follows the concept of strain decomposition by separately analyzing the viscoelastic and viscoplastic strain components. In order to calibrate the model, advanced triaxial testing was employed which included both hydrostatic and uniaxial creep and recovery cycles. The test data is presented and analyzed along with the derivation of all model parameters. It is reported that the proposed model correlates extremely well with the entire test-data in both axial and radial directions.

Mazzotti and Savoia (2003) proposed an isotropic model for creep damage of concrete under uniaxial compression, where the combined effect of nonlinear viscous strain evolution and crack nucleation and propagation at high stress levels are considered (*45*). Strain splitting

assumption is used for creep and damage contributions. Creep is modeled by a modified version of solidification theory. In the modeling of damage of concrete, a damage index based on positive strains is introduced. In particular cases, the proposed model reduces to linear viscoelasticity for long time low stress levels whereas, for very high stresses, tertiary creep causing failure at a finite time can be described. The effect of strength variation with time is also included. The model is numerically implemented to perform time integration of nonlinear equations by means of a modified version of exponential algorithm. The model was validated through comparison with experimental results and numerical examples are also presented, where the roles of concrete ageing and strength variation with time are investigated.

Huang et al (2004) presented a temperature dependent viscoplastic model that incorporated temperature and loading rate into the Hierarchical Single Surface plasticity based model (*46*). The model was able to reflect the nonlinear plasticity, as well as the temperature and loading rate dependencies of the asphalt mixtures. Triaxial compression, triaxial extension, and axial creep tests at three temperatures 28°C, 40°C and 60°C were performed to calibrate the material properties. And they proposed an algorithm to compare the numerical analysis obtained from the model and experimental results. It is reported a reasonable agreement was observed from the back calculation and the experimental results.

Chehab and Kim (2005) reported a viscoelastic-plastic continuum damage (VEPCD) model, which is developed and validated under the auspices of the National Cooperative Highway Research Program 9-19 project, entitled “Advanced Mixture Characterization for Superpave Support and Performance Models Management” (*47*). The VEPCD model was

able to characterize the viscoelastic and viscoplastic responses of asphalt concrete in addition to micro-cracking. They validated the model under thermal loading conditions that are distinctively different from the mechanical loading conditions used in model development and calibration. Measured responses and fracture parameters from thermal strain restrained specimen tensile strength tests were conducted to compare with those predicted using the VEPCD model, the viscoelastic continuum damage model, and the linear viscoelastic model. It is reported that the ability of the VEPCD model to accurately characterize the tensile behavior of asphalt concrete under thermally induced loading was confirmed.

Numerical Methods

Sepehr et al. (1994) conducted a finite element analysis of a pavement structure with the asphalt layer represented by an idealized microstructure (*48*). Air voids were simulated by imposing small stiffness values to some of the elements. This analysis revealed significant information about the influence of the micro-structural properties on the macroscopic behavior of the pavement. It was observed that increasing the air voids from 1% to 5% resulted in 1.2% increase in pavement surface deflection. It was also shown that reducing the asphalt binder stiffness from 1000MPa to 250MPa resulted in 2.25% increase in the deflection. The influence of aggregate shape on pavement behavior was also investigated and 2% decrease in surface deflection was reported when sphere shaped aggregates were replaced by aggregates of sharp edges.

Bahia et al. (1999) conducted finite element analyses using an idealized internal structure of asphalt mixture, whereby aggregates were represented by circular objects (*49*).

Binder and aggregate elements were considered linear elastic materials. The objective of this analysis was to evaluate the deformation and strain distribution in asphalt mixes and its relation to the nonlinear mix behavior. It was observed that when applying 1% strain, the binder shear strain could be as high as 46%. Therefore, they suggested that within an actual mixture, a wider range of film thickness would exist and a wider range of strain magnitude could be realized within the binder domain.

Abbas et al. (2004) incorporated a nonlinear viscoelastic material model in a FEM to analyze the asphalt concrete microstructure (*50*). The viscoelastic behavior of the asphalt mastic was defined using a mechanistic model, which was numerically solved using a convolution integral approach. To account for the asphalt binder non-linearity, the mechanical parameters were updated during the analysis according to the strain level within each element. The analysis was also used to analytically study some of the discrepancies observed between laboratory measurements of the asphalt mixture E* and G*.

Saadeh et al. (2003) extended the comparison between E* and G* to include both experimental and numerical measurements (*51*). They studied the main factors causing discrepancies between the axial and shear tests, which include the type of loading (stress versus strain-controlled), direction and reversal of principal stresses, and stress and strain distribution within the specimen. Using finite element simulations of these tests, they reported a Poisson's ratio between 1.0 and 1.5, depending on the test frequency, which is relatively smaller than that obtained experimentally. Therefore, they concluded that the FEM only captures the effect of the stress and strain distribution and does not capture the effect of the rest of these factors. It should be noted that the finite element analyses they considered

included linear viscoelastic mastics and elastic aggregates.

Rothenburg et al. (1992) presented a micromechanical model of asphalt mixture based on discrete element techniques, whereby aggregates were modeled as polygons and the inter-particle forces were described using a mechanistic viscoelastic model (*52*). The objective of this work was to relate the asphalt mixture internal structure to its deformation characteristics. Particles were considered as plane elements that interact by means of contact forces. Simulation of angular aggregate particles with an arbitrary gradation was described by a particle generation algorithm. It was found that the complex performance of the granular matrix is the main reason for the nonlinear trends in mechanical response of asphalt mixture, and to a large degree its susceptibility to rutting in field situations. Simulations indicated that mix strength increased with the increase in the fraction of contacts and that at least 30% of contacts should be bound to get nonzero strength. At least 20% of the contacts must be nonzero friction to develop shear resistance.

Chang and Meegoda (1997) used the DEM to describe different types of aggregate-aggregate and asphalt-aggregate contacts (*53*). They utilized mechanistic models to simulate the viscoelastic behavior of asphalt binder. They incorporated the Mohr-Coulomb failure criterion to account for the sliding of asphalt-coated particles due to rotation. Both macroscopic and microscopic behaviors were monitored during simulation. It was reported that the stress-strain behavior was properly captured even in the post-peak region.

Buttlar and You (2001) used DEM to simulate the behavior of asphalt mixture in the indirect tension test (IDT) (*54*). They described the internal structure using clusters of circular particles. A linear contact model along with a bonding and sliding capabilities was used to

define the particles' interaction. Their observations pointed out the significant contribution of aggregate interaction in accurately simulating the stiffness of asphalt mixtures, and hence, suggested the need for utilizing realistic aggregate shapes in microstructure models.

Given the proper mechanical contact model, the numerical simulation could avoid huge amount of sample preparation work in the lab.

Build a Digital Model by Using DEM

Several methodologies were used to represent particle geometry and the mechanical interaction between particles. For example, particle geometry has been represented using image based models (*54, 55*), and elastic, visco-elastic and cohesive models have been used to represent mechanical behaviors. How the user-defined contact model especially simple visco-elastic model represented particular materials and contact properties in PFC3d were introduced in following sections.

User Defined Contact Model in PFC3d

FIGURE 4.1 plots the flowchart of DEM simulation using User-defined contact model (UDM) in PFC3d (*56*). The input is done via the PFC interface, but the UDM dictates the behavior of all interactions within specific models. The UDM calculates the fore-displacement law each timestep. During each timestep relative motion of particles and contact forces are extracted from different models and applied in these models to dictate the force-displacement behavior between two particles in contact (*57*).

The constitutive model used in PFC3d comprises three parts:

- a contact model;

- a bond model;
- a friction slip model.

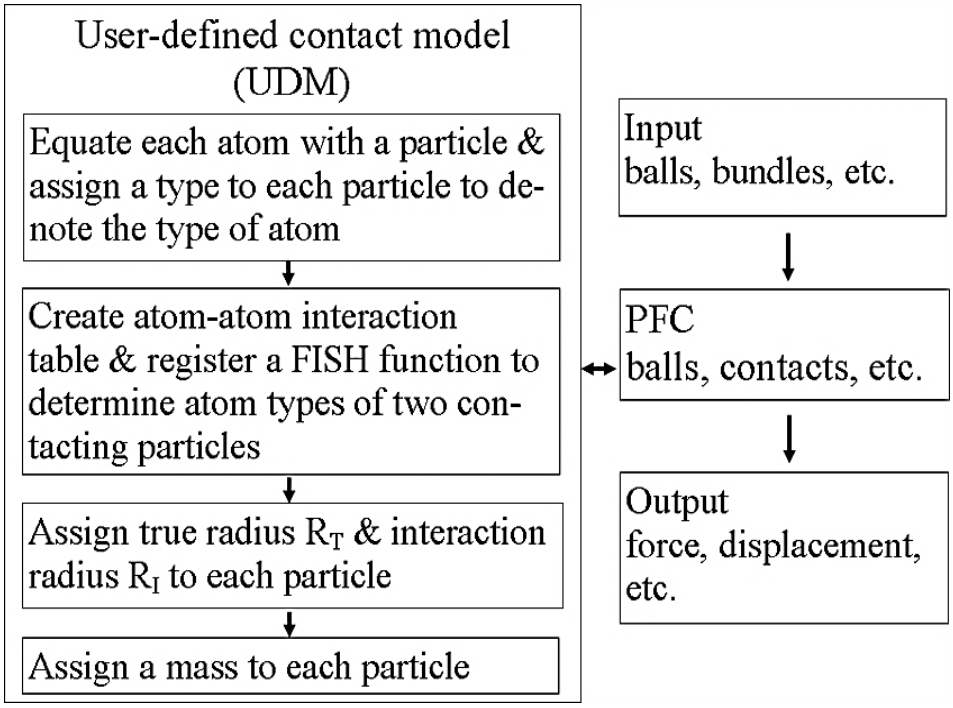

FIGURE 4.1 Flowchart of a PFC3D Program Code Using UDM (*56*)

The contact model is described in terms of a normal secant contact stiffness K_n and a shear tangent contact stiffness K_s between the two contacting entities either wall-particle or particle-particle. Note that the in-plane and out-of-plane shear parameters are assumed to be the same. PFC3d allows particles to be bonded together at contacts. If the value of the tensile normal contact force equals or exceeds the normal contact bond strength, the bond breaks, and both the normal and shear contact forces are set to zero. If the value of the shear contact force equals or exceeds the shear contact bond strength, the bond breaks and the slip model are activated. Parameters which were defined in PFC3d are the normal and shear contact stiffness K_n, K_s, the normal and shear bond strengths Pb_n, Pb_s and the coefficient of friction

between contacting particles.

Discrete element modeling was used to simulate compressive tests of asphalt mixtures with different film thicknesses. FIGURE 4.2 shows a model representing an asphalt mixture includes two aggregates and asphalt binder. Each aggregate is covered by thousands small particles which represent asphalt binder around aggregates. Between the two aggregates, several layers made of even smaller blue balls represent film. Each layer of film in the model contains 60*60=3600 particles with size:

- radius of Big aggregate = 500μm;
- radius of yellow balls = 15~30μm;
- radius of blue balls in film layers = 5μm.

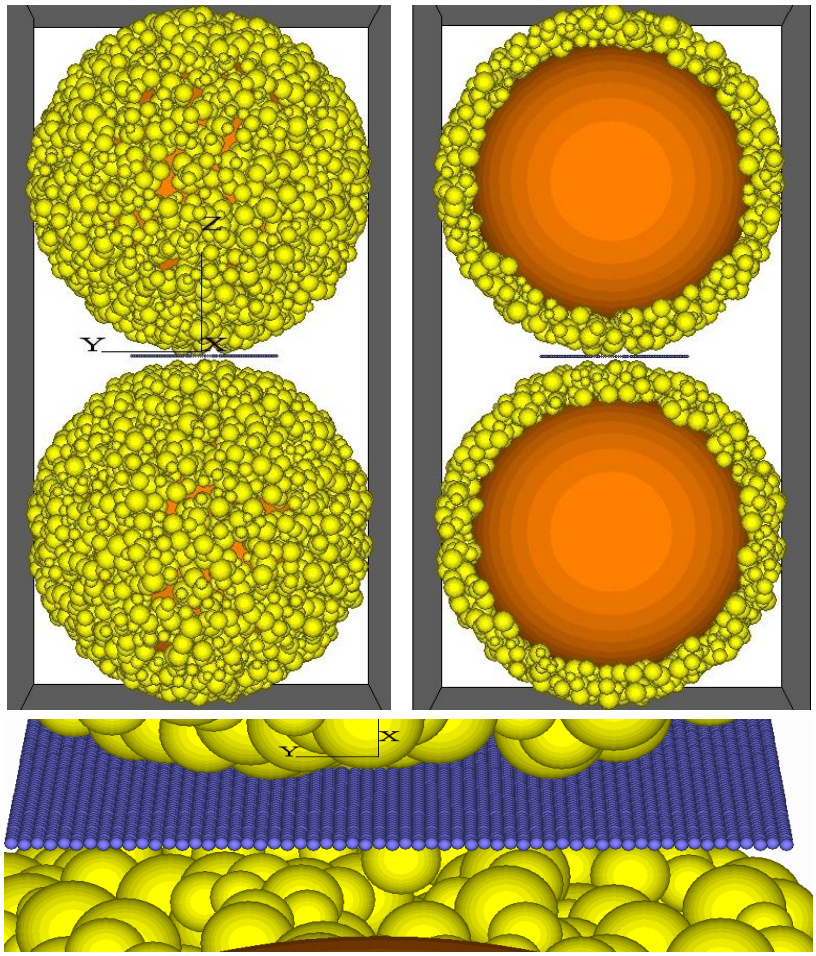

FIGURE 4.2 Asphalt Mixture Includes Two Aggregates and Asphalt Binder.

Simple Viscoelastic Model

Asphalt mixture was modeled in PFC3d. Material properties were specified by applying corresponding values of relative parameters. Such as normal stiffness, shear stiffness, friction ratio, etc. Parallel bonds were built between adjacent particles. Cracking within the structure was modeled by allowing bonds breakage. Elastic contact properties were used to investigate the effect of random variations in internal sample geometry. A simple viscoelastic model was used to introduce time dependent shear and normal contact stiffness and an elastic contact was assumed for normal contact.

Consider a simple viscoelastic model in which the shear behavior consists of a spring in series with a dashpot (*58*). The total shear velocity, $\dot{u}_s$, can be decomposed into elastic and viscous parts: Viscoelastic properties had been applied to film clump.

$$\dot{u}_s = \dot{u}_s{}^e + \dot{u}_s{}^v \tag{18}$$

For the two-dimensional case, the shear velocities and forces can be taken as scalars. Taking $F_s°$ and F_s' as the shear forces before and after one time step, respectively, we can express the components of shear velocity as

$$\dot{u}_s{}^e = -\frac{F_s' - F_s°}{k_s \Delta t} \tag{19}$$

and

$$\dot{u}_s{}^v = -\frac{F_s' + F_s°}{2\eta} \tag{20}$$

where k_s is the shear stiffness and η is the viscosity. Substituting these expressions into Equation (18) and rearranging:

$$F_s' = \frac{\mathrm{F}_s{}^{\circ}\left(\frac{1}{k_s} - \frac{\Delta t}{2\eta}\right) - \dot{u}_s \Delta t}{\frac{1}{k_s} + \frac{\Delta t}{2\eta}} \tag{21}$$

For the three-dimensional case, the shear force and relative shear velocity are both vectors, and the constitutive equation becomes

$$F_i^{s\prime} = \frac{F_i^{s^{\circ}}\left(\frac{1}{k_s} - \frac{\Delta t}{2\eta}\right) - \dot{u}_i^s \Delta t}{\frac{1}{k_s} + \frac{\Delta t}{2\eta}} \tag{22}$$

Equation (22) is encoded into a contact model accessed with the "model viscous" command. The required properties are as follows. Parameters of the contact model used in simulations are summarized in TABLE 4.1.

- *vis* k_n: viscoelastic normal stiffness
- *vis* k_s: viscoelastic shear stiffness
- *vis viscosity*: shear viscosity

TABLE 4.1 Properties Applied in Simulations

Properties for parallel bonds:	**Properties for viscoelastic contact model:**
Normal stiffness = $30*10^{15}$ Nm^{-3}; Shear stiffness = $30*10^{15}$ Nm^{-3};	Viscoelastic normal stiffness = $0.36*10^6$ N/m
Normal strength = 190 MP; Shear strength = 190MP;	Viscoelastic shear stiffness = $0.12*10^6$ N/m
Radius multiplier = real parallel bond radius/radius = $30*10^{-9}$	Shear viscosity = $0.414*10^6$ N/m

Experiment

The Skyscan 1174 cabinet X-ray tomography system was used in the experiment to verify the normal compliance model introduced before. The Skyscan 1174 system, shown in FIGURE 4.3, is a compact, cost efficient micro X-ray scanner for nondestructive

three-dimensional microscopy. It's supplied with software for system control, X-ray radiography, three-dimension (3D)-reconstruction, two-dimensional (2D) /3D image analysis and 3D realistic visualization. The SkyScan-1174 scanner supports variable magnification (6 to 30mm field of view), adjustable source energy (20 to 50KV) and flexible image format. The material testing stage of Skyscan system, shown in FIGURE 4.4, can perform compression, tension and torsion test. The loading-displacement or the stress-strain curve can be saved as an image or text file. The testing sample can be held under specific loading for scanning. The testing stage applies displacement to the top and bottom of the sample in equal amount but in opposite directions. This keeps the central part of the sample relatively static for scanning purpose.

FIGURE 4.3 Skyscan 1174 System.

FIGURE 4.4 Testing Stage of the Microscopy System (*59*)**.**

Samples were tested under uniaxial compression loads applied on top and bottom stage. With the help of X-ray scanner, the parameters needed in the compliance model were measured by the tools provided by the software. The testing stage is displacement controlled. The displacement speed was chosen according to the allowable range of the testing device, and was set at 17.5μm/s. The resistant force was monitored and recorded during the loading. When the force reaches the maximum allowable value of the testing stage, the displacement application will stop. For the sample in this study, the application of displacement was stopped when two elastic particles started to contact to each other through the asphalt layer. Prior to each test, the testing stage was calibrated according to the procedure recommended by the manufacturer. Force displacement data was stored as a text file for each sample. The specification of asphalt binder is PG 64-22 coming from the lab of the Virginia Tech Transportation Institute and the temperature at which the experiments are conducted is around 25-27C^{o} given by thermometer. The specifics of the experiment are listed in the

TABLE 4.2.

Ten compression tests are performed on samples that include two aggregates and asphalt binder by using X-ray CT. The samples are made with two sphere aggregates and PG 64-22 binder (see FIGURE 4.5). Material of the aggregates is crystal (see FIGURE 4.6). Shown in TABLE 4.2 are the load and other parameters of the experiment.

FIGURE 4.5 Crystal Aggregates Used in Compression Tests

FIGURE 4.6 Asphalt Mixture Sample Used in Compression Tests

FIGURE 4.7 - FIGURE 4.16 show the measurements and X-ray images of the ten samples. Their film thicknesses are summarized in TABLE 4.3. After compressive load applied, results of resistant force-deformation are shown in FIGURE 4.7 – FIGURE 4.16.

Since the samples are made manually, Sample 3 has the same film thickness with Sample 1. From TABLE 4.3, peak resistant force of Sample 1 and Sample 3 are almost the same, so the results are reasonable.

A relationship between film thickness and resistant force is plotted in FIGURE 4.17. Based on current results, when compressive load keeps constant and all asphalt mixtures move same displacement, the one with thinnest asphalt film had highest axial stress and resistant force. That means the mixture includes aggregates and binder will become stiffer if the film thicknesses decrease. The experimental results presents here agree well with my simulation results and theoretical analysis in my former reports.

TABLE 4.2 Experiment Specifics

Inner diameter of the chamber	10mm
Diameter of particle	12.7mm
Column diameter	9mm
Material of particle	Polyvinyl Chloride (E=2400-4100 MPa, $\upsilon = 0.41$)
Asphalt binder	PG 64-22
Test temperature	Room Temperature
Loading speed	17.5 μm/s

TABLE 4.3 Parameters and Results of Compression Test

ID	Load applied (N/step)	Speed (μm/s)	Final Deformation (μm)	Peak Resistant Force (N)	Film Thickness (μm)
1	0.22	17.5	10010.0	35.5	72
2	0.22	17.5	10010.0	37.6	36
3	0.22	17.5	10010.0	35.6	72
4	0.22	17.5	10010.0	38.8	30
5	0.22	17.5	10010.0	36.8	45
6	0.22	17.5	10010.0	41.1	21
7	0.22	17.5	10010.0	35.9	60
8	0.22	17.5	10010.0	36.4	47
9	0.22	17.5	10010.0	38.1	33
10	0.22	17.5	10010.0	35.2	90

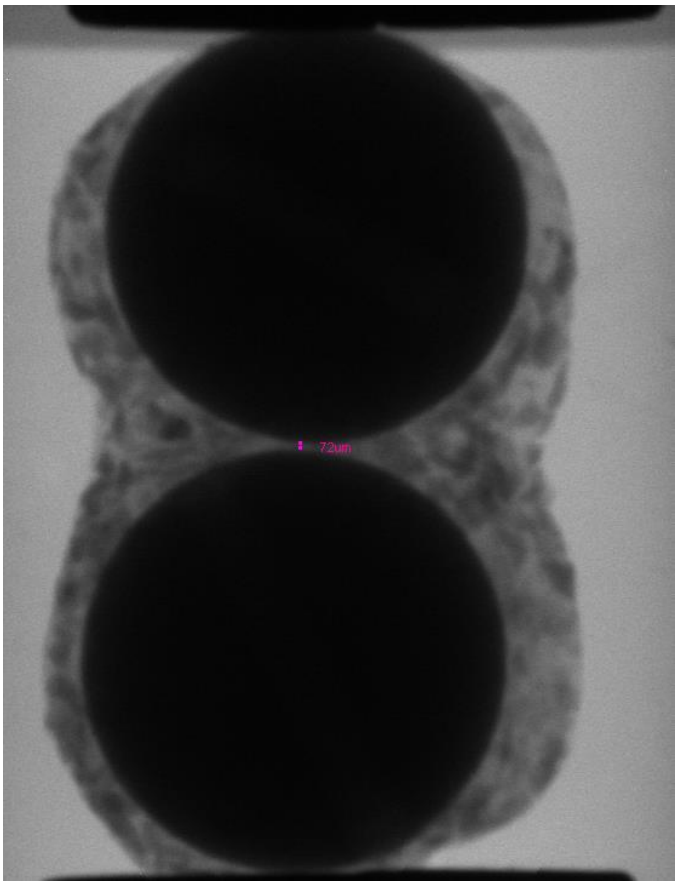

FIGURE 4.7(a) X-ray Image of Sample 1

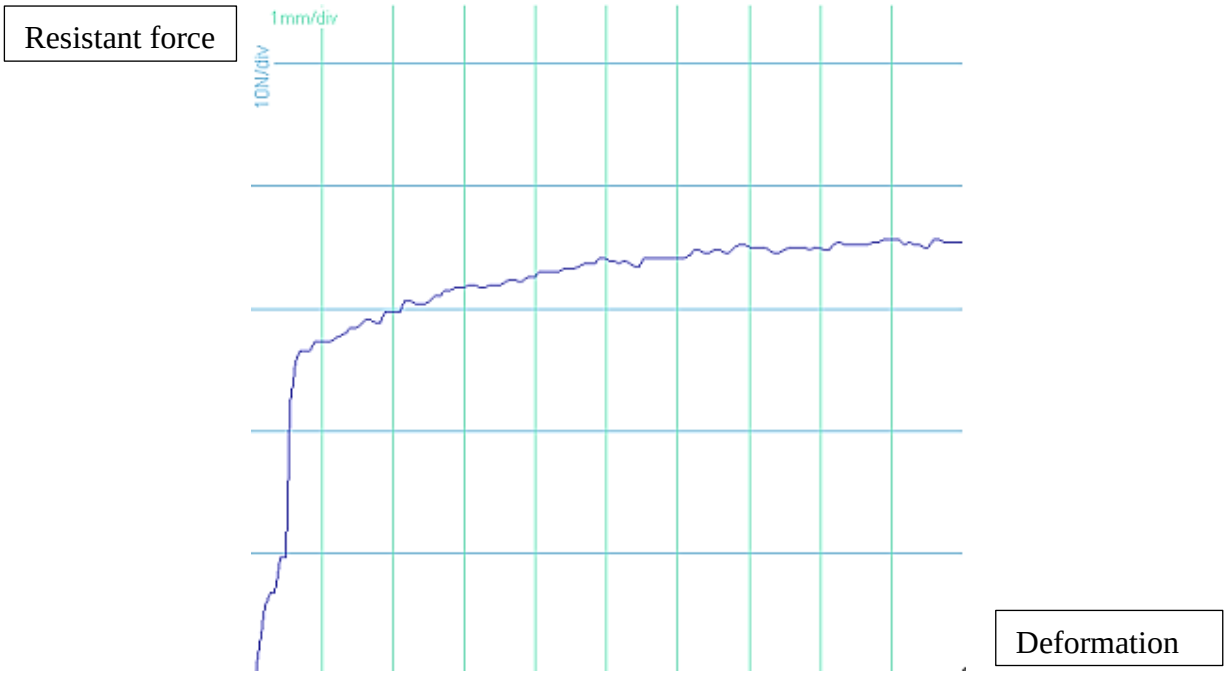

FIGURE 4.7(b) Resistant Force vs. Deformation of Sample 1

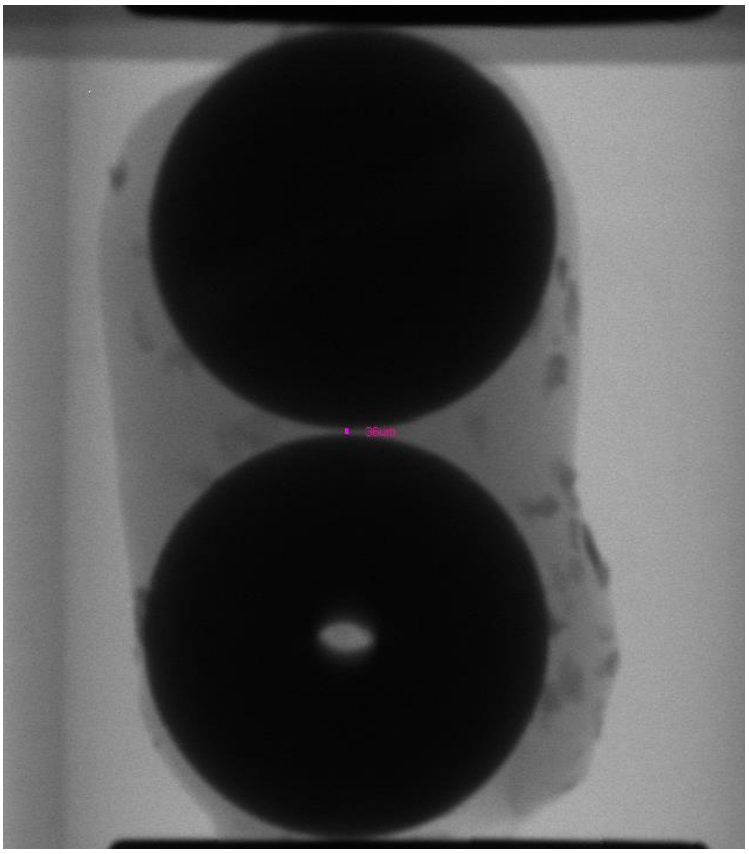

FIGURE 4.8(a) X-ray Image of Sample 2

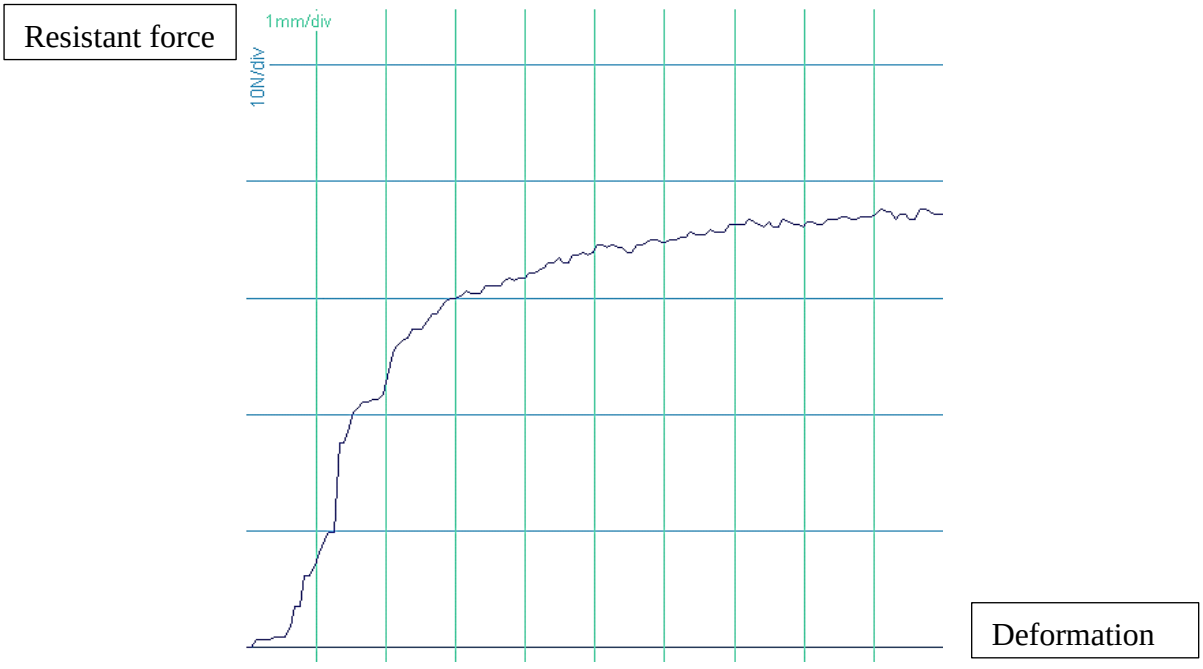

FIGURE 4.8(b) Resistant Force vs. Deformation of Sample 2

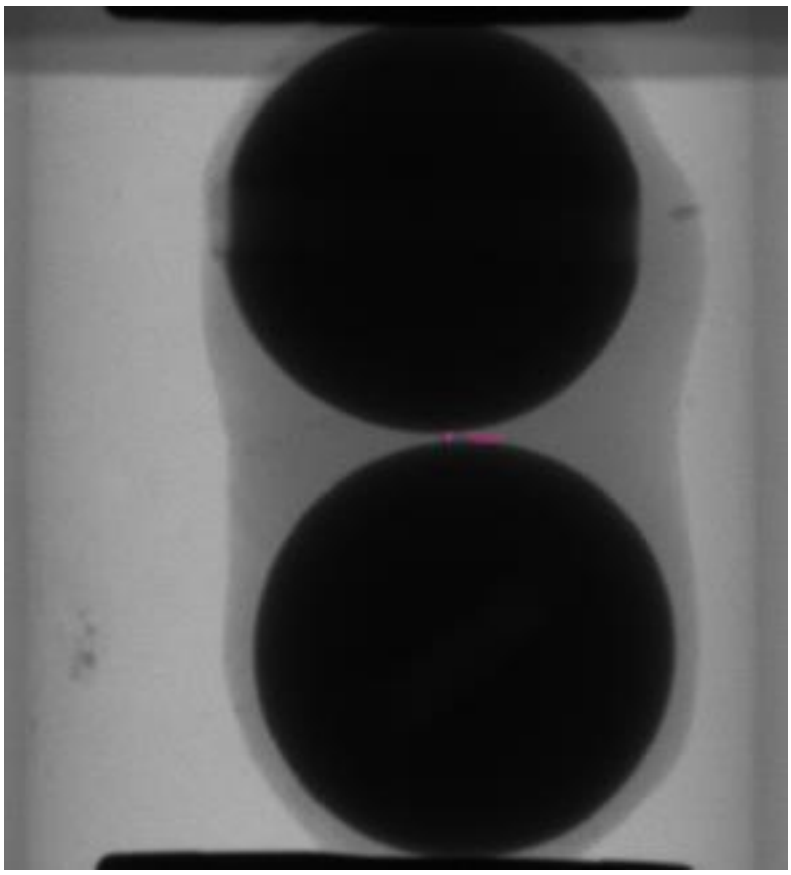

FIGURE 4.9(a) X-ray Image of Sample 3

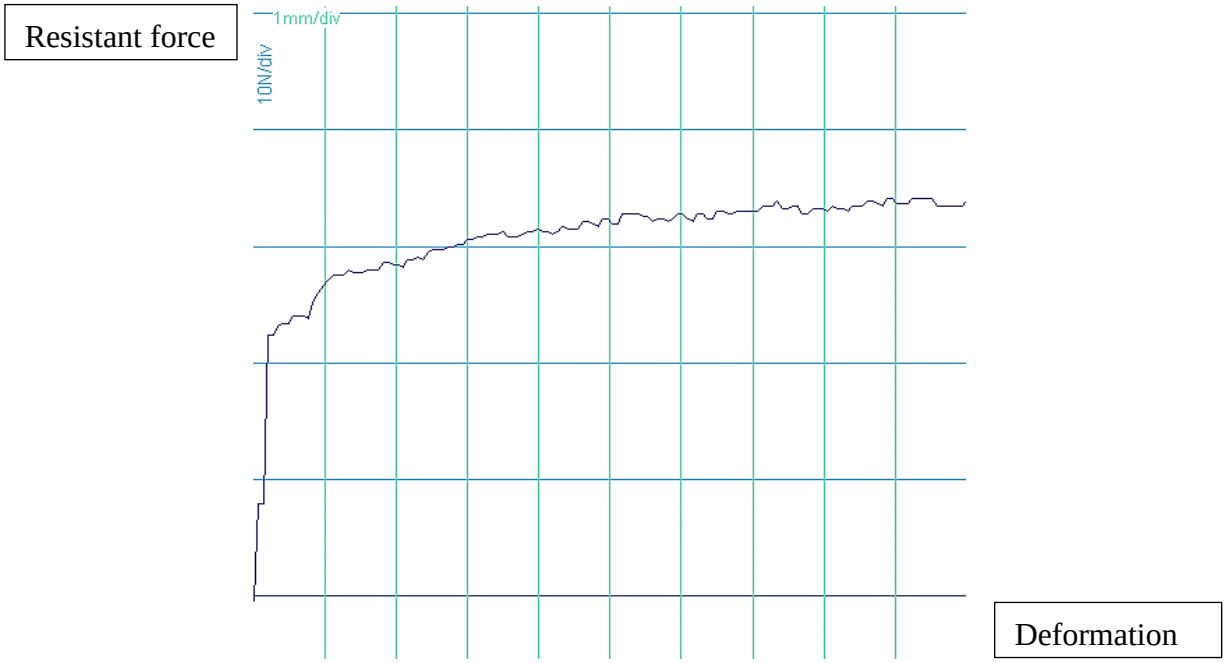

FIGURE 4.9(b) Resistant Force vs. Deformation of Sample 3

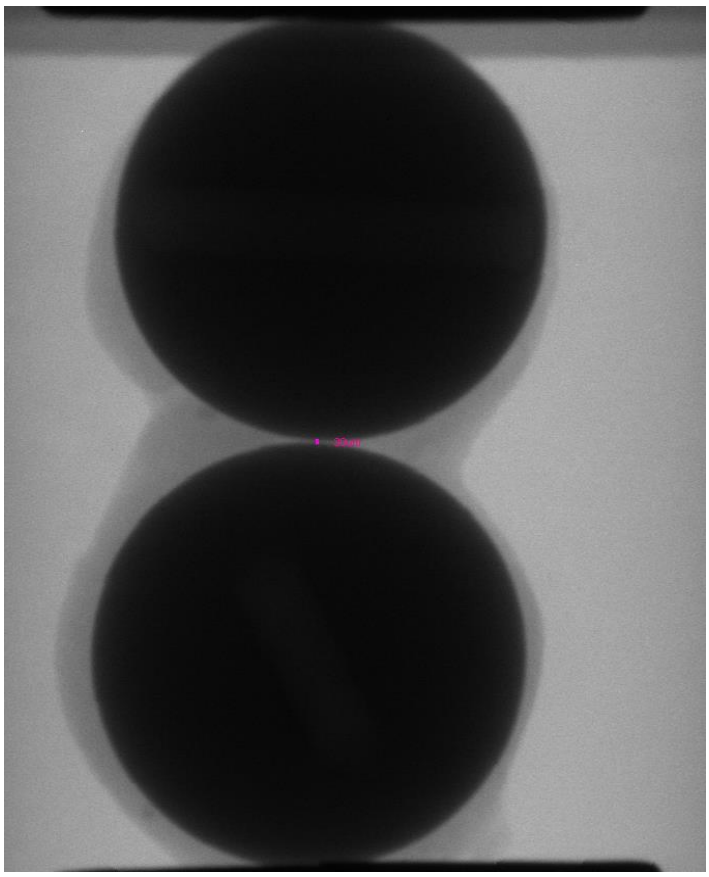

FIGURE 4.10(a) X-ray Image of Sample 4

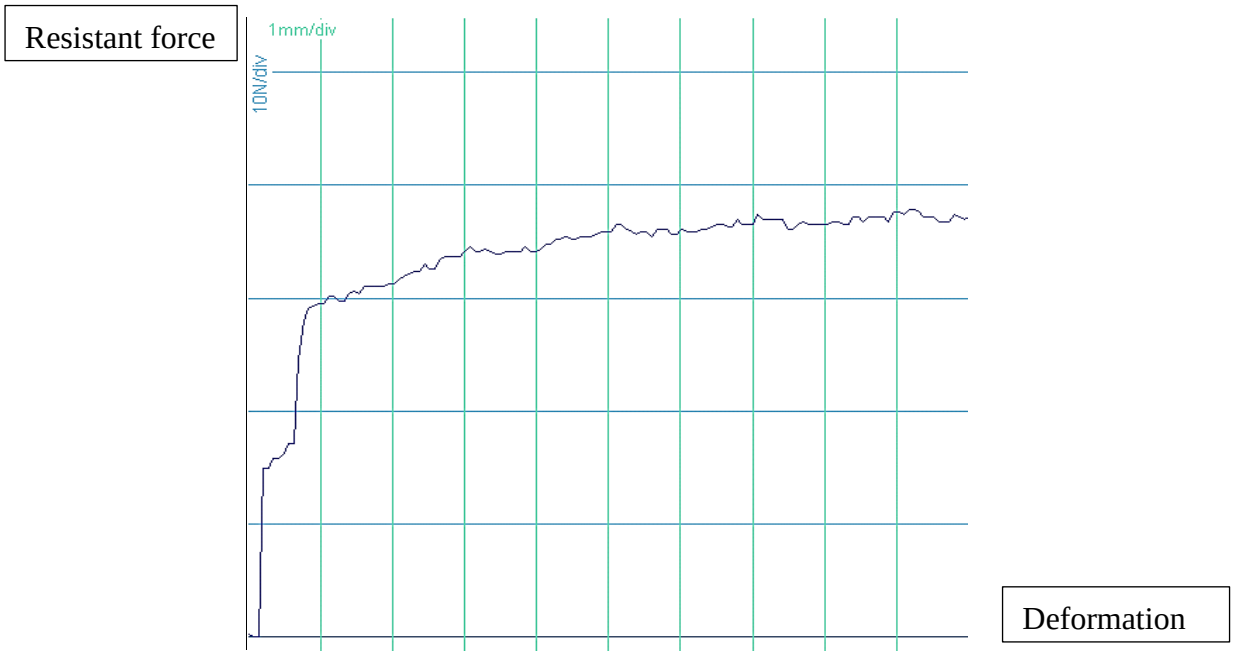

FIGURE 4.10(b) Resistant Force vs. Deformation of Sample 4

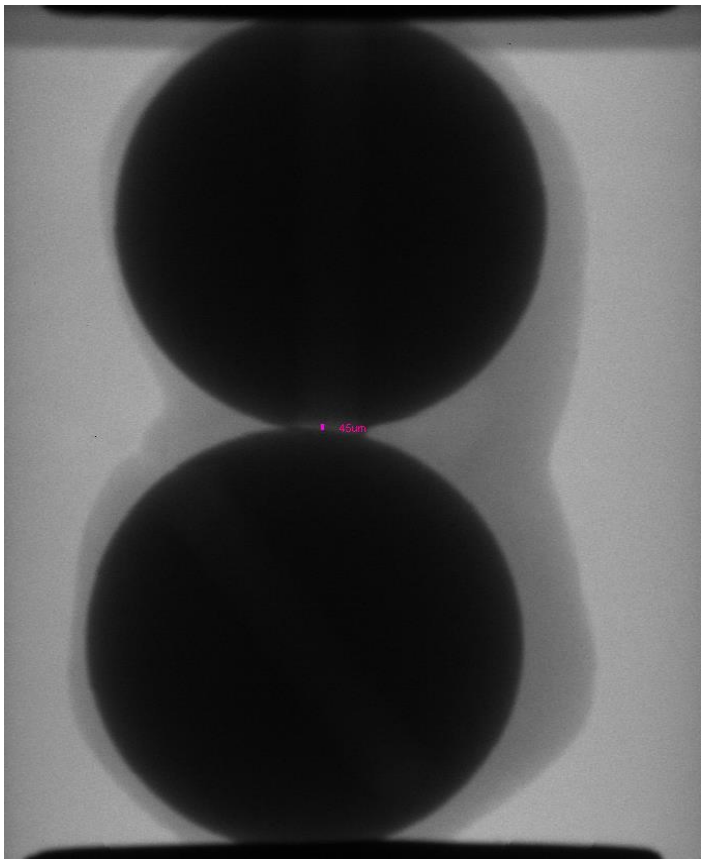

FIGURE 4.11(a) X-ray Image of Sample 5

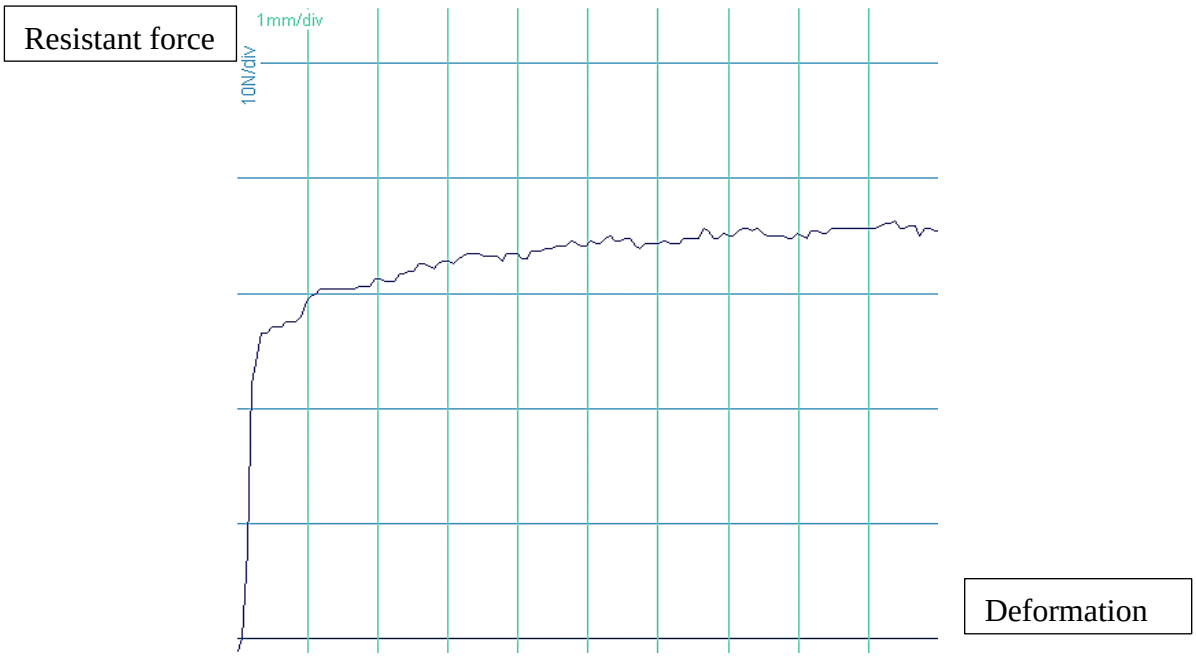

FIGURE 4.11(b) Resistant Force vs. Deformation of Sample 5

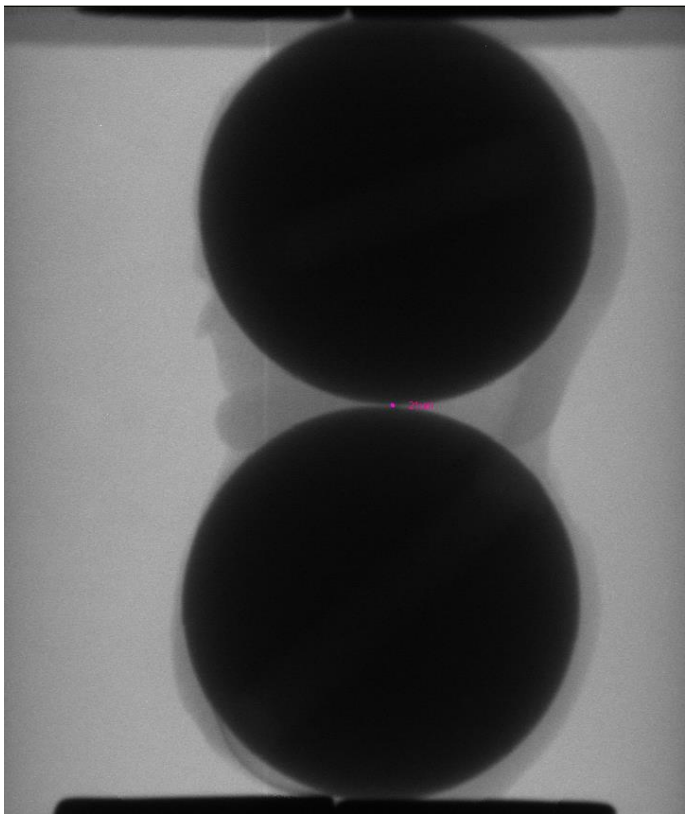

FIGURE 4.12(a) X-ray Image of Sample 6

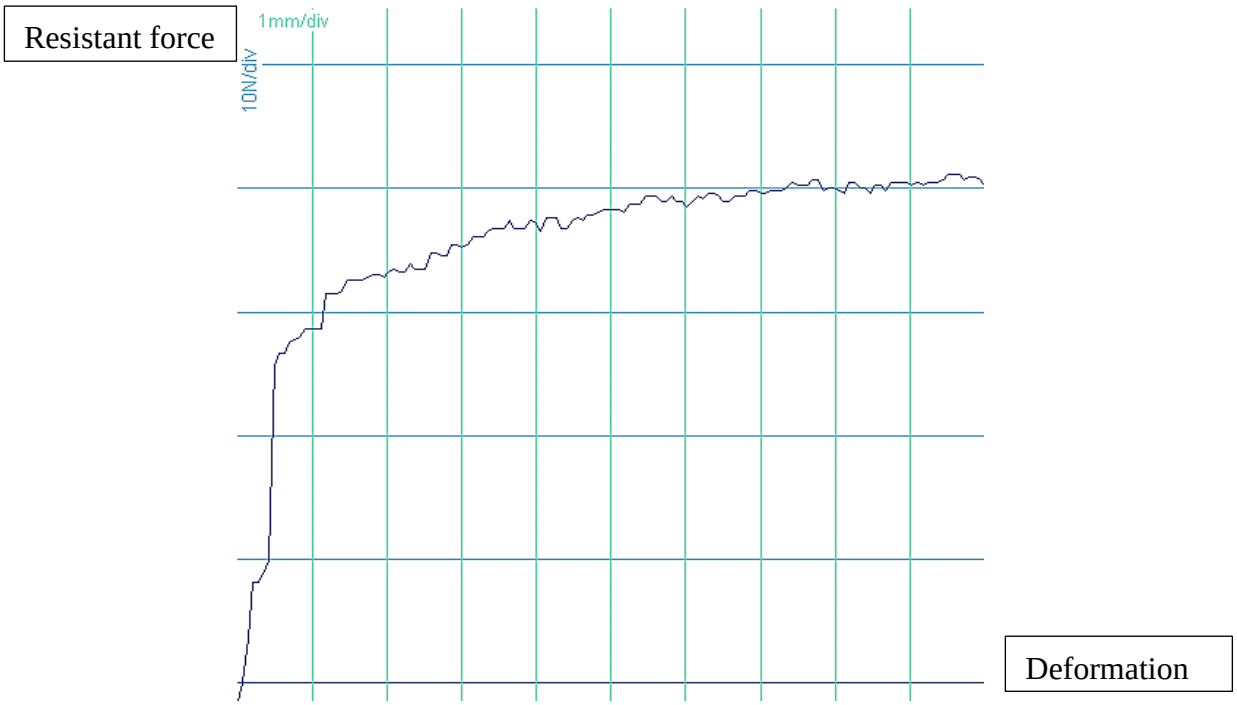

FIGURE 4.12(b) Resistant Force vs. Deformation of Sample 6

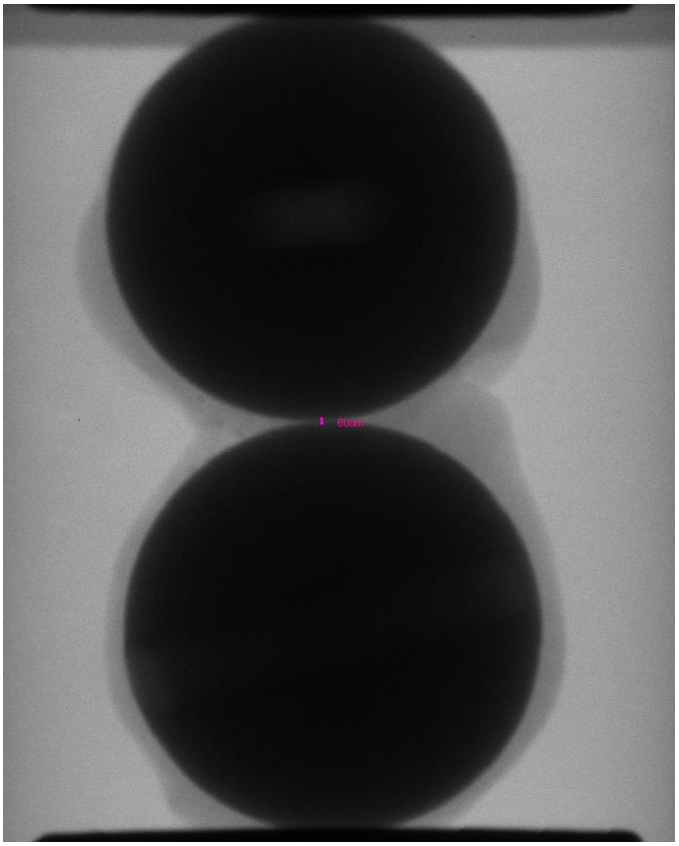

FIGURE 4.13(a) X-ray Image of Sample 7

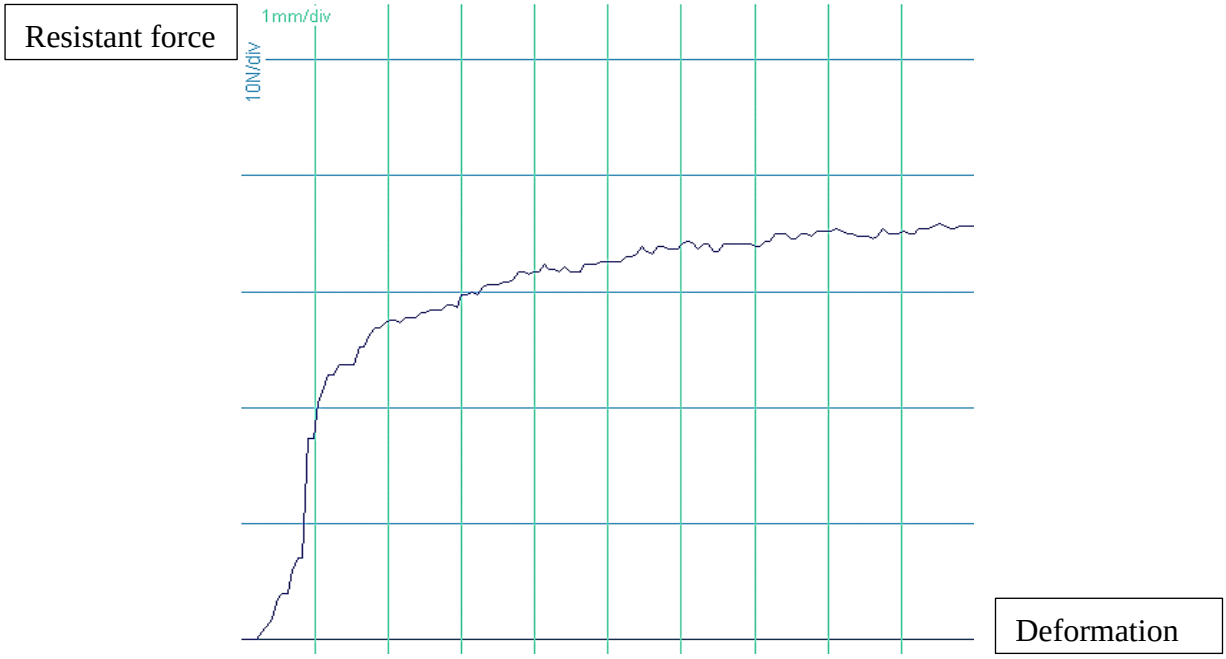

FIGURE 4.13(b) Resistant Force vs. Deformation of Sample 7

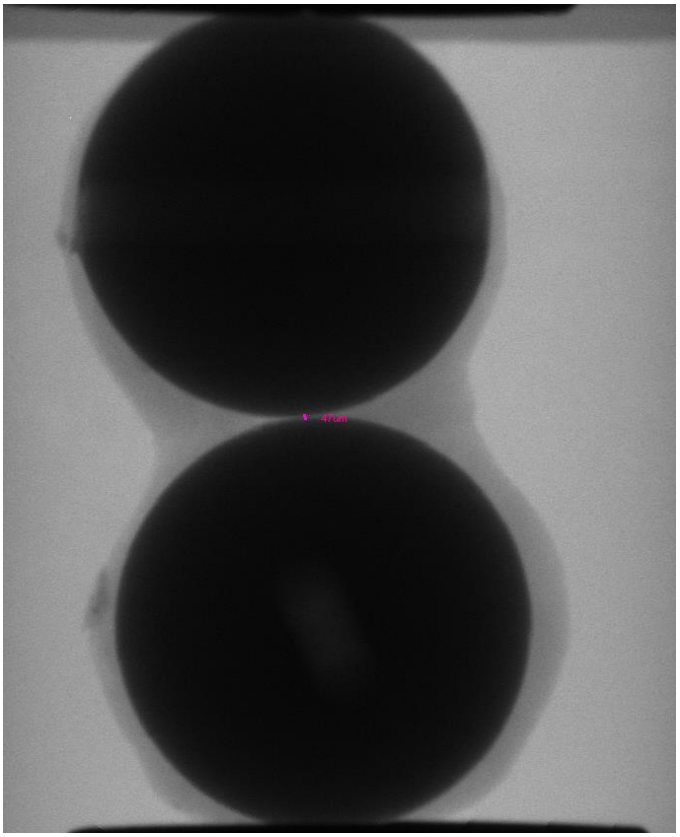

FIGURE 4.14(a) X-ray Image of Sample 8

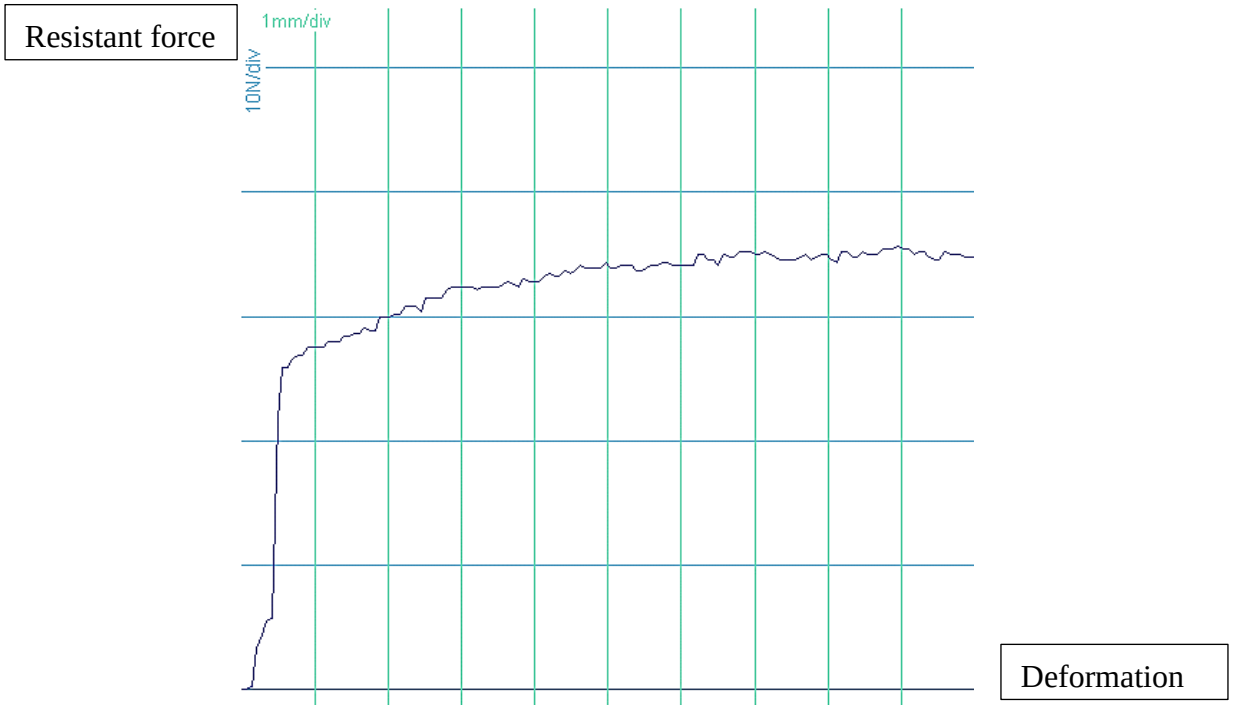

FIGURE 4.14(b) Resistant Force vs. Deformation of Sample 8

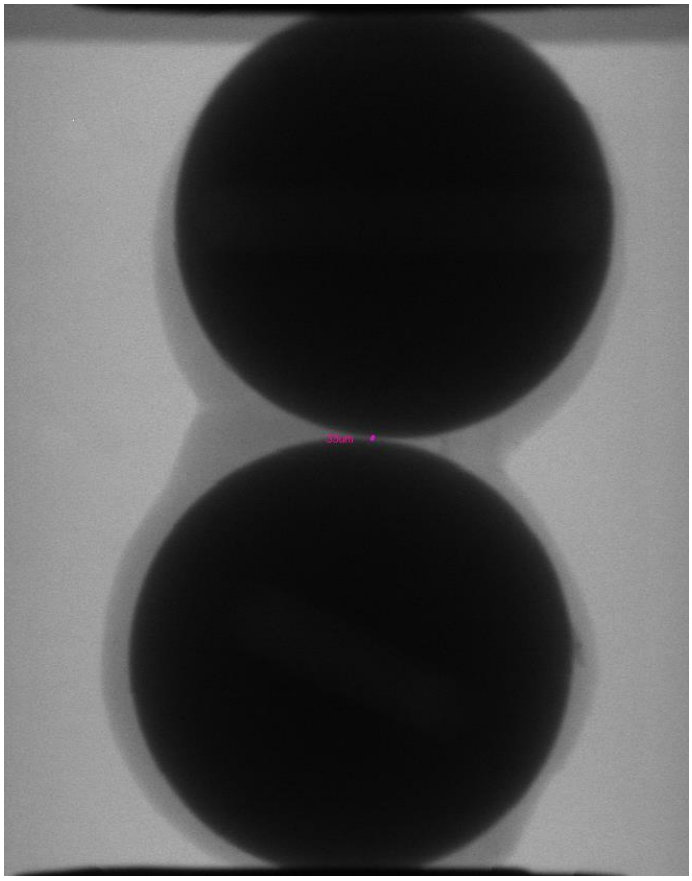

FIGURE 4.15(a) X-ray Image of Sample 9

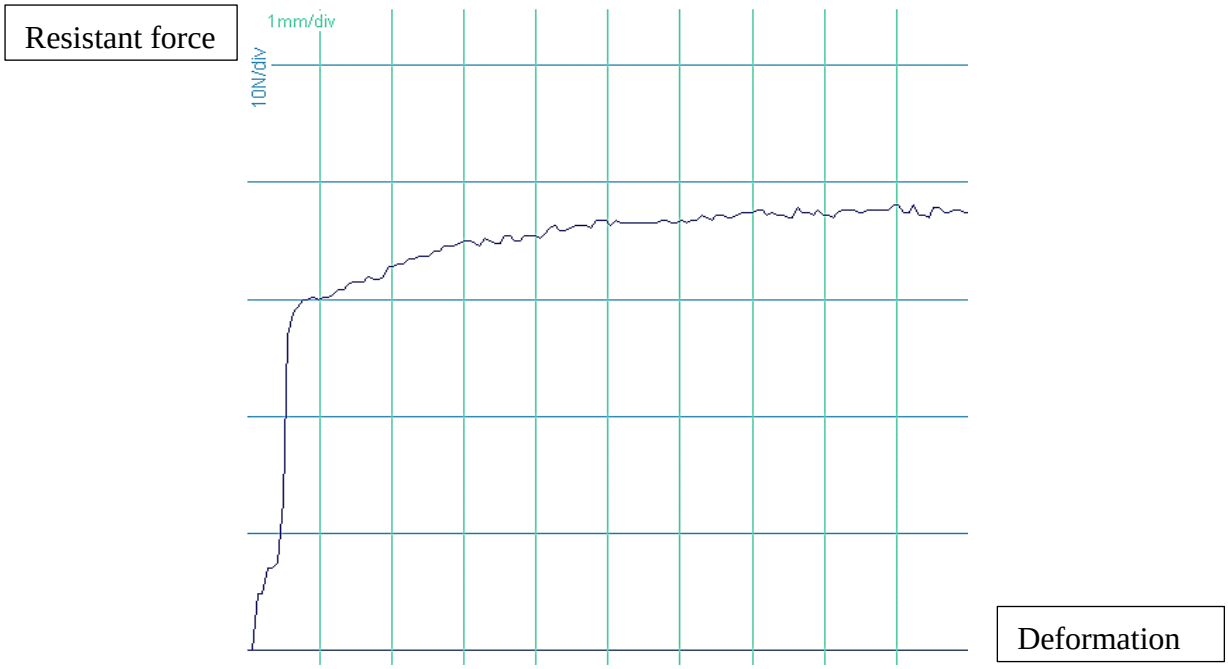

FIGURE 4.15(b) Resistant Force vs. Deformation of Sample 9

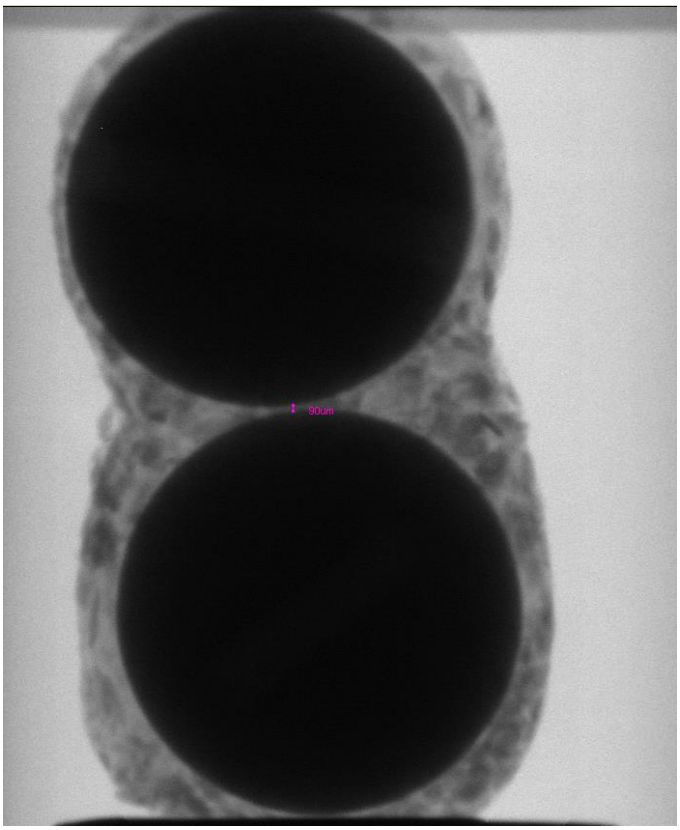

FIGURE 4.16(a) X-ray Image of Sample 10

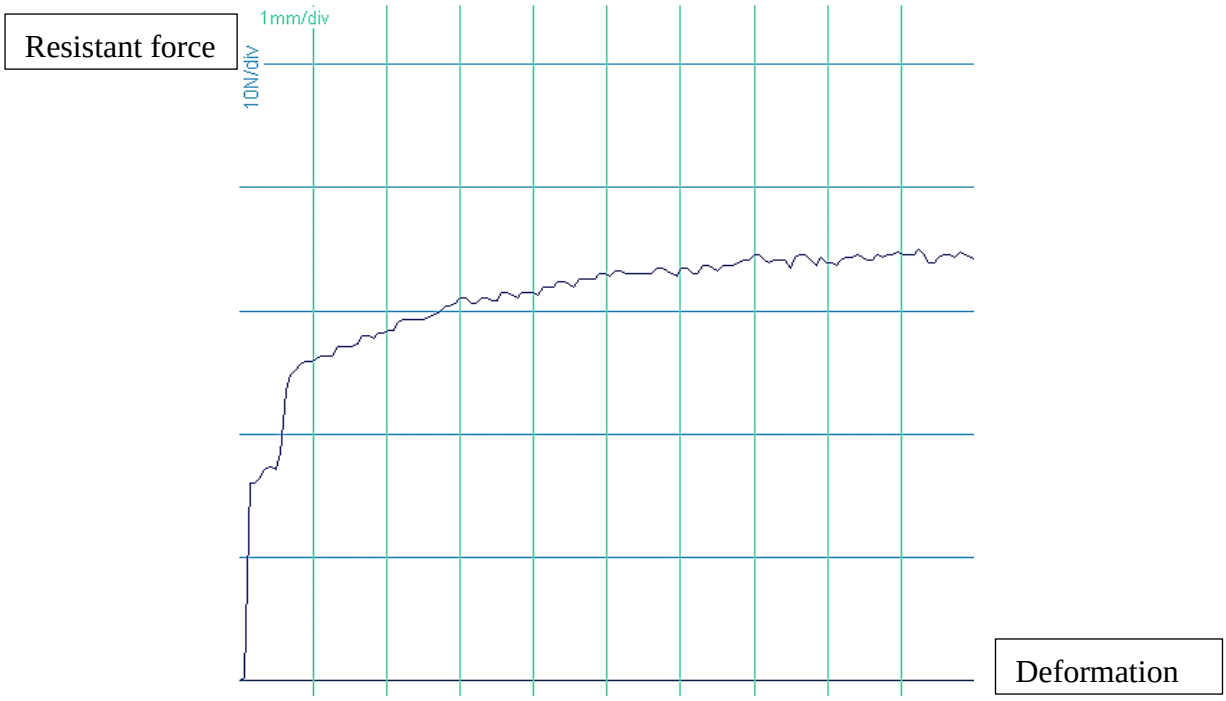

FIGURE 4.16(b) Resistant Force vs. Deformation of Sample 10

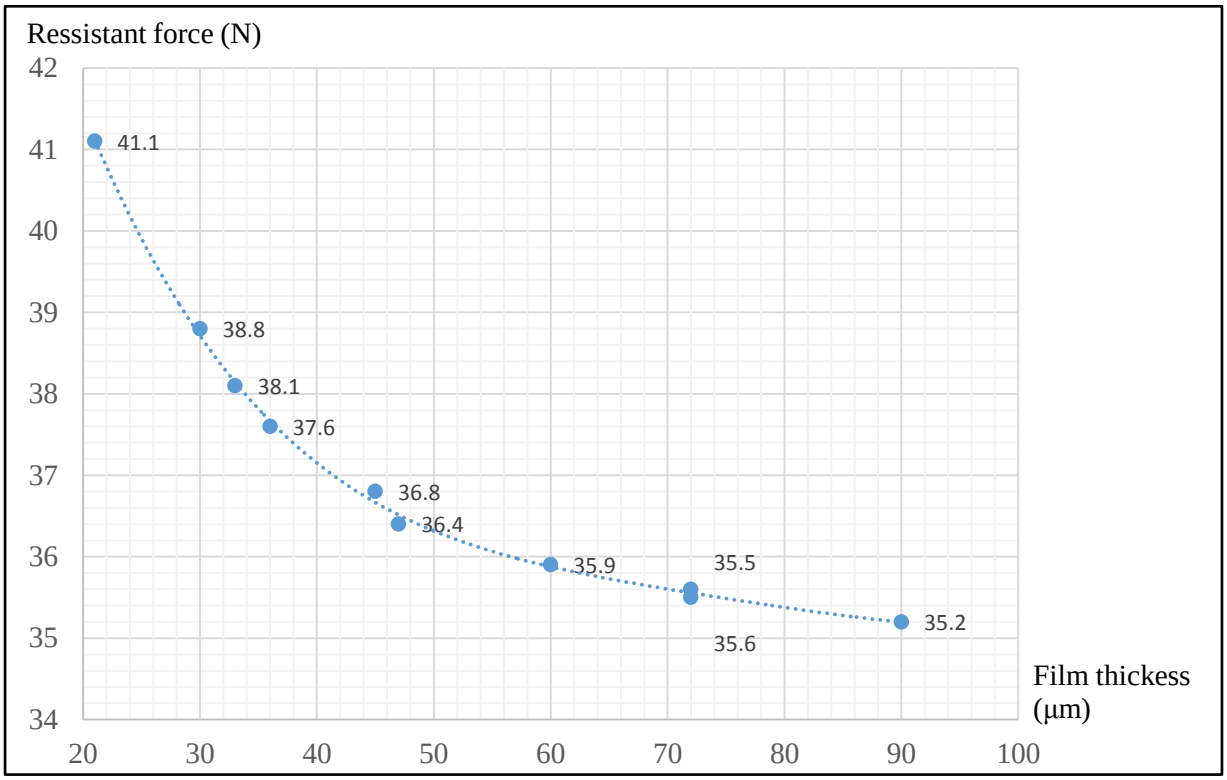

FIGURE 4.17 Relationship between Resistant Force and Film Thickness

Simulation

The model analyzes a system with two elastic particles bonded by a thin viscoelastic binder layer. Peak axial stresses are summarized in FIGURE 4.18. The only difference in comparison is film thickness. FIGURE 4.19 - FIGURE 4.23 show models simulated in PFC3d with varied thickness of 10μm to 20μm, 30μm, 40μm, 50μm, and axial stress of each case. The peak stress of asphalt mixture was found to be as a power-law function of film thickness. As Figure 8 shows, peak stress decreases with the increase of film thickness. Comparing FIGURE 4.18 with FIGURE 4.17, simulation results agree reasonably with experiment results.

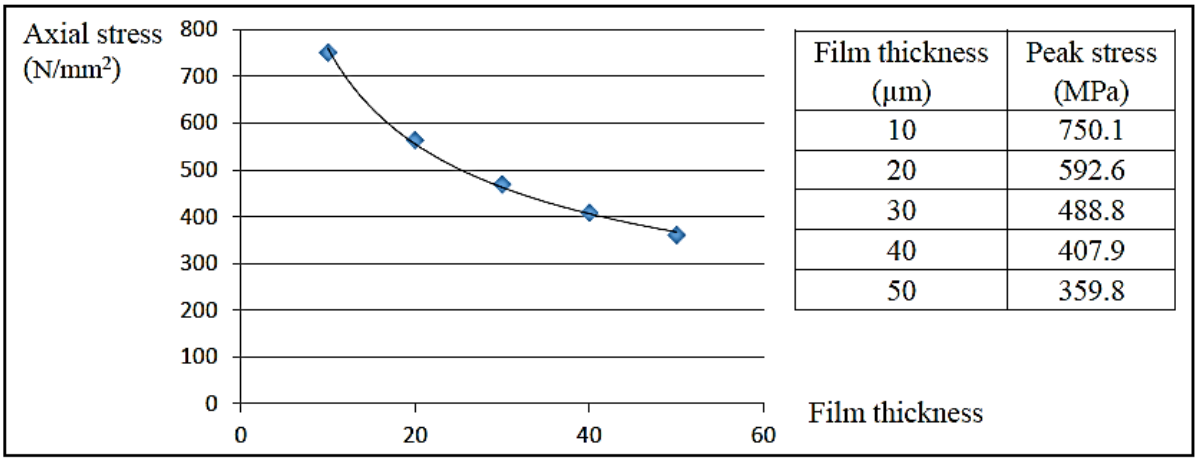

Film thickness (µm)	Peak stress (MPa)
10	750.1
20	592.6
30	488.8
40	407.9
50	359.8

FIGURE 4.18 Summary of Peak Axial Stresses

Case 1, Film Thickness = 10µm

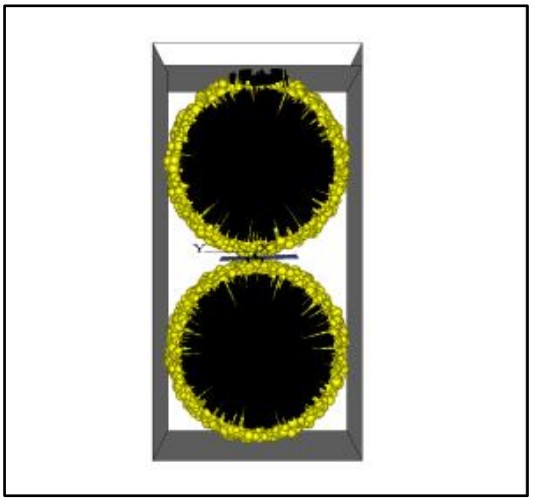

FIGURE 4.19(a) Two Aggregates and a 10µm Film Layer in Compression Test

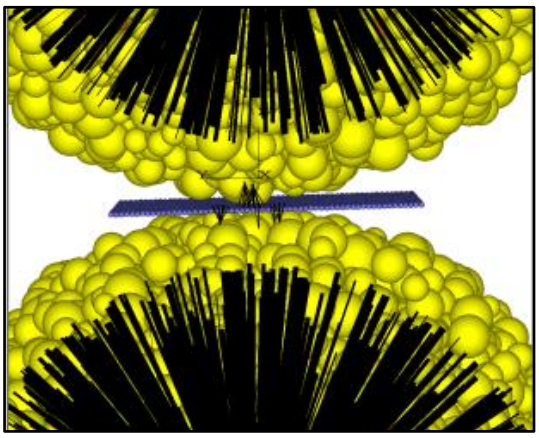

FIGURE 4.19(b) Detailed View of Film Layer, Film Thickness = 10µm

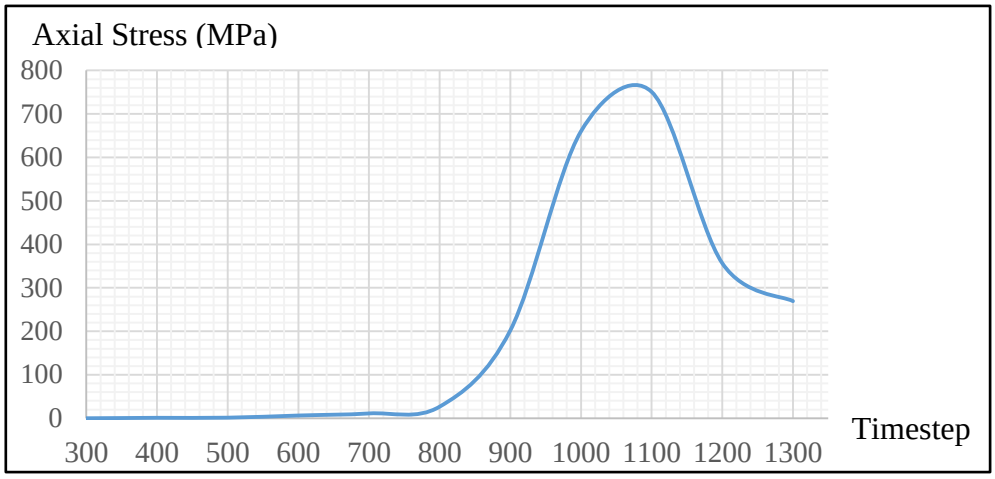

FIGURE 4.19(c) Axial Stress in Compression Test, Film Thickness = 10μm

Case 2, Film Thickness = 20μm

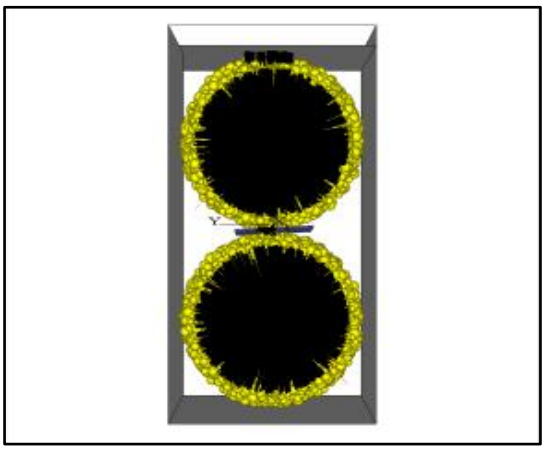

FIGURE 4.20(a) Two Aggregates and a 20μm Film Layer in Compression Test

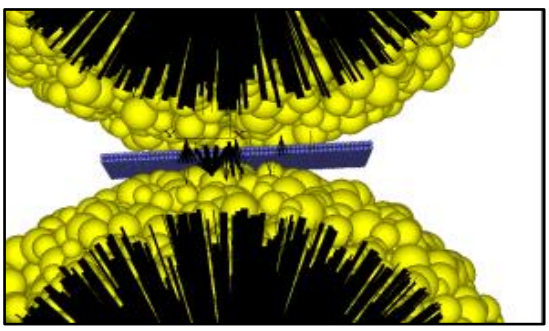

FIGURE 4.20(b) Detailed View of Film Layer, Film Thickness = 20μm

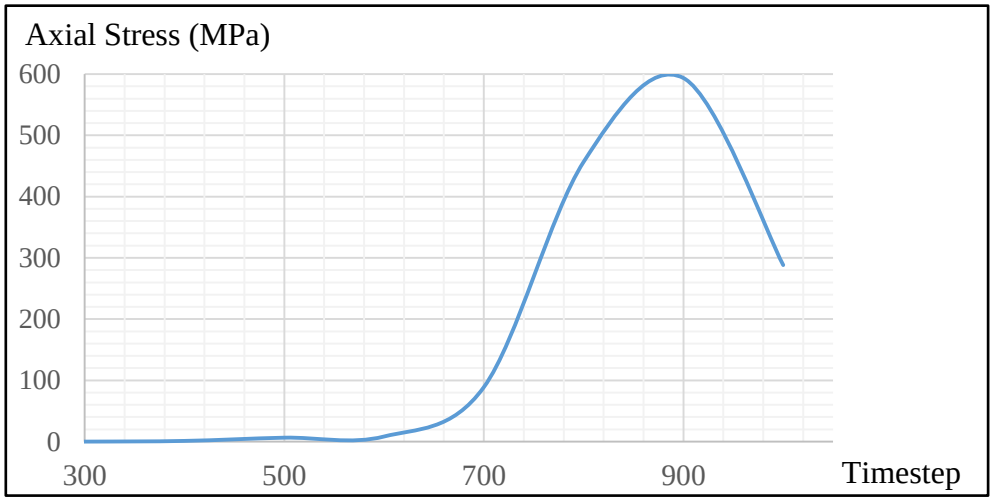

FIGURE 4.20(c) Axial Stress in Compression Test, Film Thickness = 20μm

Case 3, Film Thickness = 30μm

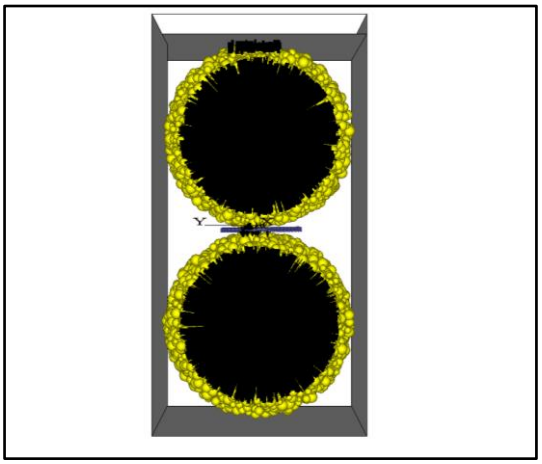

FIGURE 4.21(a) Two Aggregates and a 30μm Film Layer in Compression Test

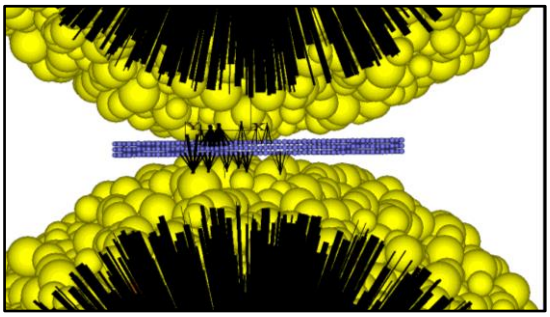

FIGURE 4.21(b) Detailed View of Film Layer, Film Thickness = 30μm

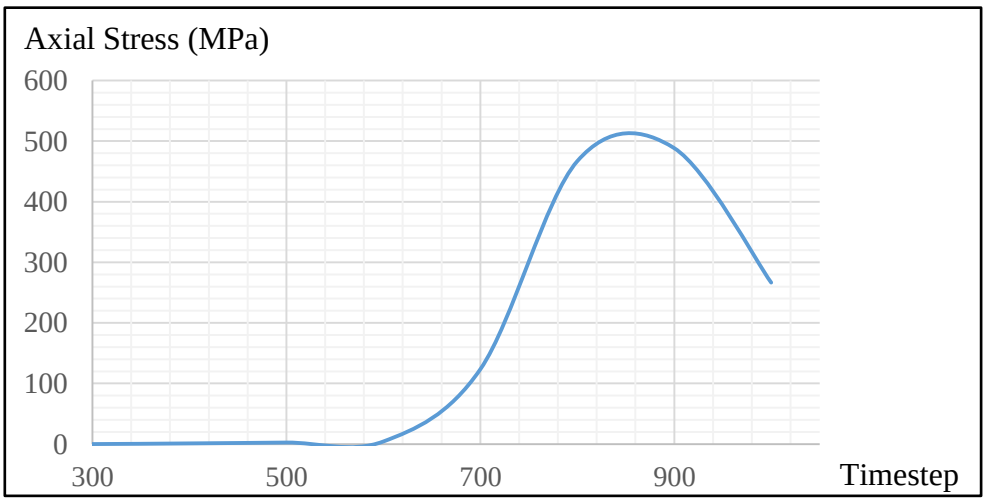

FIGURE 4.21(c) Axial Stress in Compression Test, Film Thickness = 30μm

Case 4, Film Thickness = 40μm

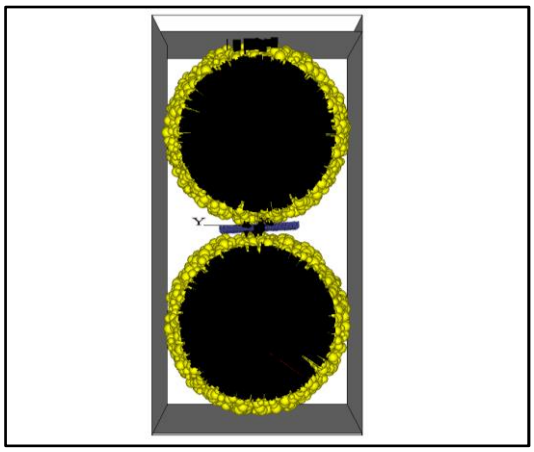

FIGURE 4.22(a) Two Aggregates and a 40μm Film Layer in Compression Test

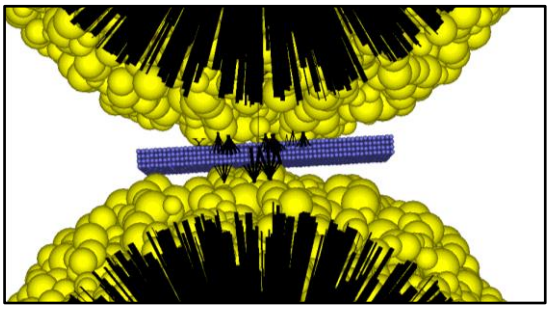

FIGURE 4.22(b) Detailed View of Film Layer, Film Thickness = 40μm

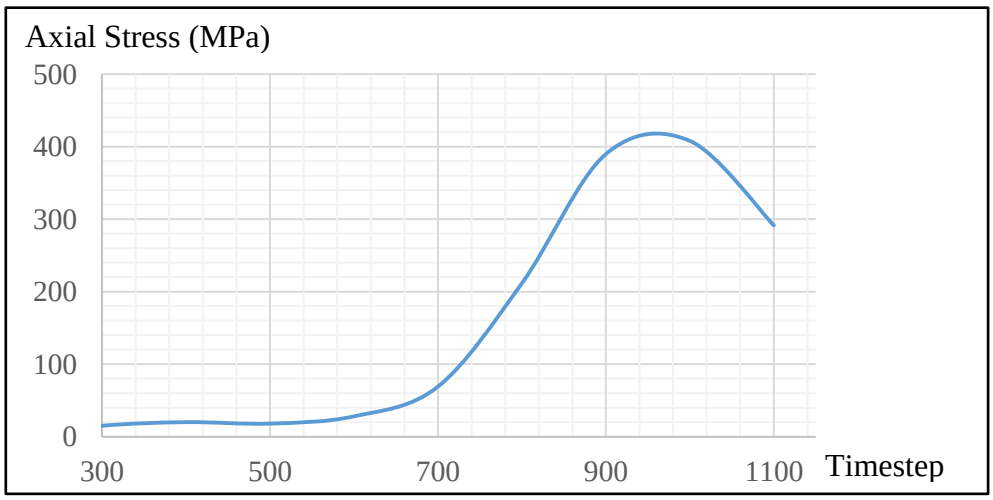

FIGURE 4.22(c) Axial Stress in Compression Test, Film Thickness = 40µm

Case 5, Film Thickness = 50µm

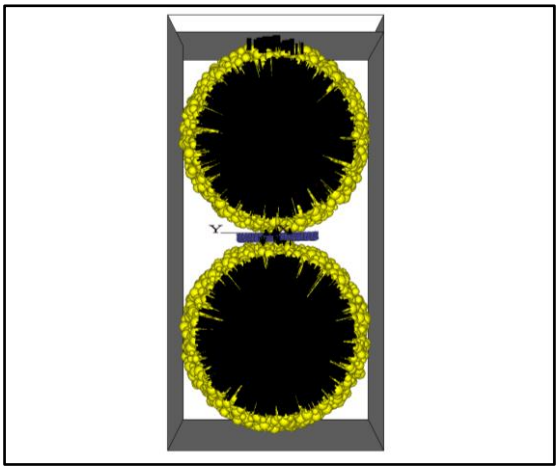

FIGURE 4.23(a) Two Aggregates and a 50µm Film Layer in Compression Test

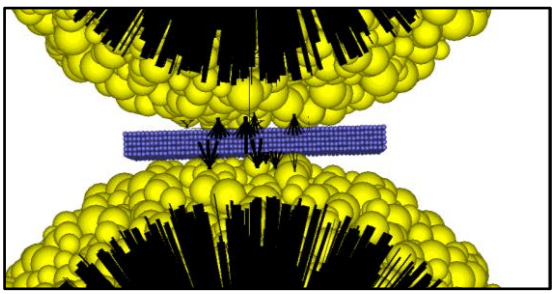

FIGURE 4.23(b) Detailed View of Film Layer, Film Thickness = 50µm

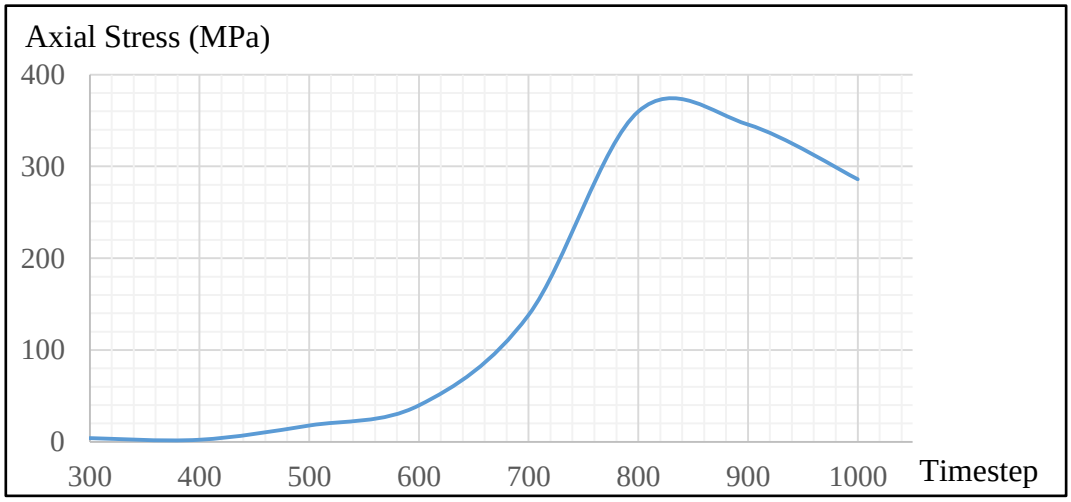

FIGURE 4.23(c) Axial Stress in Compression Test, Film Thickness = 50µm

Summary

DEM has been used to simulate the behavior of an idealized asphalt mixture with different film thicknesses under compressive load. Aggregates and asphalt binder were simulated by balls generated in PFC3d. Corresponding behaviors were achieved by applying properties to different clumps and contacts in PFC3d. These clumps represent aggregates, surrounded asphalt binder, and asphalt film layer. UDM associated with material properties provides a plate for performing visco-elastic behavior. A simple linear visco-elastic model was introduced to give time dependent shear and normal contact stiffness. Asphalt binder of asphalt mixture was successfully simulated using simple viscoelastic contact model. Results of axial stresses of models simulated in PFC3d with varied thickness of 10µm to 20µm, 30µm, 40µm, 50µm showed peak stress of asphalt mixture is a power-law function of film thickness. Peak stress decreases with the increase of film thickness.

Ten compression tests which is a validation of numerical analysis and DEM simulations were conducted using samples with different binder film thicknesses. The Skyscan 1174

cabinet X-ray tomography system was used in the experiments. Samples were tested under uniaxial compression loads. With the help of X-ray scanner, the parameters needed in the compliance model were measured. Compression tests were done by applying displacement to the top and bottom of the sample in equal amount but in opposite directions. This displacement controlled testing stage output displacement versus resistant force results. Based on the experiment results, it's clearly that by moving same displacement, the resistant force of thinner binder film system is larger than the mixture with thicker binder film.

Both simulation results and experiment results agree reasonably with theoretical analysis. When compressive load keeps constant and all asphalt mixtures move same displacement, the one with thinnest asphalt film had highest axial stress and resistant force. This means the mixture includes aggregates and binder will become stiffer if the film thicknesses decrease.

5 EFFECT OF AGGREGATE SHAPE ON ASPHALT MIXTURE

Literature Review

Aggregates consist of approximately 95% of hot-mix asphalt (HMA) by weight. Aggregate morphological characteristics such as particle size, shape, and texture influence the performance and serviceability of hot-mix asphalt pavement (*60*). Flat and elongated particles tend to break during mixing and compaction in mixture production and under traffic loads in service. Therefore, aggregate shape is one of the important properties that must be considered in the mix design of asphalt pavements to avoid premature pavement failure. The recent Strategic Highway Research Program (SHRP) targeted primarily asphalt binder properties and their contribution to pavement performance. Detailed investigations of aggregate contributions to pavement performance were excluded from the program.

There is no standard test that is capable to quantify aggregate morphological characteristics. Conflicting results have been reported on how aggregate shape influences the quality of HMA mixtures. For example, Shklarsky and Livneh (*61*) concluded that replacing uncrushed coarse aggregates with crushed coarse aggregates cannot significantly improve the properties of asphalt mixture. Krutz and Sebaaly (*62*) found a direct correlation between the rutting potential of HMA mixtures and the shape and texture of coarse aggregate particles. Li and Kett (*63*) concluded in their study that flat and elongated particles can be used in a mixture without adverse effect on its strength. Some mixes with flaky aggregates have been found to exhibit higher fatigue life than mixes with nonflaky aggregates. The percentage of crushed coarse particles had a significant effect on laboratory permanent deformation properties. As the percentage of crushed coarse particles decreased, the rutting potential of

the HMA mixtures increased. Huber and Heiman (*64*) found that crushed aggregate containing 19% flat and elongated particles did not adversely affect the volumetric properties of HMA mixtures. Stephens and Sinha (*65*) presented data on the effect of aggregate shape, and recommended blends of regular particles, flat particles, and rod-like particles to achieve optimum strength. They discussed the effect of crushing, aggregate size, and particle shape. They emphasized that asphalt usage can be reduced by increasing the size of crushed aggregate used in a mix. These conflicting statements are due to the lack of understanding on the effect of aggregate shape on engineering properties of a HMA mix. Visual examination is the most common method of judging aggregate shape. Because of the tedious task of making numerous readings, the civil engineer generally finds it impractical to identify particle shape visually. Various innovative methods are available to facilitate the quantification for aggregate shape. One of the most effective methods is digital image processing and analysis. This method provides the capability of quick and accurate measurement of the characteristics of aggregate particles. For example, Yue (*66*) used a digital image processing technique to quantify the distribution, orientation, and shape of coarse aggregate. Their quantitative results indicated that microstructural characteristics of asphalt concrete mixtures can be accurately measured using a digital image processing technique. Kuo (*67*) also used three-dimensional image analysis techniques of aggregate particles to measure the shape, size, and diameter of the particles. Therefore, the objectives of this study are (1) to quantify the morphological characteristics of coarse aggregate, and (2) to evaluate the engineering properties of HMA mixtures made of aggregate with different shapes.

Materials and Methods

Aggregate

The following procedure was performed for evaluating the effect of aggregate shape on strength of asphalt mixtures. Coarse aggregates refer to aggregate particles retained on the 4.75 mm sieve, whereas fine aggregates are aggregate particles passing through the 4.75 mm sieve. TABLE 5.1 tabulates the gradation curve.

TABLE 5.1 Aggregate Gradations

Sevier size (mm)	19	12.5	9.5	4.75	2.36	1.18	0.6	0.3	0.15	0.075
Cumulative percentage by weight (%)	100	93	80	49	32	23	17	12	8	5.2

The coarse size fractions are evaluated for the influence of aggregate shape on engineering properties of a HMA mix. Aggregate shape is determined from the longest diameter (d_L), the intermediate diameter (d_I), and the shortest diameter (d_S). The selection process was carefully conducted by an image analyzer, as discussed in the next section. The elongation ratio and the flatness ratio were used to define the aggregate shape as shown in FIGURE 5.1 – FIGURE 5.3. Four different aggregate shapes are as follows: hexagonal disk, blade, rod, and cube; their flatness ratio and elongation ratio are summarized in TABLE 5.2. Only cubical aggregates have flatness ratio and elongation ratio greater than 2/3, whereas the other three types of aggregates are flaky and oblate (i.e., either the flatness ratio or elongation ratio are greater than 2/3). The hexagonal disk-shaped aggregate is flaky and oblate, the rod-shaped is elongated, and the blade-shaped is both flaky and elongated.

TABLE 5.2 Flatness Ratio and Elongation Ratio of Four Different-shaped-aggregates

Aggregate shape	Flatness Ratio (d_S/d_I)	Elongation Ratio (d_I/d_L)
Cubic	>2/3	>2/3
Rod	>2/3	<2/3
Blade	<2/3	<2/3
Hexagonal disk	<2/3	>2/3

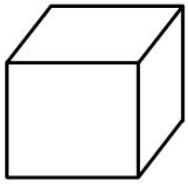

FIGURE 5.1(a) Cubic-shaped Aggregate

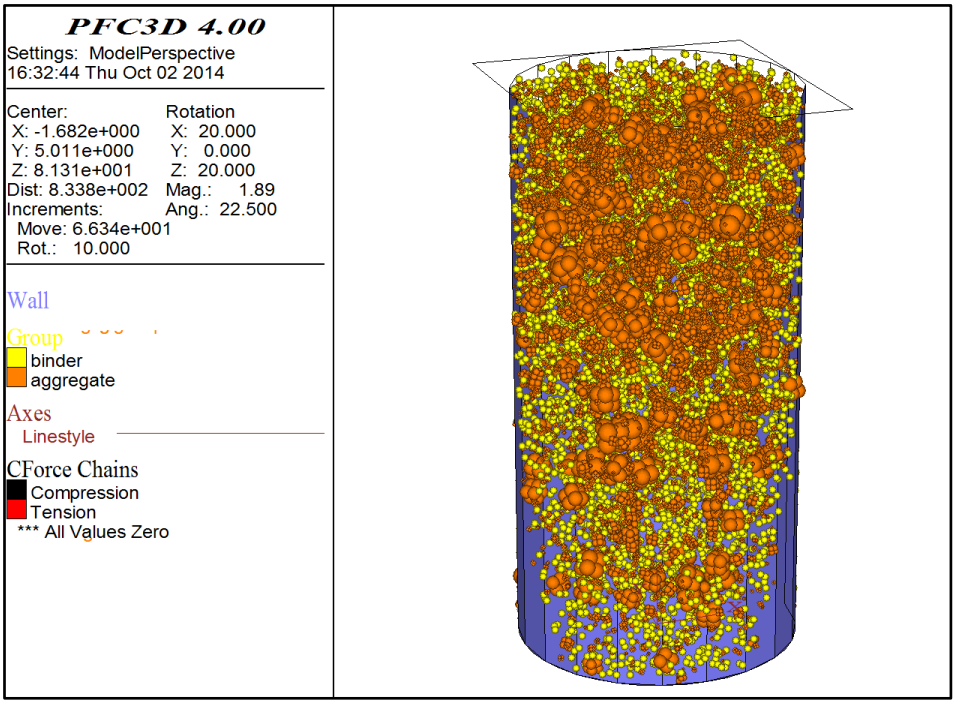

FIGURE 5.1(b) Detailed view of Cubic-shaped Aggregates in Simulation

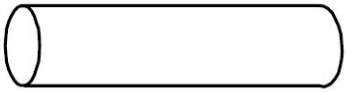

FIGURE 5.2(a) Rod-shaped Aggregate

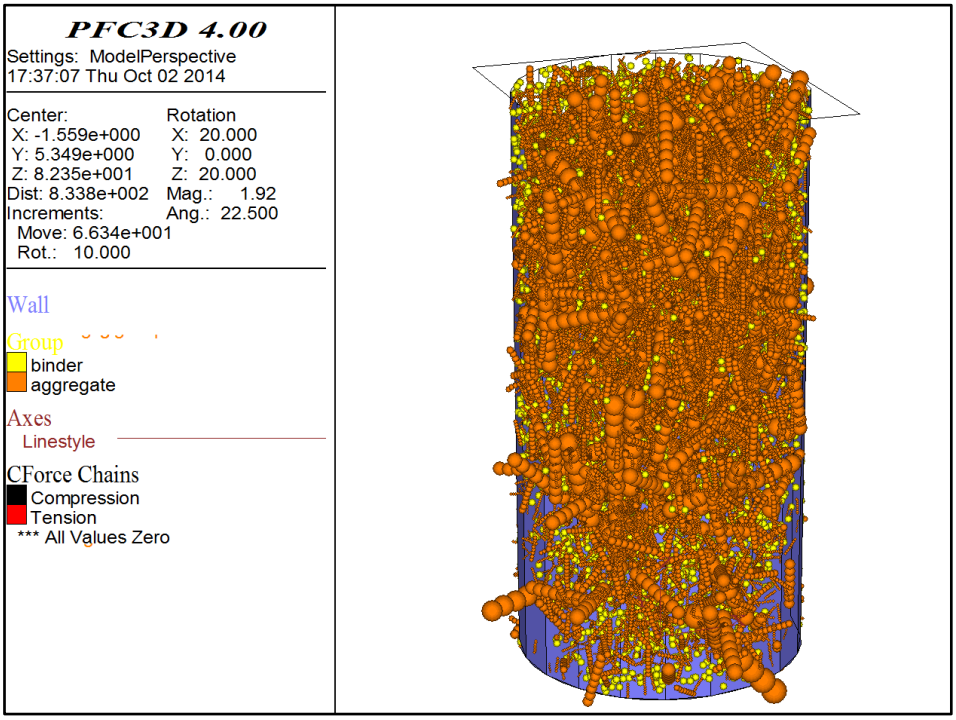

FIGURE 5.2(b) Detailed View of Rod-shaped Aggregates in Simulation

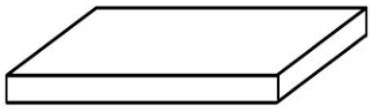

FIGURE 5.3(a) Blade-shaped Aggregate

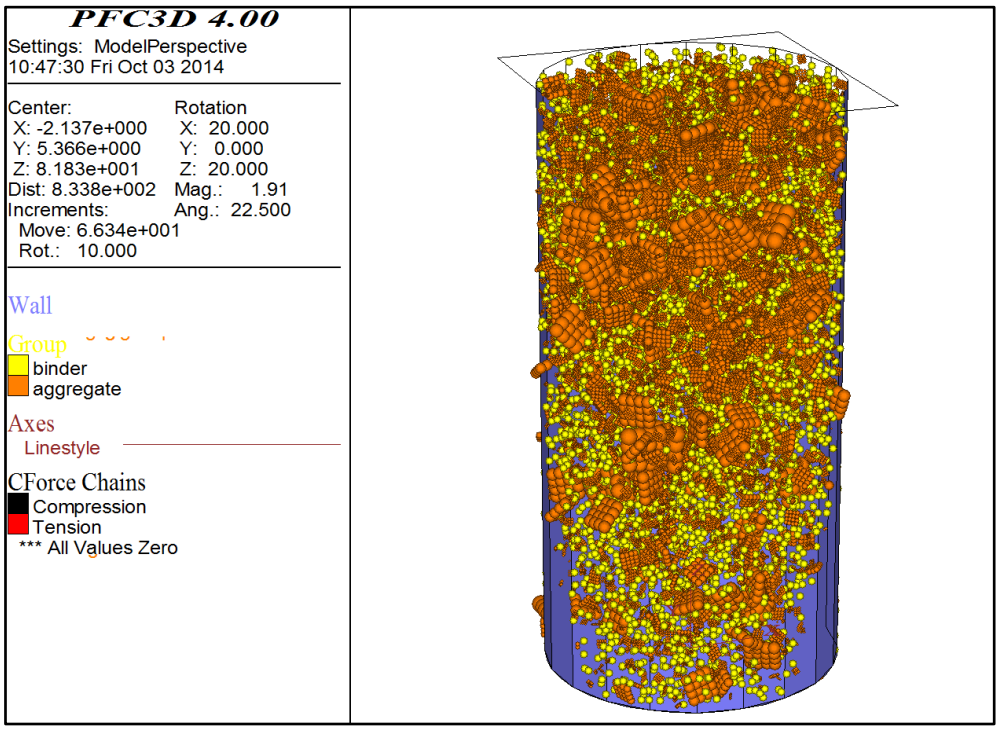

FIGURE 5.3(b) Detailed View of Blade-shaped Aggregates in Simulation

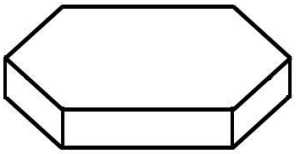

FIGURE 5.4(a) Hexagonal Disk-shaped Aggregate

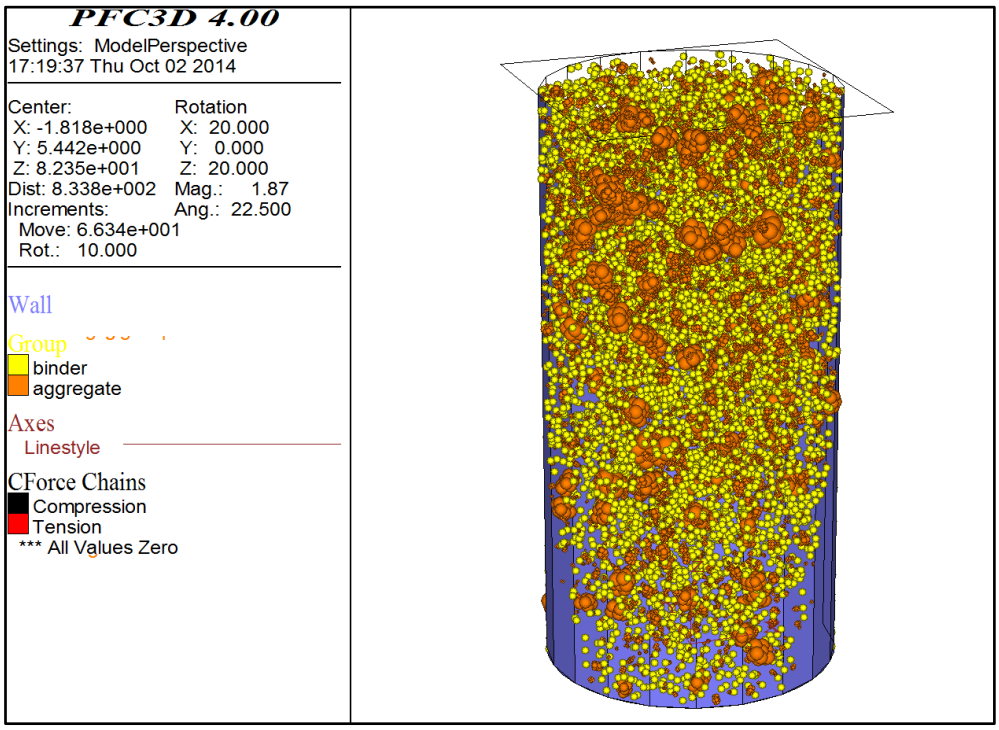

FIGURE 5.4(b) Detailed View of Hexagonal Disk-shaped Aggregates in Simulation

Image Measurements of Coarse Aggregate

Image analysis techniques were used in this study to characterize the morphological characteristics of coarse aggregate particles. The system consists of two major assemblies, including a microscope with a scanner and a rack of modules. The device named Skyscan 1174 cabinet X-ray tomography system is versatile software capable of providing full measurements of coarse aggregate.

Aggregate particles were attached to adhesive clear plastic trays with two perpendicular faces; then, the sample tray was rotated 90° to establish two orthogonal planes of measurement. Particles were placed on a light box that illuminated the sample and made definite contact between aggregate and background. The parameters of length, width, and thickness were obtained by measuring the two orthogonal planes. These parameters provided a direct method for determining the flatness and the elongation ratios of the particles.

Additionally, the image analysis method provided other shape indices that could be related to the effects of aggregates on the properties of a HMA mix. This image analysis method was more time efficient than the ASTM Test Method for Flat Particles, Elongated Particles, or Flat and Elongated Particles in Coarse Aggregate (ASTM D4791) (*68*). The imaging processing technique also provided more information.

The mean value for each aggregate size is listed in TABLE 5.3. For cubical particles, the flatness ratio is 0.80 and elongation 0.78, and both values are larger than 2/3. Note that, in cubical limestone, particles in the size range 19 to 12.5 mm are the most spherical, and those in the size range 9.5 to 4.75 mm are relatively flat and elongated. Data in TABLE 5.3 indicate that the greater the shape factor is, the more nearly cubical the aggregate is. For aggregates used in pavement construction, the shape factor is generally between 0.3 and 0.8. Aggregate used in this study falls within this range. The sphericity value represents the roundness of an aggregate regardless of its thickness. As expected sphericity value ranges between 0.5 and 0.9, and cubical particles have higher sphericity values than the others.

TABLE 5.3 Aggregate Geometric Characteristics

Shape	Size (mm)	d_L (mm)	d_I (mm)	d_S (mm)	Elongation ratio	Flatness ratio	Shape factor	Sphericity
Cubic	19-12.5	18.32	15.02	11.28	0.82	0.78	0.68	0.80
	12.5-9.5	14.05	11.34	9.08	0.81	0.80	0.72	0.80
	9.5-4.75	9.58	7.39	5.74	0.77	0.75	0.68	0.77
Average					0.80	0.78	0.69	0.79
Rod	19-12.5	26.58	14.75	11.88	0.55	0.81	0.60	0.63
	12.5-9.5	18.69	10.89	8.88	0.58	0.82	0.62	0.65
	9.5-4.75	13.85	9.06	7.18	0.65	0.79	0.64	0.70
Average					0.59	0.81	0.62	0.66
Hexagonal Disk	19-12.5	20.87	17.98	10.32	0.86	0.57	0.53	0.75
	12.5-9.5	15.36	13.02	8.01	0.85	0.62	0.57	0.76
	9.5-4.75	11.01	8.98	5.32	0.82	0.59	0.54	0.73

Average					0.84	0.59	0.55	0.75
Blade	19-12.5	29.31	17.38	11.32	0.59	0.65	0.50	0.61
	12.5-9.5	20.96	12.87	5.38	0.61	0.42	0.33	0.54
	9.5-4.75	15.85	7.98	3.25	0.50	0.41	0.29	0.47
Average					0.43	0.49	0.37	0.54

Note: Elongation ratio= d_I/d_L; Flatness ratio= d_S/d_I; Shape factor= $d_S/\sqrt{d_I \cdot d_L}$); Sphericity= $d_S \cdot \sqrt[3]{d_I \cdot d_L}$.

Calculation of Particle Index of Coarse Aggregates Based on DEM Simulations

The combined effects of particle shape and surface texture of an aggregate are determined in accordance with simulated ASTM D 3398 (*69*). FIGURE 5.5 shows the equipment of the test. Simulated tests to measure particle index (*PI*) were done by using DEM; results are summarized in TABLE 5.4. The simulation requirements for this test consists basically of a cylindrical steel mold 152 mm (6 in.) in diameter by 178 mm (7 in.) high, and a steel rod 16 mm (5/8 in.) in diameter by 610 mm (24 in.) long with the tamping end rounded to a hemispherical tip. A clean, washed, oven-dried, and single-size aggregate fraction was used for this test. The mold was filled in three equal layers, with each layer compacted with 10 well-distributed blows of the tamping rod. Each tamp consisted of a drop with the tamping rod from 51 mm (2 in.) above the surface of the layer being compacted. This procedure was repeated using the same material but applying 50 blows on each of the three layers. The weight of the contents of the mold in each case was determined and the corresponding percentage of voids was calculated using the bulk specific gravity of each aggregate fraction. The particle index (*PI*) is derived using the following equation:

$$PI = 1.25V_{10} - 0.25V_{50} - 32 \quad (23)$$

Where

V_{10} = percent voids in the aggregate compacted with 10 blows per layer;

V_{50} = percent voids in the aggregate compacted with 50 blows per layer.

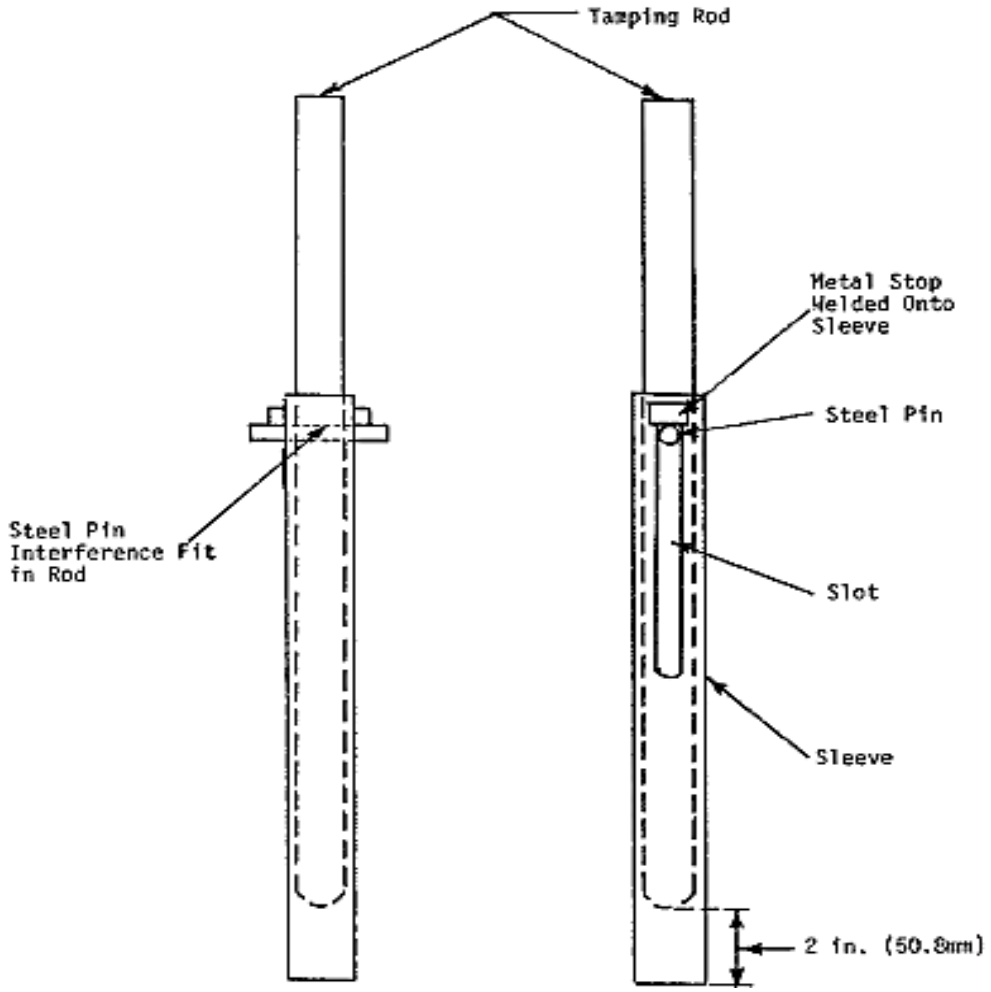

FIGURE 5.5 Tamping Rod and Sleeve (*69*)

TABLE 5.4 Measured Particle Index (*PI*) for Coarse Aggregate

Shape	Size Range (mm)	Percentage (%)	*PI* for each size	Weighted value
Cubic	19-12.5	62.7	17.6	11.0
	12.7-9.5	14.5	15.7	2.3
	9.5-4.75	22.8	15.2	3.5
PI				16.8
Rod	19-12.5	62.7	16.3	10.2
	12.7-9.5	14.5	14.9	2.2
	9.5-4.75	22.8	14.0	3.2
PI				15.6
Hexagonal disk	19-12.5	62.7	15.1	9.5
	12.7-9.5	14.5	14.1	2.0
	9.5-4.75	22.8	13.3	3.1

PI				14.6
Blade	19-12.5	62.7	12.8	8.0
	12.7-9.5	14.5	12.3	1.8
	9.5-4.75	22.8	11.2	2.6
PI				12.4

Simulated Indirect Tensile Tests on Digital Samples with Selected Grading Aggregates Using DEM

The indirect tensile strength of HMA is used often to evaluate the relative quality of materials. The repeated-load indirect tension test for determining the resilient modulus was conducted by applying compressive loads according to ASTM D4123 (*70*). The load was applied vertically in the vertical diameter plane of a cylindrical specimen of asphalt concrete through a curved loading strip. The resulting horizontal deformation was measured and used to calculate the total resilient modulus (M_r) as follows:

$$M_r = \frac{P \cdot (v + 0.27)}{t \cdot H} \tag{24}$$

Where

P = repeated load,

v = Poisson's ratio,

t = thickness of specimen,

H = total recoverable horizontal deformation.

Poisson's ratio was calculated using the measured recoverable vertical and horizontal deformation. The tensile strength (S_T) is calculated as follows:

$$S_T = \frac{1.96 \cdot P_{ult}}{\pi \cdot t \cdot D} \tag{25}$$

Where

P_{ult} = ultimate applied load required to cause to the specimen to fail,

t = thickness of specimen,

D = diameter of specimen.

Conventionally, the indirect tensile test is conducted to indicate the internal resistance in a mix. Mixes were prepared to observe the effect of aggregate shape on the strength of the mixes. TABLE 5.5 shows peak strength of mixtures include different aggregates. FIGURE 5.6 shows the test results for different aggregate shapes vs. *PI* values. A trend was observed for indirect tensile strength. Coarse aggregates with lower *PI* provide lower stiffness than those with higher *PI*. Blade and hexagonal disk particles impede compaction and thus may prevent the development of satisfactory properties in HMA. In compacted mixtures, cubical particles provide great interlocking internal friction between aggregates and, resulting in greater mechanical stability than flat, thin, and/or elongated particles. The *PI* value is a quantitative measure of the aggregate shape that influences the characteristics of HMA mixtures.

TABLE 5.5 Peak Normal Strengths Achieved in Indirect Tensile Test

Aggregate Shape	Loading Rate (mm/min)	Temperature (^{o}C)	Specimen Diameter (mm)	Peak Normal Strength (MPa)
Cubic	50	25	100	1.69
Rod	50	25	100	1.40
Hexagonal disk	50	25	100	1.35
Blade	50	25	100	1.31

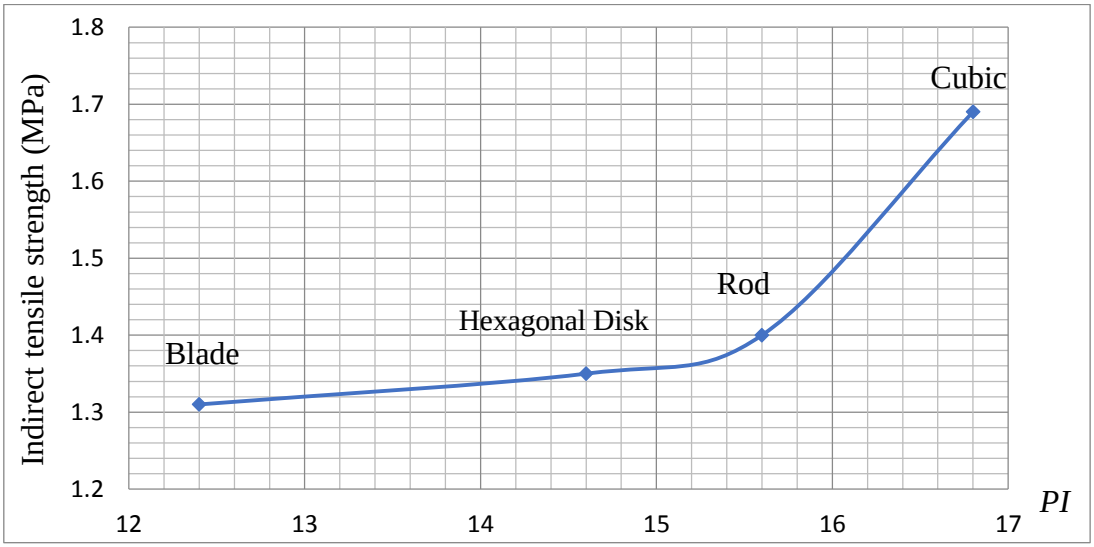

FIGURE 5.6 Effect of Aggregate Shape on Indirect Tensile Strength

Simulated Compression Tests on Digital Samples with Ten Aggregates in Each of Them Using DEM

Summary of DEM Properties

Different form the indirection tensile test, digital model of the samples used in the compression test are built on a smaller scale. Each sample is created by asphalt binder and 10 aggregates. Same compression load has been applied on 36 digital samples, 12 of them include only sphere aggregates, 12 of them include only cubic aggregates, and the other 12 include randomly shaped aggregates. These samples are true to size with the specimens that are tested by an X-ray scanner, Skyscan 1174 system. Details of the X-ray aided compression experiments are summarized in next session.

FIGURE 5.7, 5.8 and 5.9 show the views of the digital samples in DEM simulation. Geometry information of the samples could be found in TABLE 5.6. Two different contact models are applied to aggregates and asphalt binders (see TABLE 5.7). Small yellows balls

represent asphalt binder and orange clusters represent aggregates. Though 10 aggregates are included in each sample, some of them are located more close to center, so it's hard to see all of them on the pictures.

TABLE 5.6 Geometry Information of the Samples used in Simulated Compression Test

Sample	**Aggregate**		
Height = 16mm	**Sphere**	**Cubic**	**Random**
Diameter = 8mm	Diameter = 4mm	Side length = 3mm	Longest diameter = 4mm; Shortest diameter = 2mm

TABLE 5.7 Contact Model and Mechanic Property

Aggregate (Elastic)	Asphalt binder (Viscoelastic)
Density: 2.34 g/ml	Shear viscosity = $0.414*10^6$ N/m
Normal stiffness	Viscoelastic normal stiffness = $0.36*10^6$ N/m
Shear stiffness	Viscoelastic shear stiffness = $0.12*10^6$ N/m

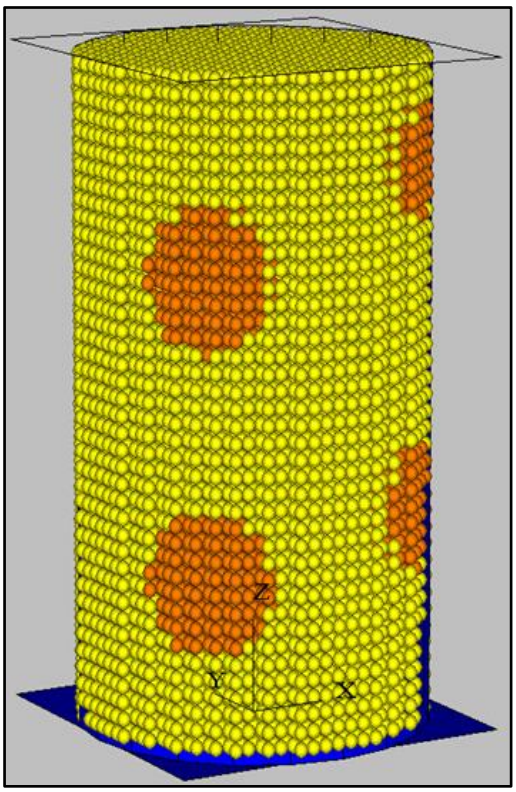

FIGURE 5.7 Digital Sample Include 10 Sphere Aggregates

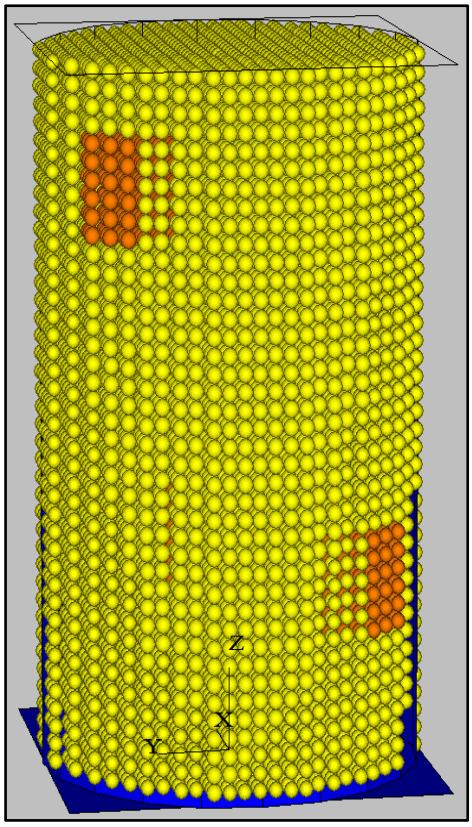

FIGURE 5.8 Digital Sample Include 10 Cubic Aggregates

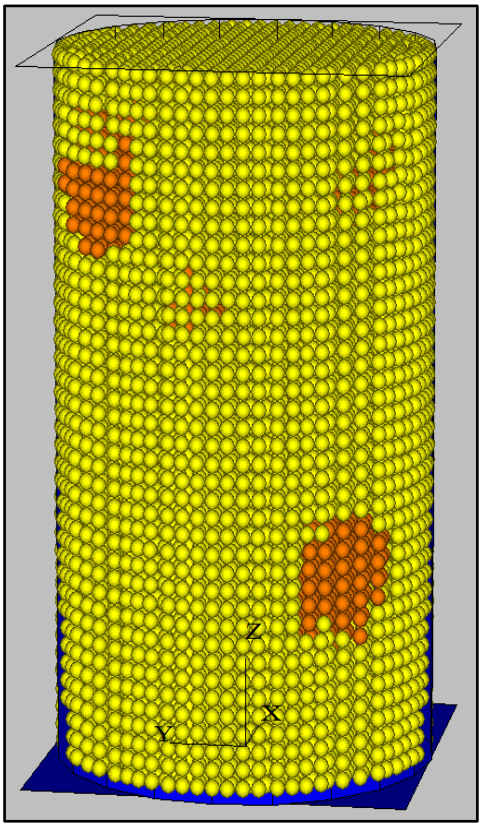

FIGURE 5.9 Digital Sample Include 10 Random Aggregates

Results and Analysis

TABLE 5.8 Peak Normal Strengths Achieved in Compression Test on Digital Samples with Ten Aggregates in Each of Them

Aggregate Shape	Loading Rate (μm/s)	Temperature (^{o}C)	Peak Normal Strength (MPa)
Sphere	17.5	25	1.12
Cubic	17.5	25	1.68
Random	17.5	25	1.34

Similar with the results of indirect tensile test, specimen with cubic aggregates reached the greatest peak normal strength. The values of the strength of the digital specimens in both of the simulated tests are pretty close to each other. This means contact models and physical properties applied to the digital models in PFC3d perfectly represent what real asphalt binder and aggregate should have. These results are also verified by experiments in the following session.

Compression Tests Using X-ray Image Scanner

Equipment and Specimens Preparation

The Skyscan 1174 cabinet X-ray tomography system was used in the experiment to verify the simulation results from DEM models introduced before. The Skyscan 1174 system, shown in FIGURE 5.10, is a compact, cost efficient micro X-ray scanner for nondestructive three-dimensional microscopy. It’s supplied with software for system control, X-ray radiography, t hree-dimension (3D)-reconstruction, two-dimensional (2D) /3D image analysis and 3D realistic visualization. The SkyScan-1174 scanner supports variable magnification (6

to 30mm field of view), adjustable source energy (20 to 50KV) and flexible image format. The material testing stage of Skyscan system, shown in FIGURE 5.11, can perform compression, tension and torsion test. The loading-displacement or the stress-strain curve can be saved as an image or text file. The testing sample can be held under specific loading for scanning. The testing stage applies displacement to the top and bottom of the sample in equal amount but in opposite directions. This keeps the central part of the sample relatively static for scanning purpose.

FIGURE 5.10 Skyscan 1174 System

FIGURE 5.11 Testing Stage of the Microscopy System

Samples were tested under uniaxial compression loads applied on top and bottom stages. With the help of X-ray scanner, the parameters needed in the compliance model were measured by the tools provided by the software. The testing stage is displacement controlled. The displacement speed was set at 17.5μm/s, chosen according to the allowable range of the

testing device, and was set at 17.5μm/s. The resistant force was monitored and recorded during the loading. When the force reaches the maximum allowable value of the testing stage, the displacement application will stop. For the sample in this study, the application of displacement was stopped when two elastic particles started to contact to each other through the asphalt layer. Prior to each test, the testing stage was calibrated according to the procedure recommended by the manufacturer. Stress vs. Strain data was stored as a text file for each sample. The PG 64-22 asphalt binder is used and the test temperature is 25-27C^{o} according to the thermometer.

Compression tests are performed on samples that include ten aggregates and asphalt binder by using X-ray CT. The samples are made with aggregates with different shapes and PG 64-22 binder (see FIGURE 5.12 and FIGURE 5.13).

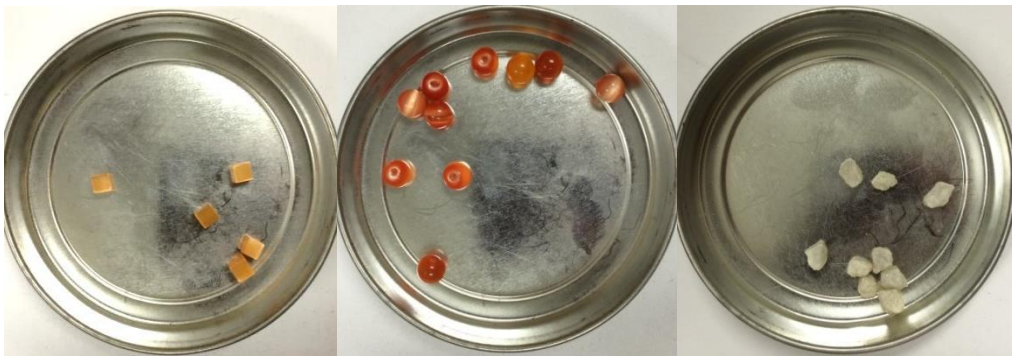

FIGURE 5.12 Crystal Particles and Aggregates Used in Compression Test

FIGURE 5.13 Asphalt Mixture Specimen Used in Compression Test

Test and Results Analysis

There are 36 specimens (12 with sphere aggregates, 12 with cubic aggregates, and 12 with random aggregates) tested under compression load by using Skyscan 1174 X-ray scanner. Weight of the aggregates and asphalt binder used in each specimen are summarized in TABLE 5.9. These specimens were taken from a freezer to and mounted to a stage placed as vertically as possible. Once mounted and imaged, the stage was first pulled using a tension load, in order to make sure the specimen had adequate space to compress properly, then the compression test was performed. Throughout the compression test, X-ray images of the specimens were taken to show the positions of the aggregates within the specimens (See FIGURE 5.14). The compression test software was also calibrated to the numbers shown in TABLE 5.10. TABLE 5.11 tabulated the test results, and FIGURE 5.15 plots the stress-strain relationship.

TABLE 5.9 Weights of Aggregates and Asphalt Binder

Sample	Cubic Aggregate (g)	Asphalt Binder in Random Specimens (g)	Sphere Aggregate (g)	Asphalt Binder in Random Specimens (g)	Random Aggregate (g)	Asphalt Binder in Random Specimens (g)
1	0.7	0.4	0.4	0.3	0.5	0.3
2	0.8	0.3	0.4	0.3	0.4	0.1
3	0.8	0.4	0.4	0.5	0.5	0.3
4	0.7	0.3	0.4	0.3	0.3	0.3
5	0.7	0.5	0.4	0.3	0.4	0.2
6	0.7	0.7	0.4	0.4	0.6	0.5
7	0.7	0.5	0.4	0.4	0.5	0.4
8	0.8	0.7	0.4	0.4	0.3	0.2
9	0.7	0.9	0.4	0.4	0.3	0.4
10	0.7	0.5	0.4	0.4	0.9	0.4
11	0.7	0.6	0.4	0.3	0.5	0.5
12	0.7	0.3	0.4	0.4	0.6	0.3

TABLE 5.10 Loading Information of Compression Test

Force (N/step)	0.22
Torque (N*cm/step)	0.08
Speed (μm/s)	17.5
Angle (deg/sec)	52.80
Linearization (%)	2
Symmetry (%)	110

TABLE 5.11 Peak Normal Strength of Each Specimen Achieved in Compression Test

Sample	**Peak Normal Strength of Specimens with Sphere Aggregates (MPa)**	**Peak Normal Strength of Specimens with Cubic Aggregates (MPa)**	**Peak Normal Strength of Specimens with Random Aggregates (MPa)**
1	1.139	1.656	1.269
2	1.135	1.785	1.386
3	1.068	1.761	1.268
4	1.136	1.699	1.234
5	1.132	1.640	1.359
6	1.119	1.627	1.215
7	1.116	1.642	1.247
8	1.109	1.683	1.354
9	1.118	1.605	1.238
10	1.110	1.651	1.275
11	1.133	1.647	1.263
12	1.114	1.684	1.346
Mean Peak Strength	*1.119* (MPa)	*1.673* (MPa)	*1.288* (MPa)

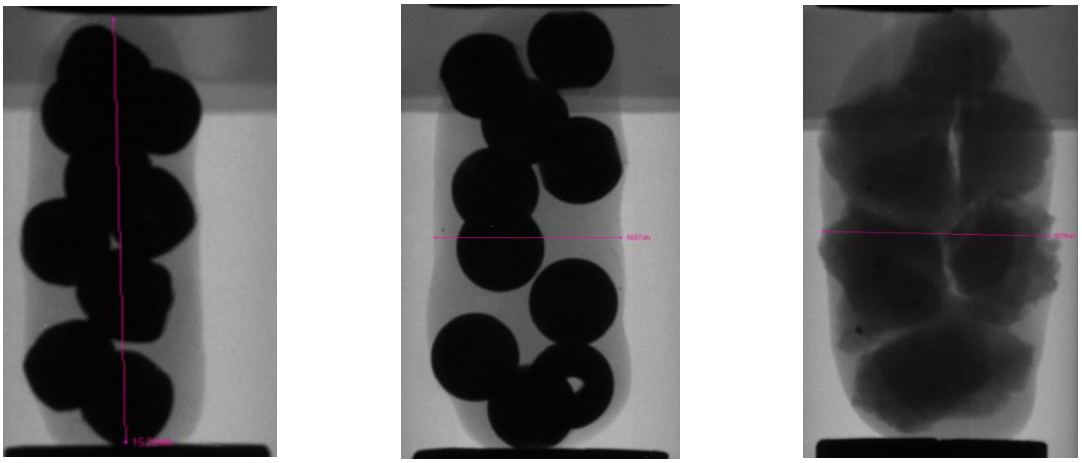

(a) (b) (c)

FIGURE 5.14 X-ray Images of Specimens with Asphalt Binder and (a) Ten Cubic Aggregates, (b) Ten Sphere Aggregates, and (c) Ten Random Aggregates

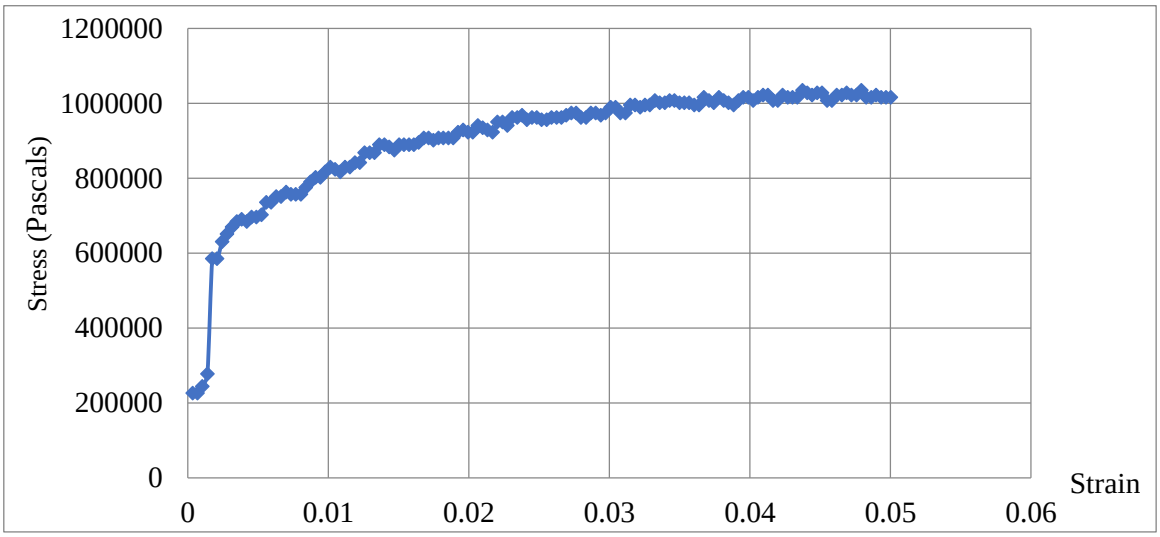

FIGURE 5.15 Stress vs. Strain of One Specimen with Ten Sphere Aggregates

There is a good agreement between simulations and experiments. Specimens with cubic aggregates have the greatest peak normal strength in both the simulation test and experimental test. However, there are some discrepancies. In the simulation the specimen was able to reach its ultimate strength, which was hard in the experiment due to the allowed loading of the specimen by the testing software. Finally, the simulation was much more detailed and spiky because the PFC3d software could tell exactly how the contact force changed between particles, rather than the experiment software, which could only read the stress and strain of the total specimen.

Summary

The indirect tensile strength of HMA with four different shapes of aggregate was evaluated in simulated test to evaluate the relative quality of materials. The image analyzer was shown to be a useful tool for quantifying the morphological characteristics of coarse aggregates. Image evaluation provided quantitative indices such as geometric measurement

and angle rotation of granular materials. Data showed that the morphological characteristics of coarse aggregate correlated well with the results of other indirect tests such as the particle index. Cubical particles possessed the best resistance over the other shapes. The particle index (*PI*) was shown to be an adequate measure of the combined contribution of particle shape, angularity, and surface texture to the stability of an aggregate. The *PI* value correlated well to aggregate geometric characteristics including elongation ratio, flatness ratio, shape factor, and sphericity. The particle shape determined how aggregate was packed into a dense configuration and also determined the internal resistance of a mix. The morphological characteristics of coarse aggregates found from both digital test and image analysis were in good agreement with the engineering properties of HMA mixtures. This study presents a precise method to evaluate the aggregate characteristics in a HMA mix and demonstrates their effects on pavement performance. The results of this study would provide useful guidelines for highway engineers to construct a long-lasting pavement.

6 EVALUATION OF COMPACTION TEMPERATURE SENSITIVITY

Literature Review

One of the most traditional constructed materials is “Hot Mix Asphalt (HMA)”. Mechanical performance of HMA depends on solid production, temperature control, and moisture, it is still being paid attention by many people. Determination of volumetric parameters of HMA samples has vital importance for quality control of constructed roads. The compaction temperature is one of the parameters that can change the HMA volumetric parameters. In HMA pavement construction, compaction is defined as the process by which the volume of air in a HMA mixture is reduced through the application of external forces. Compaction is an essential factor in the design and subsequent production of asphalt mixtures. The expulsion of air enables the mix to occupy a smaller space, thereby increasing the unit weight or density of the mix.

The compaction temperature influences workability which is related to the achieved density of the mixture. According to the ASTM D6926, the compaction temperature is the temperature at which bituminous should be heated to produce viscosities of 0.28 ± 0.03 pa·s. (*71*). This requirement was based on experience with conventional asphalt binders. In general, the binder in modified asphalt mixture is stiffer than in conventional mixtures, therefor, there is a need for a higher compaction temperature. However, previous studies (Bahia 2000; Huner and Brown 2001) on the effect of compaction temperature on the volumetric properties of asphalt mixture reported that specimens could have the same volumetric properties over a very wide range of compaction temperatures (*72, 73*). Azari et al. (2003) also suggested that a temperature range from 119 ^{o}C to 159 ^{o}C could be used for modified mixtures with the

limestion - Novophalt binder (*74*).

The compaction temperature is one of the major issues in HMA and also one of important criteria in the process of producing good quality of hot mix asphalt. Also, the temperature is a key factor in the control of bitumen viscosity, which affects its ability to coat and provide adequate lubrication for aggregates.

Viscosity is simply a measure of a fluid resistance to flow and is described by the following equation:

$$\mu = \frac{\tau}{\gamma} \tag{26}$$

Where: μ = viscosity (in cgs units of poise); poise = dyne-sec/cm^2 = g/cm-sec (the SI unit of viscosity is the Pa·s = N^{-sec}/m^2 = 10 poise)

τ = shear stress

γ = shear rate

Aggregate Grading

In this study two mix designs were used and the gradation of the aggregates has been shown in the TABLE 6.1. Gradation of surface course layer is the optimal one selected in the chapter “Determination of Gradation”.

TABLE 6.1 Gradations of Aggregates Used in Simulation

Sieve size (mm)	25	19	12.5	9.5	4.75	2.36	1.18	0.6	0.3	0.15	0.075
Surface Course Layer, Percentage passing sieve size (%)		100	93	80	49	32	23	17	12	8	5
Binder Course Layer, Percentage passing sieve size (%)	100	95	69		50	35			10		5

Asphalt Binder Selection

Considering this fact that the most consuming asphalt binder is the bitumen of 60-70, in this study asphalt binder PG 64-22 was used and FIGURE 6.1 shows the temperature and viscosity tested by Freddy L. Roberts and Prithvi S. Kandhal, et al (*75*). TABLE 6.2 shows the properties of asphalt binder specified in DEM simulation.

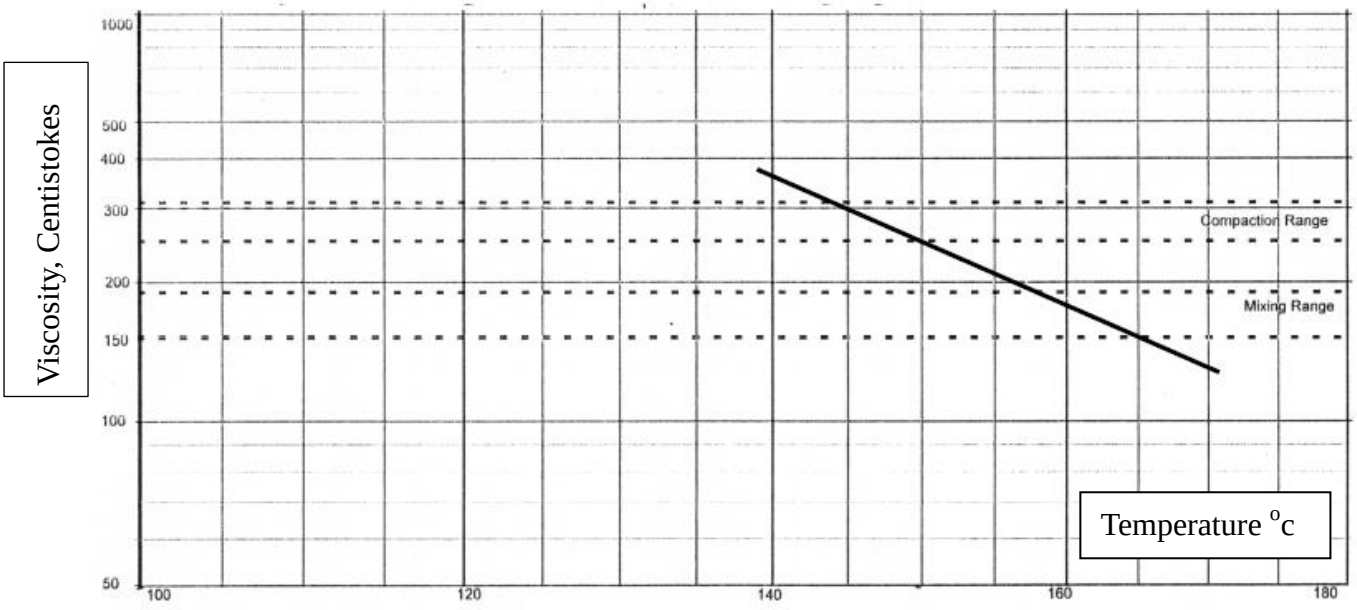

FIGURE 6.1 Viscosity-Temperature of Bitumen for Determination of Compaction Temperatures (*75*)

TABLE 6.2 Properties of Asphalt Binder Used in DEM Simulation

Density at 25 ^{o}C	1.017 (g/cm^{3})
Penetration of asphalt binder at 25 ^{o}C (100g, 5sec)	80 (d-mm)
Softening point of asphalt binder	50 (^{o}C)
Ductility at 25 ^{o}C	+100
Solubility in trichloroethylene	99.7 (% by mass)
Flash and fire points by cleveland open cup	296 (^{o}C)
Kinematic viscosity at 120 ^{o}C	884 (Pa·s)
Kinematic viscosity at 125 ^{o}C	690 (Pa·s)
Kinematic viscosity at 130 ^{o}C	525 (Pa·s)
Kinematic viscosity at 135 ^{o}C	415 (Pa·s)
Kinematic viscosity at 140 ^{o}C	313 (Pa·s)
Kinematic viscosity at 145 ^{o}C	246 (Pa·s)

Kinematic viscosity at 150 ^{o}C	202 (Pa·s)
Kinematic viscosity at 155 ^{o}C	181 (Pa·s)
Kinematic viscosity at 160 ^{o}C	172 (Pa·s)

DEM Simulation Process of Superpave Gyratory Compactor (SGC) Compaction

Gyratory compaction is the commonly used compaction method to prepare asphalt mixture specimen. In the DEM simulation of gyratory compaction, the vertical pressure was set at 600 kPa and the angle of gyration was set at 1.25º. The gyration was applied at a rate of 30 revolutions per minute. The gyratory kneading action in PFC3d was applied by a rotary compression plate which is controlled by two separate DEM simulation engines: rotation plate engine and constant pressure engine. The rotation plate engine applies a constant rotation speed on the compression plate around a specific axis. The function of constant pressure engine is to apply a specific pressure to the underneath particles by specified.

The procedures of the DEM simulation process is summarized as follows:

1) Generate compaction cylinder and funnel (FIGURE 6.2a);
2) Calculate particle numbers of each particle size according to gradation curve;
3) Randomly generate particles in specific space (FIGURE 6.2b);
4) Pack particles under gravity force until it is stable (FIGURE 6.2c and FIGURE 6.2d);
5) Generate compression plate and gyratory compact asphalt mixture by constant pressure (FIGURE 6.2e and FIGURE 6.2f);
6) Record the position of compression plate and spheres during compaction process;
7) Calculate air void content of the mixture.

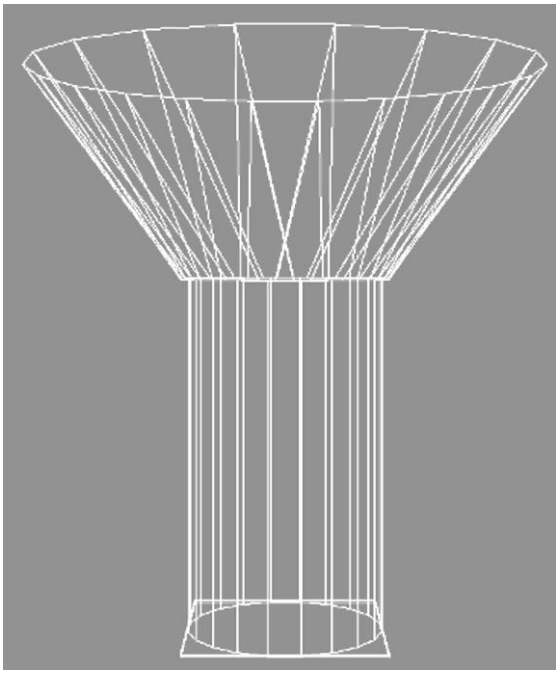

(a)

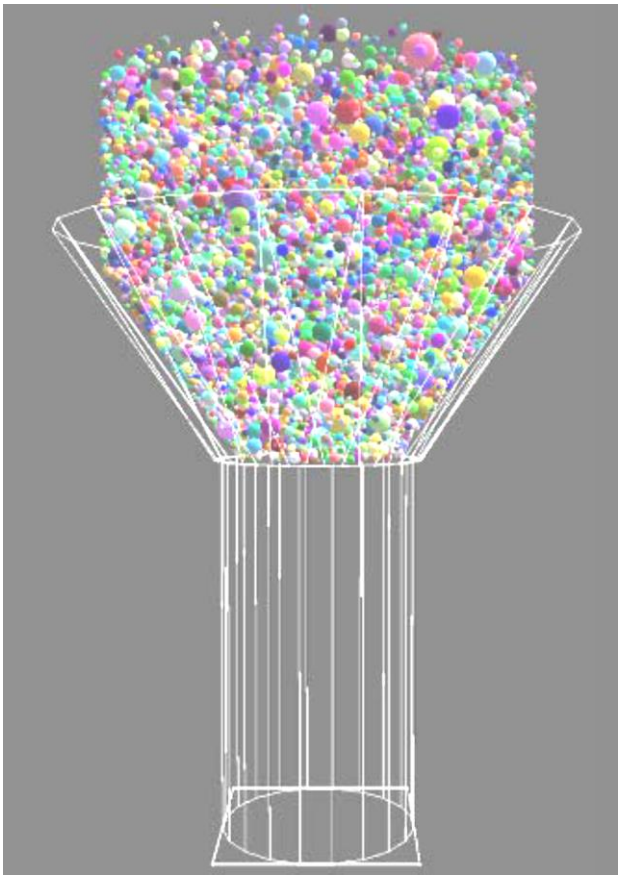

(b)

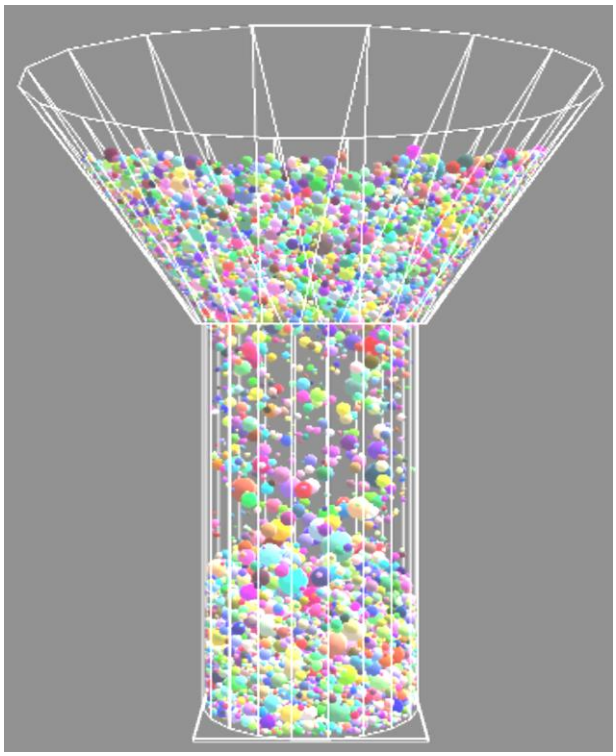

(c)

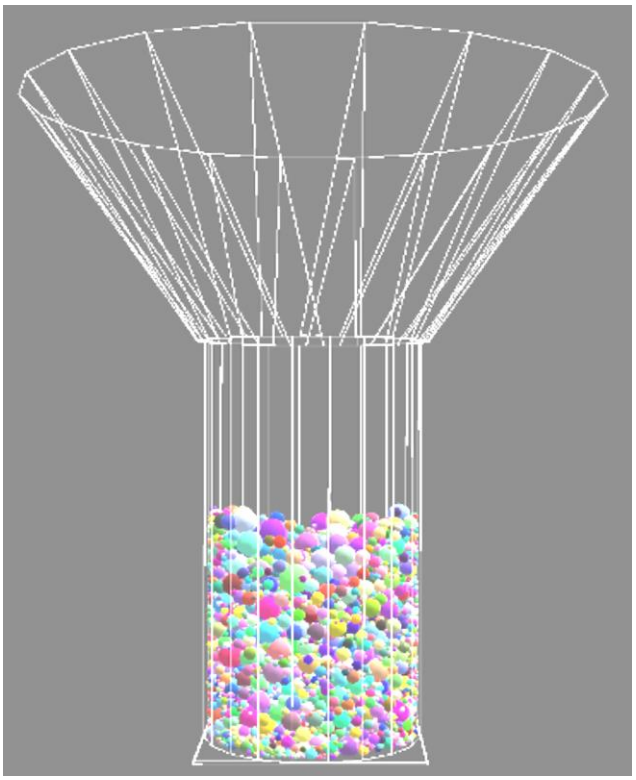

(d)

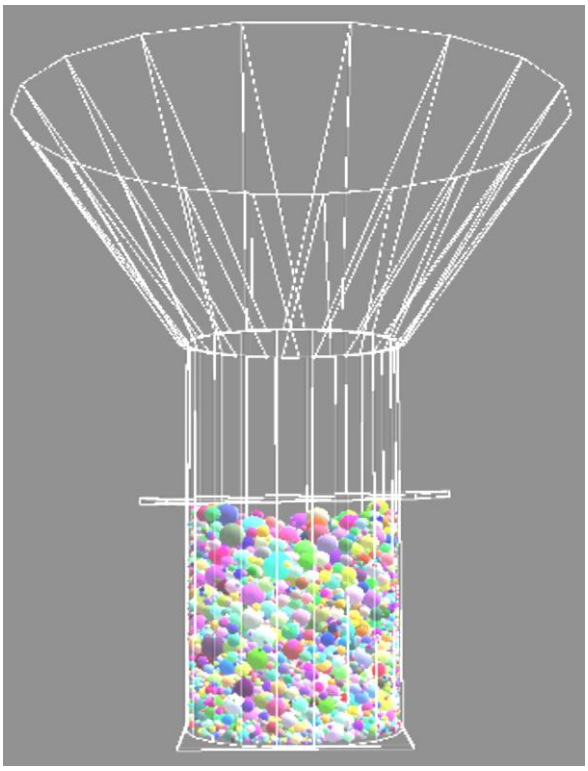

(e)

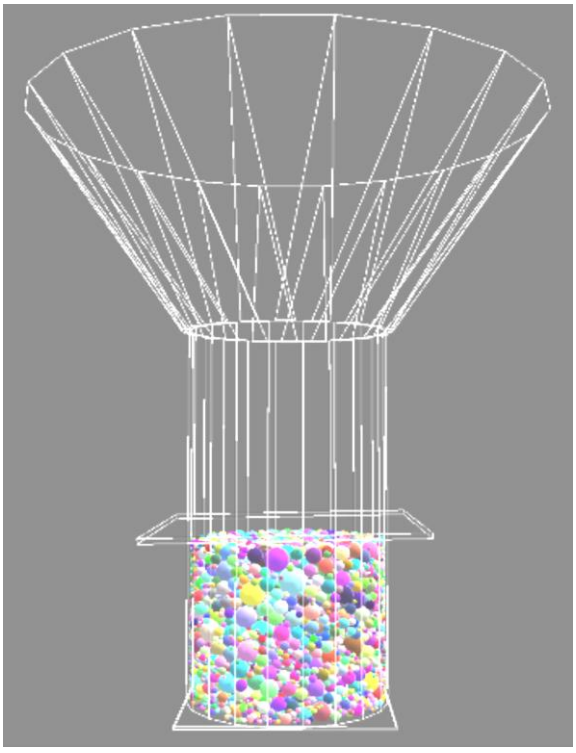

(f)

FIGURE 6.2 DEM Simulation Process of SGC

Result and Analysis

Simulated compactions were done at different temperatures; several results were recorded (see TABLE 6.3). In this study, the temperature of the asphalt binder during mixing with aggregate that with continuous grading in mixer increases from 120 ^{o}C to 160 ^{o}C.

TABLE 6.3 Data Measured at a Serial of Modeling Temperatures

T (^{o}C)	Stiffness of asphalt binder (kg/mm)	Density (g/cm^{3})		Air voids (VA, %)		Voids filled with asphalt (VFA, %)		Flow (mm)	
		Binder course	Surface course	Binder course	Surface course	Binder course	Surface course	Binder course	Surface course
120	407.19	2.199	2.175	5.4	5.0	66.6	67.1	2.76	2.76
125	416.32	2.204	2.184	5.2	4.8	67.9	68.3	2.79	2.91
130	429.28	2.208	2.192	4.9	4.5	69.6	69.9	2.83	3.00
135	443.97	2.216	2.198	4.7	4.3	70.7	71.2	2.88	3.08
140	466.54	2.222	2.203	4.5	4.2	71.8	72.2	2.91	3.17
145	481.66	2.229	2.208	4.4	4.1	72.7	73.1	2.95	3.24
150	499.58	2.227	2.207	4.2	4.0	73.3	73.7	2.98	3.29
155	519.09	2.226	2.207	4.1	3.9	73.8	74.3	3.03	3.35
160	541.08	2.225	2.206	4.0	3.8	74.4	74.7	3.05	3.40

Analysis of Density

FIGURE 6.3 shows the following results: Density of binder course layer is slightly greater than surface course layer. Density of binder course layer and surface course layer is being simultaneously increased with increasing compaction temperature, which is as a result of asphalt cement viscosity due to temperature increase and subsequently, the location of aggregates beside each other becomes denser.

The highest density of binder course and surface course is being occurred over the temperature of 145 °C. High correlation of binder course and surface course indicates the

strong relationship between density and compaction temperature. (For the surface course aggregate, R^2 = 0.936 and for the binder course aggregate R^2 = 0.951).

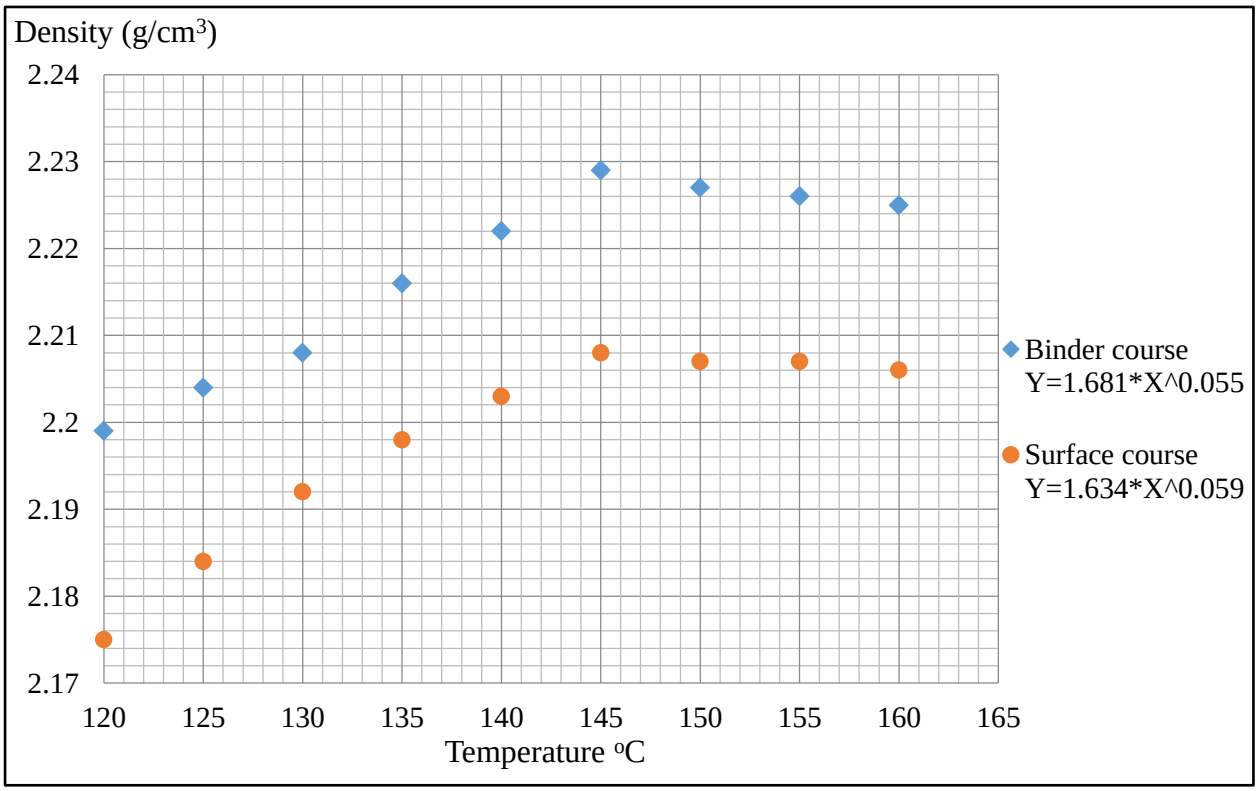

FIGURE 6.3 Density vs. Compaction Temperature

Analysis of Percent of Air Voids (VA)

Air voids (VA) of aggregate of binder course layer is higher comparing to the VA of aggregate of surface course layer. Furthermore, FIGURE 6.4 shows high R^2 value for binder course layer and surface course layer is indicator of the strong relationship between air void and compaction temperature. (For the surface course layer aggregate, R^2= 0.970 and for the binder course layer aggregate, R^2= 0.986) The higher compaction temperature results in the change of asphalt binder viscosity and more asphalt binder dispersion on the surface. It

makes a thin film of asphalt binder becomes enough for covering the coarse aggregates, and finally since the volume of asphalt binder is constant, consequently, the temperature increase only decreases the percent air void.

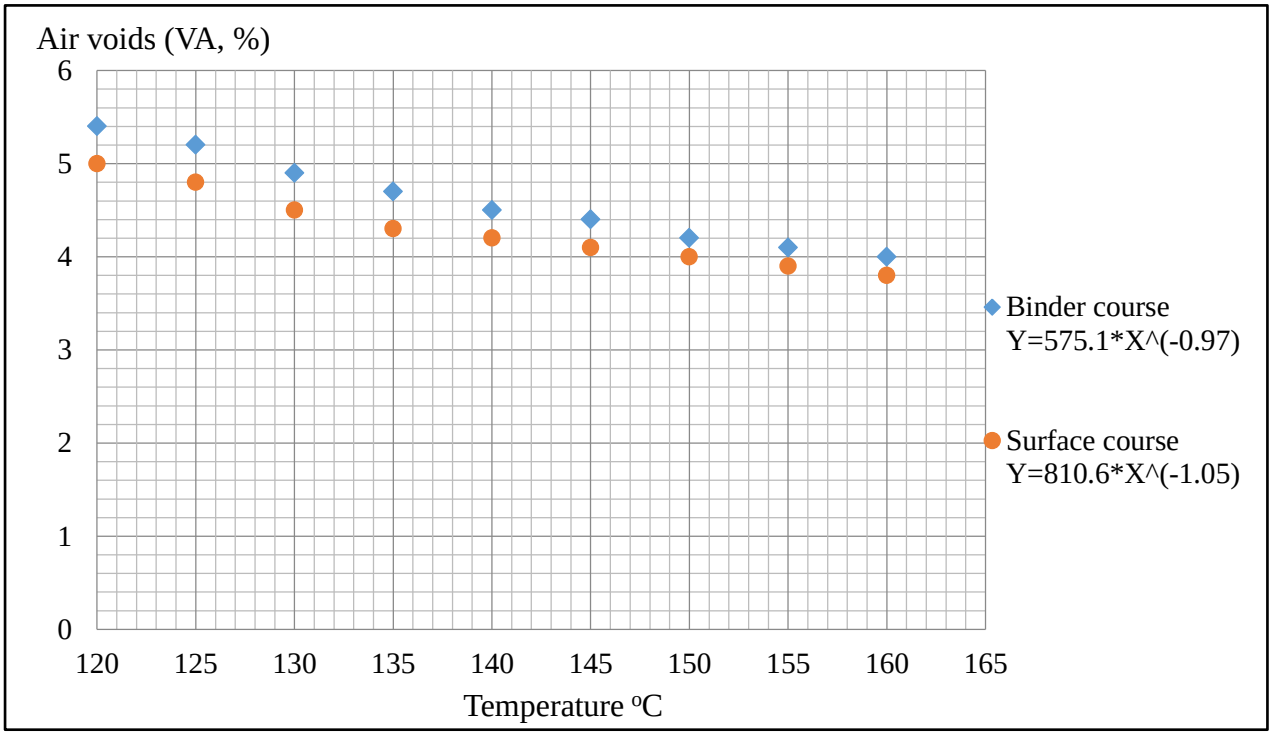

FIGURE 6.4 Air voids vs. Compaction Temperature

Analysis of Percent Voids Filled with Asphalt (VFA)

FIGURE 6.5 shows that voids filled with asphalt (VFA) simultaneously increases with the increase of compaction temperature. The amount of VFA in the binder course is more than that in the surface course, as the optimum asphalt content in the surface course is greater than that in the binder course. However, due to the lack of inequality of air void percent difference of surface course comparing to the binder course at different temperatures, the amount of surface course VFA are not exactly equal to the binder course VFA. Also, the

drawn curves for binder course and surface course show an attended move of VFA versus the increase of temperature. This figure also indicates a strong relationship between VFA and compaction temperature (because of the high correlation of binder course and surface course, for the surface course aggregate, $R^2 = 0.990$ and for the binder course aggregate $R^2 = 0.970$).

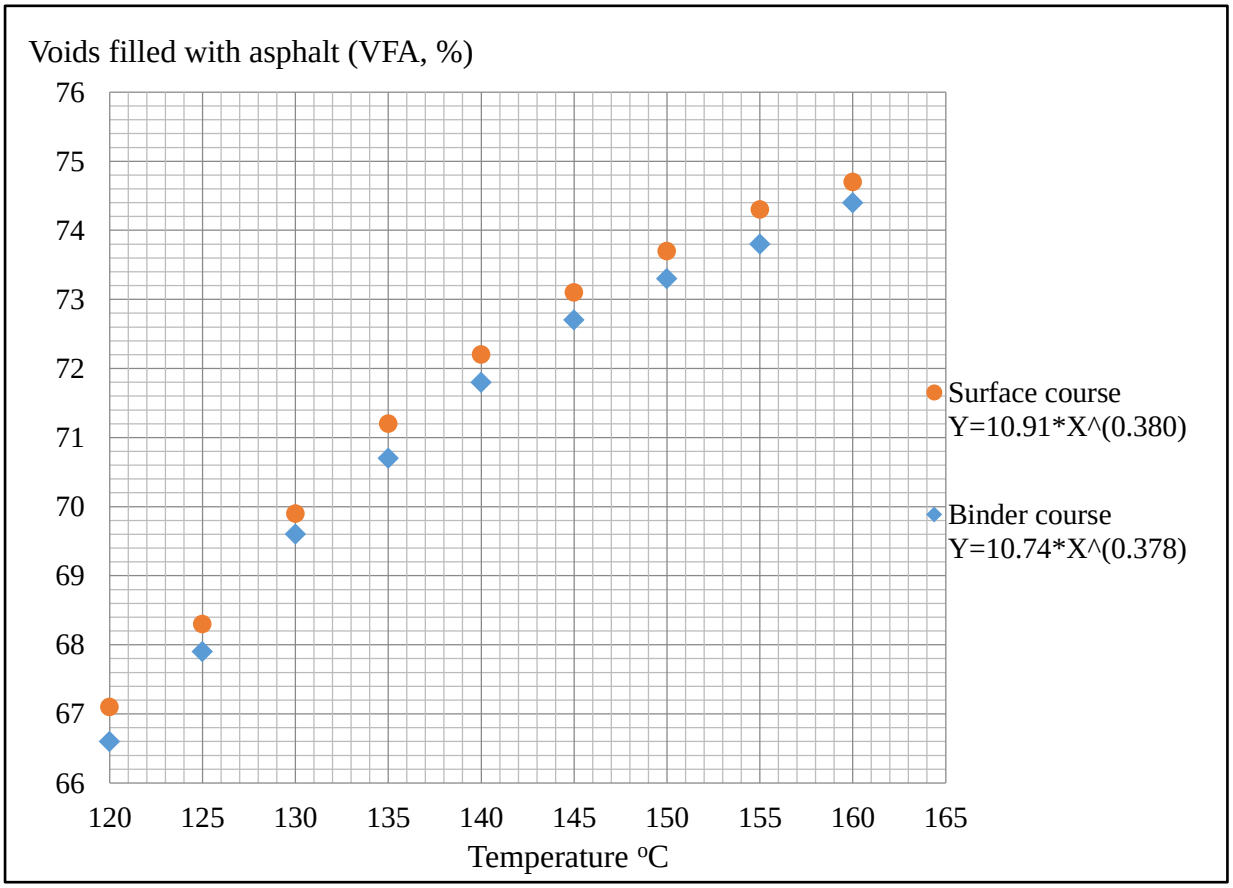

FIGURE 6.5 VFA vs. Compaction Temperature

Analysis of Flow

The quantity of Marshall Flow in surface course and binder course increases with the increase of compaction temperature. FIGURE 6.6 indicates that the difference between flows of surface course and binder course becomes greater at higher temperatures. This figure

shows a strong relationship between flow and compaction temperature (because of the high R^2 value for binder course = 0.966 and 0.989 for surface course). According to the minimum and maximum authorized quantity for flow in the Asphalt Institute Manual Series MS-2 (2-3.5mm) (*76*), FIGURE 6.6 shows that all of the attained flow quantities for surface course and binder course are within the authorized limitation.

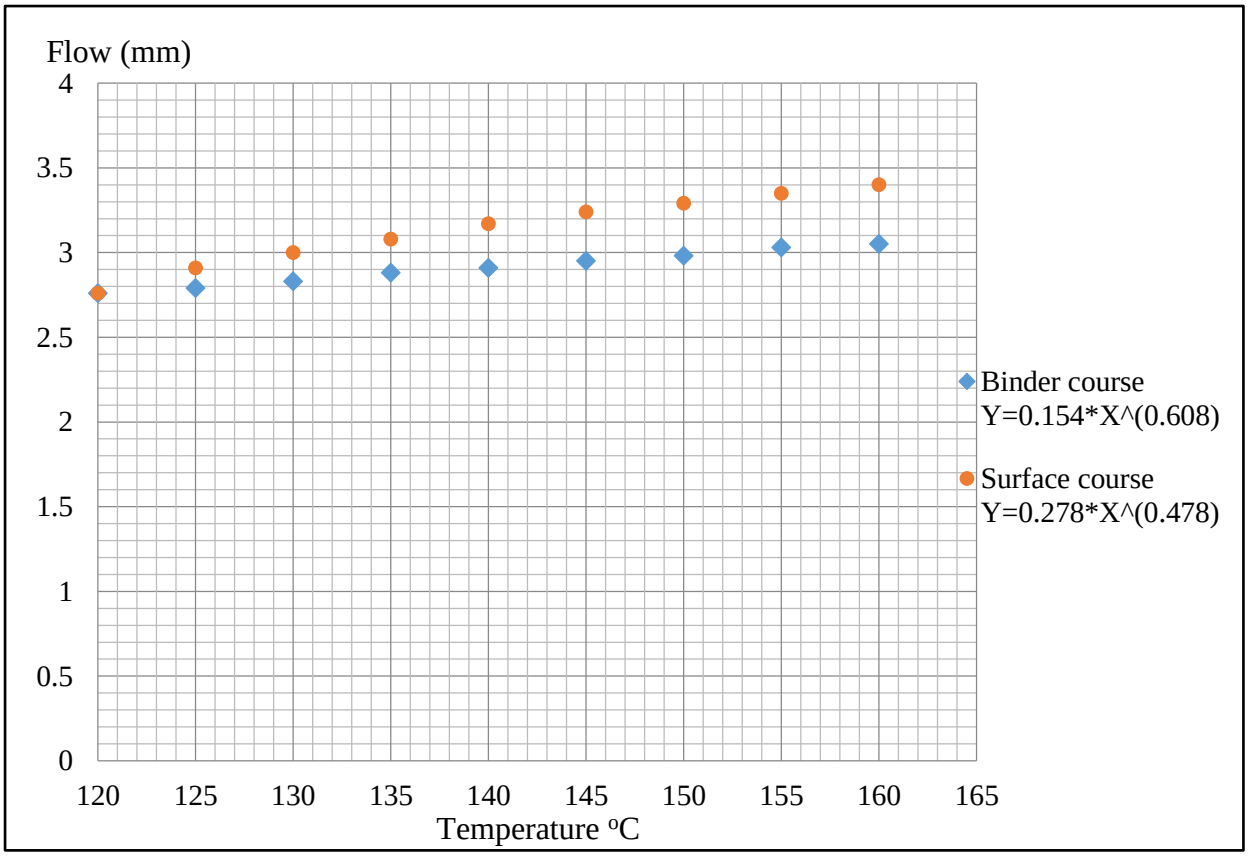

FIGURE 6.6 Flow vs. Compaction Temperature

Summary

This study indicates that the temperature has significant impression on hot mix asphalt properties. From the discovered high correlation value (R^2 over 0.9) in the drawn figures, we can realize that there is a strong relation between various parameters of asphalt mixture samples and compaction temperature. So, observing the compaction temperature during the

performing hot mix asphalt, can help us to avoid from considerable changes which there are in the asphalt specifications.

Increasing compaction temperature makes density to be increased, but there is a limitation for this increase and afterwards density will be decreased.

Considering the mentioned minimum and maximum for VA and VFA in MS-2 and other references, the amount of authorized temperature parallel with them can be achieved.

Increasing the temperature makes flow to be increased. The difference between flows of surface course and binder course becomes greater at higher temperatures.

7 EVALUATION OF MOISTURE DAMAGE POTENTIAL

Literature Review

The liquefaction behaviors of concrete have received a considerable amount of attention. Because flow-type landslides are strongly associated with the liquefaction phenomenon (*77, 78, 79*), the extensive geo-technical tests, especially the undrained triaxial compression tests, have been performed under both dynamic stress-loading and static conditions. It was concluded that the collapse of loose meta-stable structures due to the compressive deformation produced excessive pore-water pressure resulting in the liquefaction (*80*). Since the triaxial compression tests cannot investigate the undrained shear behaviour subjected to a large shear displacement, the studies using the ring-type direct shear testing apparatus have also been conducted. Sassa proposed the sliding surface liquefaction that occurred within the shear zone where particles were crushed and comminuted (*77*). Note that the sliding surface liquefaction takes place even when the specimens are medium-dense through dense, whereas the liquefaction can only occur in the loose specimens. Okada et al. (2004) stated that the crushed and comminuted particles can form the less-permeable shear zone, and it hindered the dissipation of generated excessive pore-water pressure in the ring shear tests (*81*). Cundall and Strack (1979) proposed a discrete numerical method, to model the shear behavior of granular assemblies. In discrete element method, the contacts between ball and ball (in three dimensions) or disc and disc (in two dimensions) are modeled by the mechanical elements of elastic spring and viscous damper (FIGURE 7.1) (*82*). Gravity flow of granular materials were numerically simulated by two-dimensional discrete element method. Although the discrete element method has difficulties in tuning up the setting parameters and it consumes

rather too much time with limited number of elements, it is a very strong tool to investigate non-continuum problems.

Previous work also has revealed that the pore water pressure (PWP) reduction of cement-based materials such as paste, mortar and concrete reflects rather well the stiffness evolution and volume change of such materials from time zero and through the time of set (*83*). Furthermore, it has revealed that PWP is a good indicator for susceptibility of "plastic shrinkage cracking" and for friction against panels in forming slips (*84*). Early PWP reductions are caused by two interacting mechanisms: vacuum effect caused by chemical shrinkage and meniscus effect (capillary tension). Air voids will alter the early age PWP. This is because they may grow as long as the stiffness of the paste-mortar-concrete is low, which results in PWP release.

Initially and in a sealed condition (no moisture exchange with the surroundings), PWP corresponds to the hydrostatic pressure of the liquid paste-mortar-concrete given by the height over the point of measuring and the density. PWP will decrease and reach the water pressure given by the height over the point of measuring when the paste-mortar-concrete is able to support its own weight (point of self-support, PSS). Note that PSS occurs before time of initial set (*83).* In the time before PSS the body is too week to resist the total volume change (chemical shrinkage). Beyond PSS, the total volume change will be resisted, more and more as the stiffness increases. It results in compression force in the solid and tension force of the pore water, forming so-called vacuum effect. Beyond final setting (i.e. beyond the time period considered here), emptying of capillary pores (self-desiccation) forms menisci, resulting in capillary tension.

The buffer effect and the fact that the amount of air pores in cement paste varies from nominally zero in pure cement paste, to 20% in the cement paste of concrete with air entraining mixture (AEM), suggest that air voids play an important role in the present period in time. The study presents and discusses some results from a limited test program of cement paste with and without AEM as well as concretes with and without AEM, conducted in order to evaluate the influence of air voids on the mentioned properties, both from a fundamental and practical point of view.

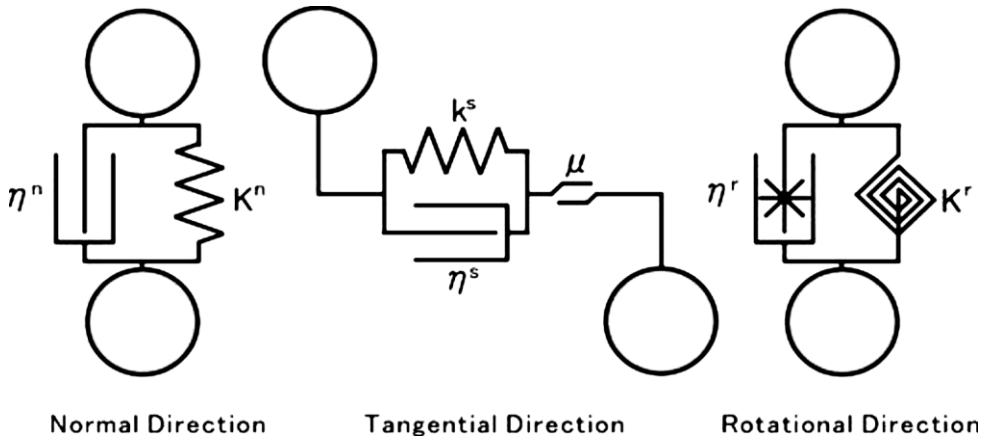

FIGURE 7.1 Mechanical Elements Introduced in Ball–ball Contacts in Normal, Tangential and Rotational Directions in DEM

Procedure of Numerical Calculation of Pore Water Pressure

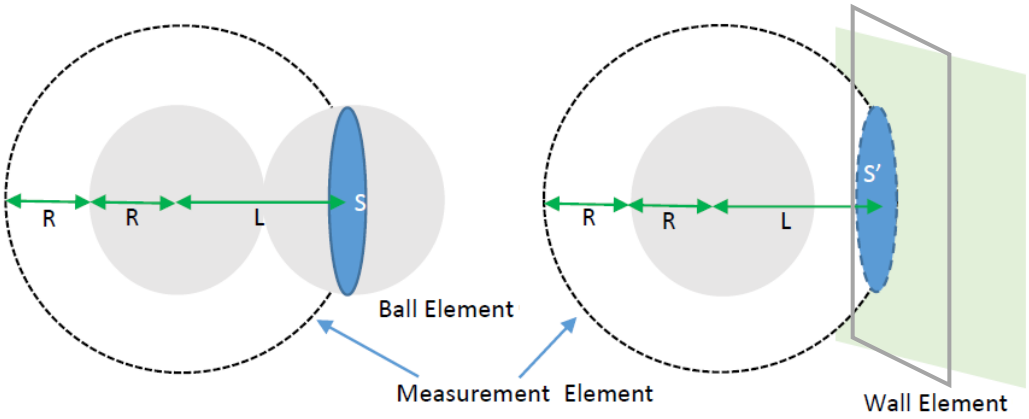

FIGURE 7.2 Schematic Illustrations of Measurement Sphere and Cross Section Areas

The detailed procedure of the fluid-coupled discrete element method is highlighted. First, the measurement sphere, which assigns the pore water pressure, is introduced, and then the calculation scheme is shown. The measurement sphere surrounds and coincides with the center of each ball element with the radius *R* (FIGURE 7.2). The radius of the measurement sphere is twice of that of the ball element, i.e. 2R. The mean velocity and center position of the ball and wall elements that intersect a given measurement sphere are calculated as follows:

$$\overline{V_i} = \frac{\sum_N V_i}{N}, \qquad \overline{X_i} = \frac{\sum_N X_i}{N} \qquad (i = 1,2,3) \tag{27}$$

in which N is the total number of ball and wall elements contained in the measurement sphere, V_i is the translational velocity, and X_i is centroid location of ball and wall elements. The relative velocity and position of ball and wall elements from the mean values could be written as:

$$\tilde{V}_i = V_i - \overline{V_i}, \qquad \tilde{X}_i = X_i - \overline{X_i} \qquad (i = 1,2,3) \tag{28}$$

In this model, the relative velocity is estimated by using strain rate tensor $\dot{\beta}_{ij}$. It's expressed as:

$$\tilde{V}_i' = \dot{\beta}_{ij}\tilde{X}_j \qquad (i = 1,2,3) \tag{29}$$

The strain rate tensor $\dot{\beta}_{ij}$ that minimizes the difference between relative velocity $\tilde{V}_i$ and the estimated relative $\tilde{V}_i'$ is computed using the least square method, in which the following nine equations are resolved. In this calculation, LU decomposition based on the Crout's algorithm, and backward and forward substitutions were conducted.

$$\sum_N \dot{\beta}_{ik}\tilde{X}_k\,\tilde{X}_j = \sum_N \tilde{V}_i\,\tilde{V}_j \qquad (i,j = 1,2,3) \tag{30}$$

The volumetric strain during the increment of time, Δt is obtained like:

$$\varepsilon_v = \dot{\varepsilon}_v \Delta t = \left(\dot{\beta}_{11} + \dot{\beta}_{22} + \dot{\beta}_{33}\right)\Delta t \tag{31}$$

The changes in pore-water pressure due to the volume change is given by the product of volumetric strain and the modulus of compressibility of water, and it is applied as forces to the centers of ball and wall elements, which are within a given measurement sphere as follows:

$$F_{ball} = P_A' S = (P_A + \Delta P)S = (P_A + E_w \varepsilon_v)\pi r^2 \tag{32}$$

$$F_{wall} = P_A' S' = (P_A + \Delta P)S' = (P_A + E_w \varepsilon_v)\pi[(2r)^2 - L^2] \tag{33}$$

in which PA is the pore-water pressure of the measurement sphere A, ΔP is incremental changes in pore-water pressure within Δt, S and S' are the areas on which pore-water pressure acts (FIGURE 7.2), Ew is the modulus of compressibility of water. The fluid-flow due to the difference of pore-water pressure values between the neighboring measurement spheres is given based on the Darcy's law by:

$$\Delta Q_{AB} = k \cdot \pi r^2 \frac{P_B' - P_A'}{\rho \cdot g \cdot L_{AB}} \Delta t \tag{34}$$

in which P_A' and P_B' are the pore-water pressure of the measurement spheres A and B, and g is the gravitational acceleration, L_{AB} is the distance between the measurement spheres A and B. The total change in pore-water pressure (P_A) because of the fluid-flow is given by:

$$P_A = \sum_N \Delta P_{AB} = \sum_N \frac{E_w \Delta Q_{AB}}{V_A} \quad (35)$$

where V_A is the volume of the measurement sphere A.

Simulated Measurement of Pore Water Pressure in Asphalt Mixture

Digital Model and Properties Used in DEM Simulation

A dynamic load was applied on the asphalt mixture model. The simulated asphalt mixture follows an elastic model. The numerical specimens were cylindrical in shape (0.10 m in diameter and 0.20 m in high) formed by three wall elements, including a circumferential wall cylindrical in shape, upper end and lower end walls (FIGURE 7.3). These wall elements were not deformed during the numerical simulation. The upper and lower end walls moved vertically, and the circumferential wall cylindrical in shape contracted or expanded radially. The ball elements had the uniform size of 0.015 m in diameter. The packing of the ball elements was conducted such that certain numbers of ball elements with a reduced diameter of 0.0031 m (0.625 times of 0.015 m) were created to effectively make assembly at the positions determined by the pseudo-random numbers within the cylindrical numerical space surrounded by wall elements. After that, the diameter of ball elements created within the wall elements was restored to 0.015 m to form the designated specimens. Initial confining stress of 20 kPa was given to normally (isotropic) consolidate the numerical specimens, then compressed with a constant axial speed of 0.01 m/sec (the upper end wall elements moved down vertically). The input parameters used are given in TABLE 7.1. The bulk permeability used in the simulation was the input value that was selected to be similar to the one found in

the sandy soils. The bulk permeability was constant all through in the simulation, neglecting the changes in the void ratio in microscopic scale due to deformation of the assembly of ball elements during compression.

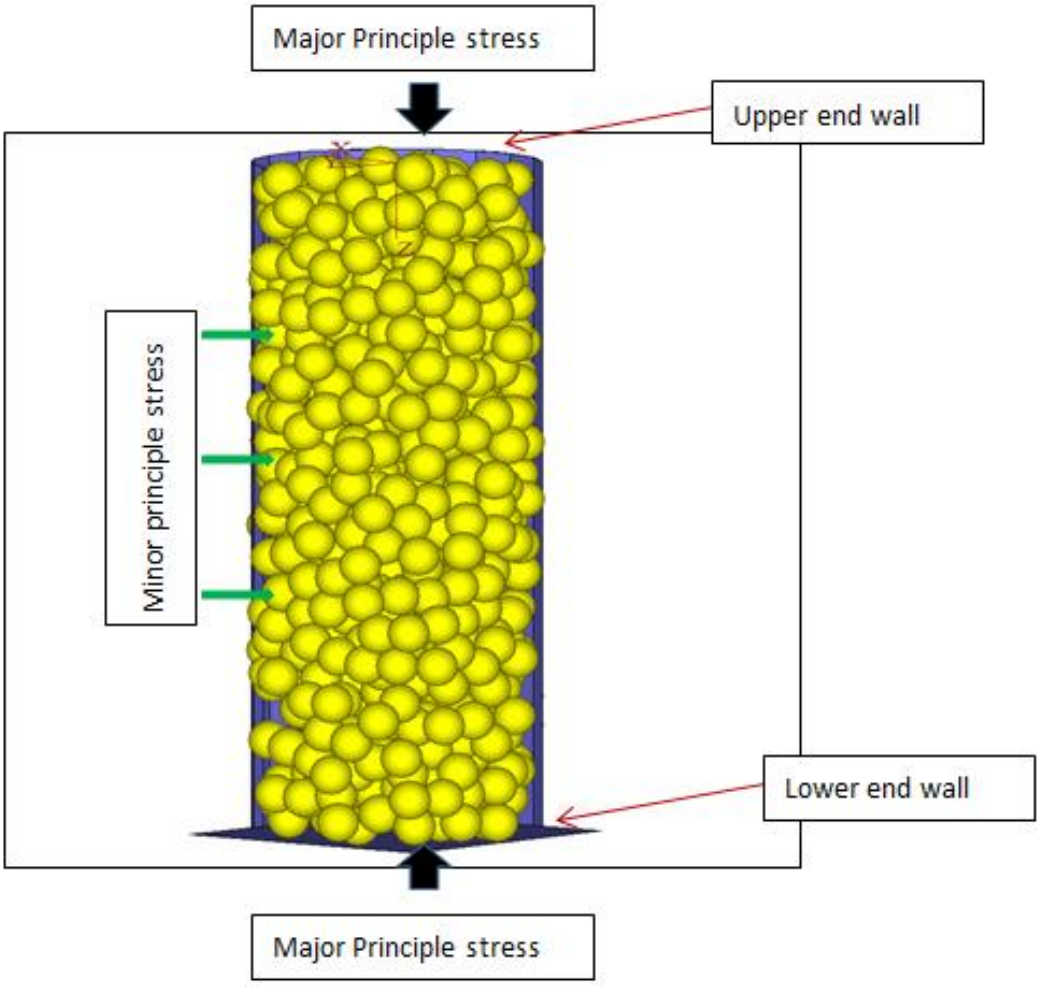

FIGURE 7.3 Numerical Specimen for Undrained Triaxial Compression Test

TABLE 7.1 Input Parameters of The Simulated Specimen

Normal elastic spring stiffness	5.00×10^{6} N/m
Tangential elastic spring stiffness	1.25×10^{6} N/m
Rotational elastic spring stiffness	7.03×10^{1} Nm
Normal viscous damping coefficient	2.27×10^{5} Ns/m
Tangential viscous damping coefficient	1.13×10^{5} Ns/m
Rotational viscous damping coefficient	1.00×10^{-3} Nms
Frictional coefficient of wall element	0.01
Passion radio	0.30

Confining pressure	2.00×10^{4} Pa
Modulus of compressibility of water	2.10×10^{6} Pa
Axial loading speed	1.00×10^{-2} m/s
Bulk permeability	1.00×10^{-3} m/s
Thermal expansion at 25^{o}C	$12\times10^{-6}K^{-1}$
Thermal conductivity at 25^{o}C	0.75 W/(m.K)

The simulated asphalt mixture follows an elastic model; properties of the model are summarized in TABLE 7.1.

Result and Analysis

The change of pore water pressure is linear along with dynamic load growth (see FIGUER 7.4). Both positive and negative pore water pressures were produced in the process of dynamic load applying repeatedly. Such an erosion of high pore water pressure on the pavement will spray outward a mortar with a scoured material from crevice, resulting in peel off and loose of asphalt surface. Then the performance of the mixture will rapidly decline in the overall structure, and damage will occur.

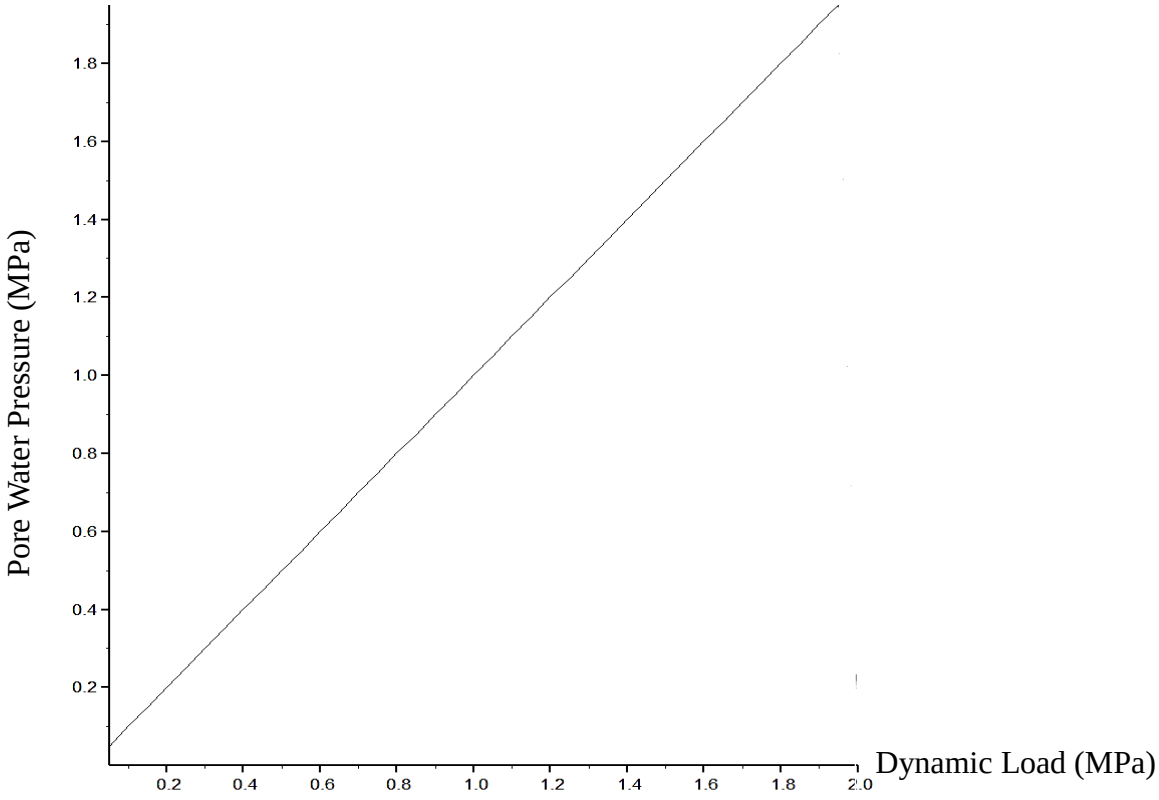

FIGURE 7.4 Pore Water Pressure vs. Dynamic Load

As a result, calculated pore water pressure decreases along with an increasing elastic modulus (see FIGURE 7.5). Air voids of the model equals to 8%. Pore water pressure that calculated from a model with a 2500 MPa elastic modulus equals to 0.31 MPa, this value increases to 0.59, 0.92 and 1.8 MPa when the elastic modulus was changed to 1500, 1000 and 500 MPa, respectively (See TABLE 7.2).

TABLE 7.2 Elastic Modulus and Pore Water Pressure

Elastic Modulus (MPa)	Air Voids	Pore Water Pressure (MPa)
2500	0.08	0.31
500	0.08	1.80
1000	0.08	0.92
1500	0.08	0.59

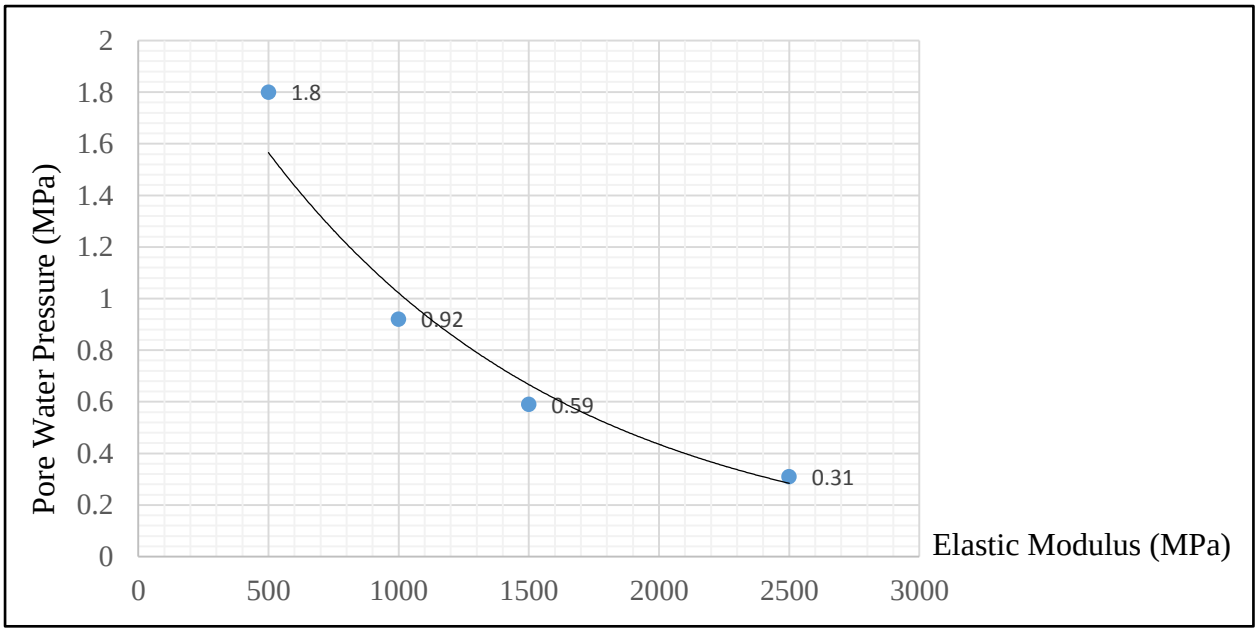

FIGURE 7.5 Pore Water Pressure vs. Elastic Modulus in Compression Tests, Air void = 8%

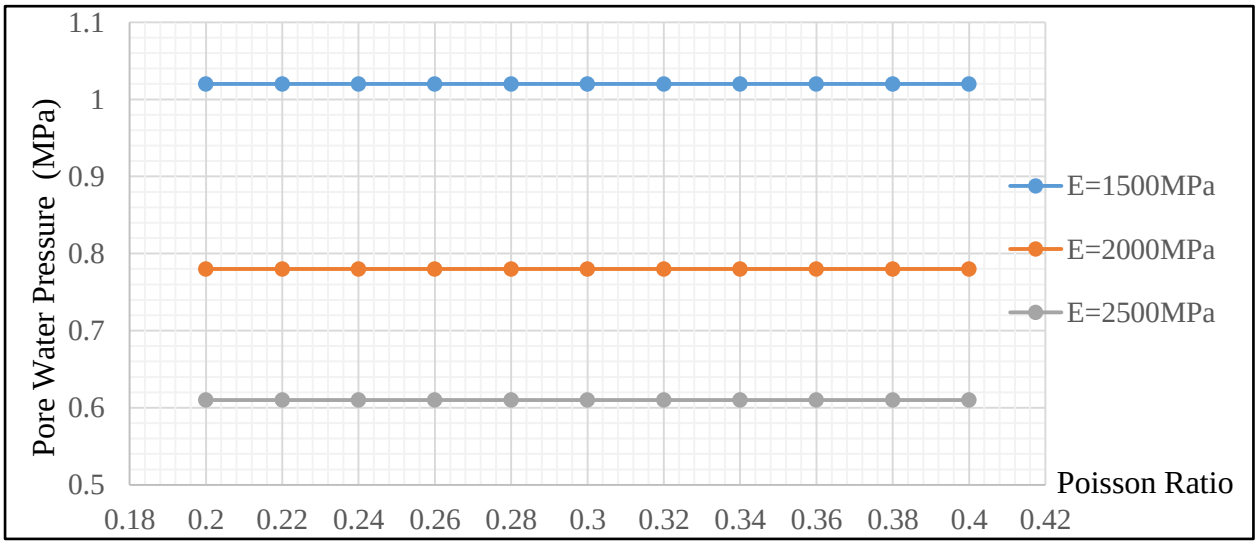

FIGURE 7.6 Pore Water Pressure vs. Elastic Modulus with Varied Poisson Ratios

In order to analyze how Poisson ratio effect pore water pressure on asphalt mixture, different Poisson ratios have been set to the digital model. Compare with influence of elastic modulus, Poisson ratio rarely affects pore water pressure (see FIGURE 7.6).

As we known, there is pore water in the pavement structure. Under high traffic loads, pore water pressure becomes an important reason of moisture damage. Many properties of

asphalt mixtures are closely related to air voids. Shown in FIGURE 7.7, Hydraulic conductivity is very small when air voids is smaller than 8%, and become pretty high when air voids is larger than 15%. That means water can flow freely and be discharged easily when air voids is larger than 15%. So air voids significantly affect pore water pressure; moisture damage rarely exists when air voids is smaller than 8% or larger than 15%. It's clearly in FIGURE 7.8 that pore water pressure changed visibly when air voids equals to 8%.

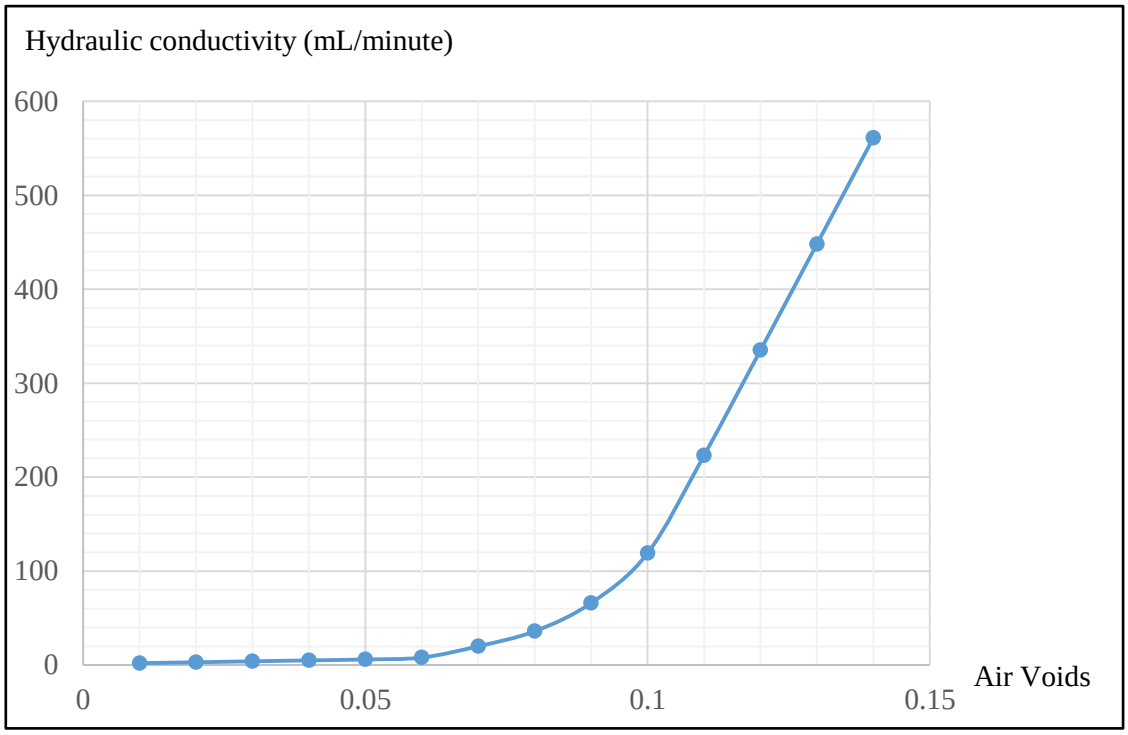

FIGURE 7.7 Hydraulic Conductivity vs. Air Voids

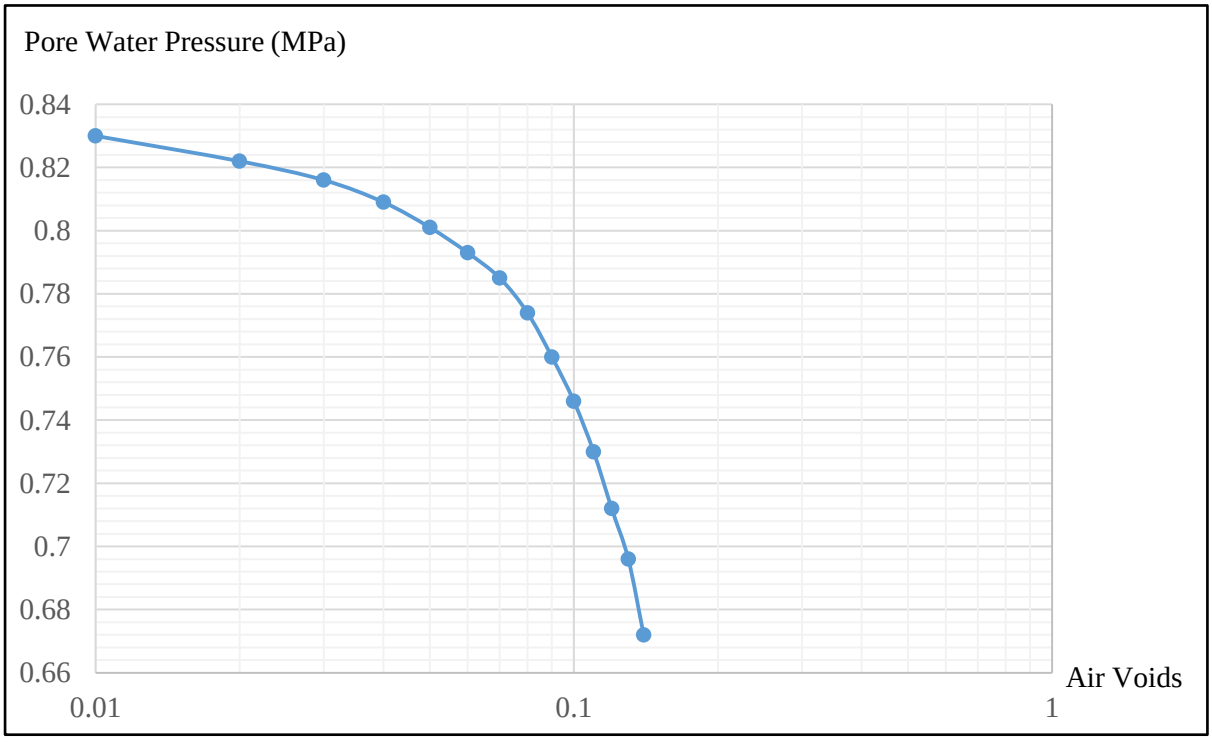

FIGURE 7.8 Pore Water Pressure vs. Air Voids.

Influence of Entrained Air Voids on Pore Water Pressure and Shrinkage on Asphalt Concrete

Numerical Analysis

Shrinkage of the asphalt binder in asphalt concrete is restrained by the stiff, non-shrinking aggregates. Measurements of asphalt concrete shrinkage presented are in fact the result of the interaction between a shrinking asphalt binder, whose mechanical properties change during hardening, and the inert inclusions. A challenge in the modeling of autogenous shrinkage is to calculate shrinkage of asphalt concrete based on shrinkage of the corresponding asphalt binder. If this would be accomplished, it would save experiments on asphalt mixture. In fact, the autogenous deformation of mixtures can be predicted from the

autogenous shrinkage of the corresponding asphalt binder. There is no agreement on the feasibility of this approach. According to Tazawa et al. (2000), autogenous shrinkage of asphalt concrete at 28 days can be calculated from autogenous deformation of asphalt binder with a simple composite model (*85*). On the other hand, Hammer et al. (2002) excluded that shrinkage of a concrete mixture can be calculated from shrinkage of an asphalt binder using composite models (*86*).

In the following calculations, asphalt concrete is assumed to consist of two phases, namely aggregate particles dispersed in an asphalt binder matrix. If the shrinkage of the asphalt binder is greater than that of the aggregates, the aggregates restrain the shrinkage of the asphalt binder. According to this approach, asphalt concrete shrinkage is a function of the asphalt binder shrinkage, the aggregate shrinkage, the stiffness of the asphalt binder and of the aggregate, and the aggregate volume concentration.

Some attempts (Pickett 1956, Hansen & Nielsen 1965, Hobbs 1969) have been made to obtain expressions for the dependence of the asphalt concrete shrinkage upon the aggregate volume concentration and the properties of the constituents (*87, 88, 89*). However, exact solutions for asphalt concrete shrinkage cannot be obtained because of the geometric complexity of concrete and the many interacting particles. In order to obtain a solution, simplified assumptions are made and as a consequence the solutions are only approximate.

Analytical models for asphalt concrete shrinkage are discussed in (Hobbs 1974) (*90*). Basic assumptions are as follows:

1) Asphalt concrete consists of two homogenous phases, aggregates and asphalt binder.

2) Aggregate and asphalt binder behave elastically.

3) Elastic properties are not influenced by shrinkage, i.e. micro-craking of the asphalt binder, if it occurs, does not reduce the stiffness.

4) The total volume occupied by shrinkage cracks is independent of aggregate grading.

In the following, Pickett's model (Pickett 1956) and Hobbs' model (Hobbs 1969) will be discussed and applied to quantify autogenous shrinkage of asphalt concrete (*87*, *89*).

Pickett's model

Pickett (1956) derived an expression for the effects of aggregates on concrete shrinkage (*87*). The formula is derived by considering the restraining effect of one small spherical aggregate particle embedded in a large body of shrinking concrete. The concrete surrounding the aggregate particle is considered as a homogeneous material and both the particle and the concrete are assumed to be elastic. As further particles are added, the elastic properties and the shrinkage are recalculated, while the body is still considered to remain homogenous. Integration and a number of assumptions lead to the expression:

$$\varepsilon_C = \varepsilon_P \cdot (1 - \emptyset_A)^{\alpha_P} \tag{36}$$

where ε_C (m/m) is the shrinkage of concrete, ε_P (m/m) is the shrinkage of the asphalt binder, $\emptyset_A$ (m^3/m^3) the volume fraction of the aggregates and α_P is a parameter defined as:

$$\alpha_P = \frac{3 \cdot (1 - V_C)}{1 + V_c + 2 \cdot (1 - 2V_A) \cdot E_C/E_A} \tag{37}$$

where V_C and V_A are the Poisson's ratio of the concrete and of the aggregates, E_C and E_A (MPa) are the elastic moduli of the concrete and of the aggregates, respectively.

According to Equation (1) and (2) $\varepsilon_C = \varepsilon_P$ only when the ratio E_C/E_A becomes ∞.

Hobbs' model

Hobbs' model (*89*, *90*), also called C&CA model, was developed for drying shrinkage,

where the elastic modulus of the paste is constant. According to the model, the shrinkage of the concrete, ε_C (m/m), is equal to:

$$\varepsilon_C = \frac{\varepsilon_P \cdot (1 - \emptyset_A) \cdot (G_P + G_A) + 2 \cdot \varepsilon_A \cdot \emptyset_A \cdot G_A}{G_P + G_A + \emptyset_A \cdot (G_A - G_P)} \quad (38)$$

where ε_P (m/m) is the shrinkage of the cement paste, ε_A (m/m) is the shrinkage of the aggregates, G_A (MPa) is the shear modulus of the aggregates, and G_P (MPa) the shear modulus of the paste.

This model is more general than Pickett's, taking into account the possible shrinkage of aggregates upon drying. Another difference is that the elastic modulus of the paste is used in the computation in Hobb's model, whereas the modulus of concrete is used in Pickett's model.

Traditional Method of Experiment Test

Autogenous deformation of concrete varies enormously in magnitude and even in sign between different publications (Hammer et al. 2002) (86). Since concrete is the material which is used in practical application, the principal aim of autogenous deformation measurements on cement paste is to understand and possibly predict autogenous deformation of concrete made with the same paste. However, this approach suffers of a series of drawbacks of which one of the most serious lies in the measuring methods.

Cement paste

Linear measurement of autogenous deformation is frequently performed by placing the cement paste in a rigid mold with low friction. The length change of the asphalt binder is recorded by a displacement transducer at the end of the specimen, see FIGURE 7.9.

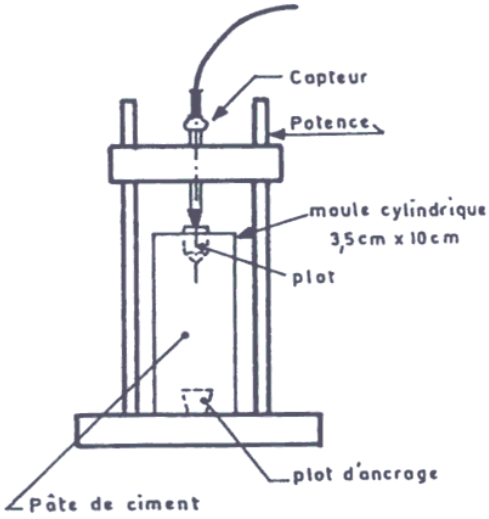

FIGURE 7.9 Equipment for Measuring Linear Autogenous Deformation of Cement Paste (*91*)

Concrete

Different linear methods have been used to measure autogenous deformation of concrete on beams, slabs or cylinders (FIGURES 7.10-7.14):

1) Cast-in nails through a hole in the middle of the end plates with the nail heads embedded in a concrete beam (FIGURE 7.10).

2) Moveable endplates with plugs in a concrete beam (FIGURE 7.11).

3) Horizontal transverse cast-in bars through a concrete beam (FIGURE 7.12).

4) Vertical cast-in bars in a concrete slab (FIGURE 7.13).

5) Cast-in strain gage (Hanehara et al. 1999).

6) Metal plates placed on top of cylinders (FIGURE 7.14).

For all the measuring systems presented, the main problems to overcome are ensuring a good contact between the measuring points and the concrete, minimizing restraint and moisture loss and keeping the temperature constant. The systems presented in FIGURES

7.9-7.12, solve these problems in a similar way: embedment of rods or bars in the fresh cast, to which later the measuring points are fixed; reduction of friction on the lower face with low-friction foils; moisture loss is reduced by a plastic or aluminum foil on the upper face after casting; constant temperature is obtained with temperature-controlled baths or by circulation of cooling liquid in the mold. The system in FIGURE 7.14, on the other hand, presents different solutions and is analogous to the one designed for cement paste.

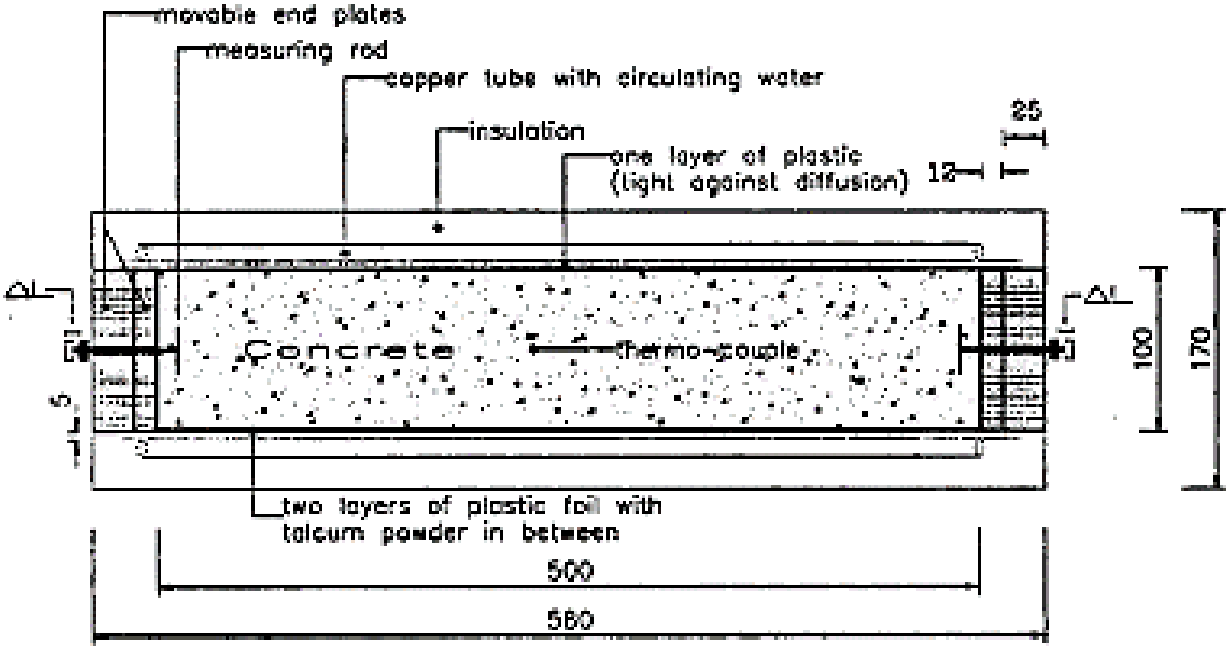

FIGURE 7.10 Measuring System with Cast-in Nails (*92*)

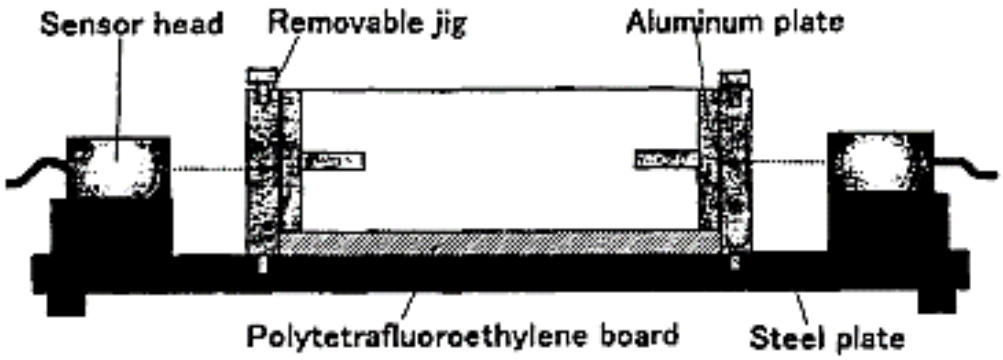

FIGURE 7.11 Measuring System with Moveable End Plates in a 40×40×160 mm^3 Beam (*93*)

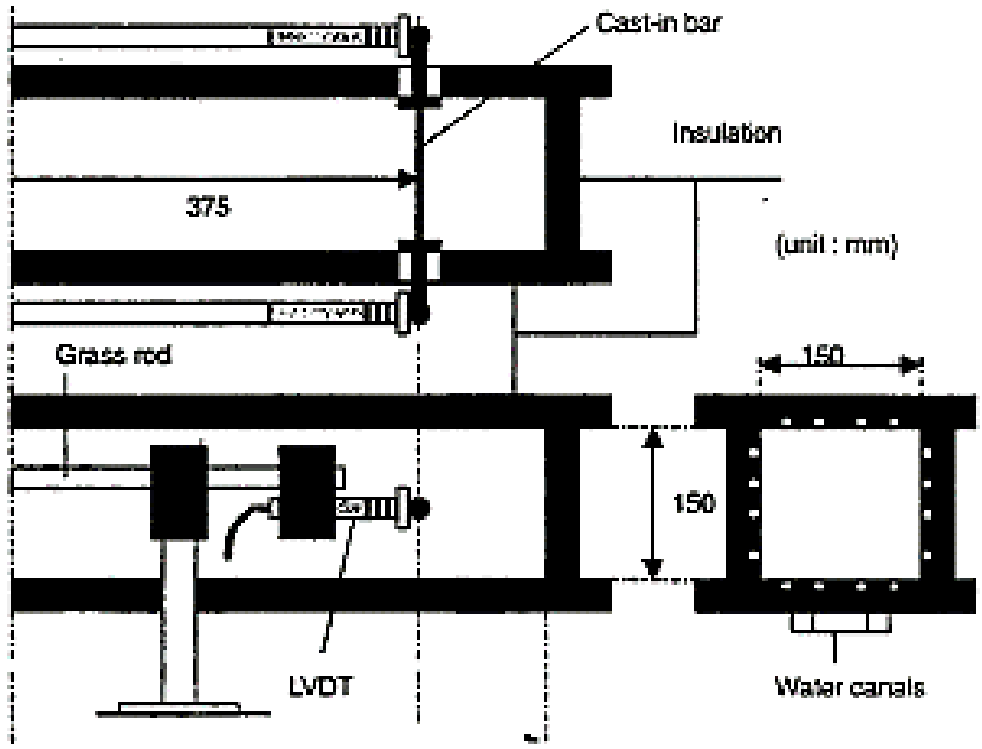

FIGURE 7.12 Measuring System with Horizontal Cast-in Bars in a 150×150×1000 mm^3 Beam (*94*)

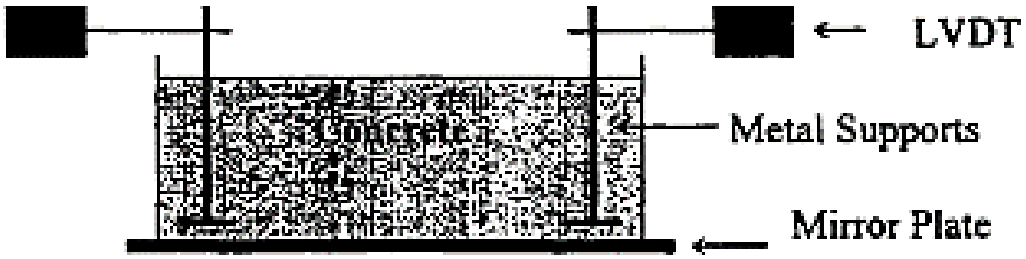

FIGURE 7.13 Measuring System with Vertical Cast-in Bars in a 270×270×100 mm^3 Slab (*95*)

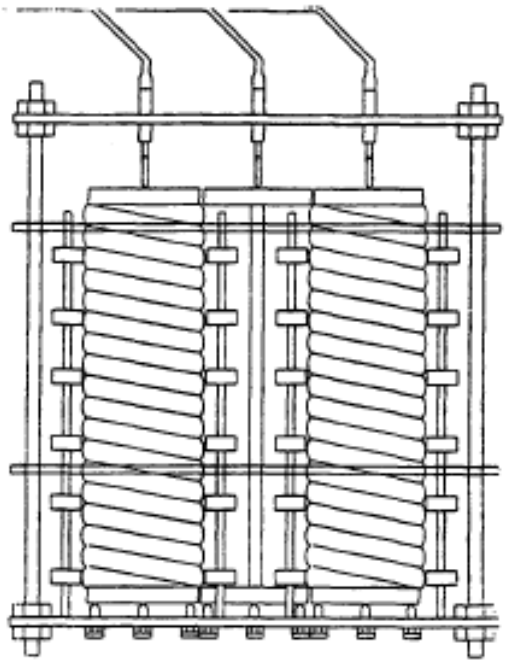

FIGURE 7.14 Measuring System with Flexible Tubes (diameter 100 mm and length 375 mm) and Vertical Length Measurement (*96*)

As pointed out in the previous section about cement paste, linear measurements of autogenous deformation on a concrete mix before setting are not only associated with a large scatter, but are also intrinsically ambiguous, since the length is not defined in a fluid system. Start of the measurement should coincide with setting, but exact determination of the fluid-solid transition is difficult and subjective. A possible approach, which was followed in the measurements is to start measuring before setting and to register at the same time the self-induced stress of a restrained specimen. The deformations are then zeroed at the moment when a stress is recorded in the restrained specimen. This ensures that only the deformations measured on a solid system, which is able to exert an external stress, are taken into account.

Simulated Shrinkage Process Using DEM

The shrinkage is measured on a digital model that represents beams in a steel mold with

length/thickness/height of 280/100/100 mm. The shrinkage is defined as the linear autogenous deformation at horizontal direction, it's measured as horizontal movement of two "nails" placed centric in both ends of the specimen. The nails are made of 3mm thick steel rods with a 15 × 15mm steel plate soldered to the end of each rod, placed 30mm in the concrete. The other end is wedged and screwed into inductive displacement transducers through a hole in the ends of the mold. The transducers are fixed to the mold. All data (shrinkage and pore water pressure) were recorded every second minute. The water loss may also be recorded.

Different with experiment method, material used in simulation is asphalt concrete instead of cement concrete. PG 64-22 asphalt binder is used. Elastic and simple viscoelastic contact models are adopted in DEM simulations. Contacts properties and other governing parameters in the DEM model in PFC 3d are summarized in TABLE 7.3.

TABLE 7.3 Contacts Properties and Other Governing Parameters Specified in DEM Model

Normal elastic spring stiffness	5.00×10^{6} N/m
Tangential elastic spring stiffness	1.25×10^{6} N/m
Rotational elastic spring stiffness	7.03×10^{1} Nm
Normal viscous damping coefficient	2.27×10^{5} Ns/m
Tangential viscous damping coefficient	1.13×10^{5} Ns/m
Rotational viscous damping coefficient	1.00×10^{-3} Nms
Frictional coefficient of wall element	0.01
Passion radio	0.30
Confining pressure	2.00×10^{4} Pa
Modulus of compressibility of water	2.10×10^{6} Pa
Axial loading speed	1.00×10^{-2} m/s
Bulk permeability	1.00×10^{-3} m/s
Thermal expansion at 25^{o}C	$12\times10^{-6}K^{-1}$
Thermal conductivity at 25^{o}C	0.75 W/(m.K)

Result and Analysis

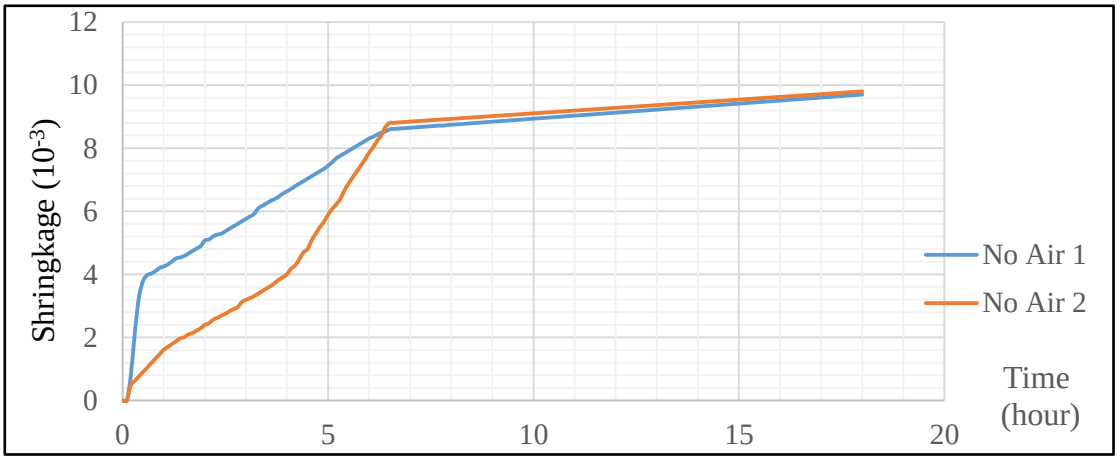

FIGURE 7.15 Shrinkage of Asphalt Concrete without Air Entraining Mixture

Firstly, pore water pressure and deformation are measured on two asphalt concrete samples, one with AEM and the other one without AEM. Tests on asphalt mixture without AEM were repeated once, results of shrinkage of the tests are shown in FIGURE 7.15.

It is a difficult task to generate a stable air pore system in the asphalt concrete and to reach the target air content of 8-15%. The air content was calculated from the difference in density assuming that the asphalt binder sample without AEM contains no air. The asphalt binder sample showed sufficient fluidity to allow good compaction during filling. The asphalt binder sample did not show significant bleeding, and thus, the deformation test was performed without rotation.

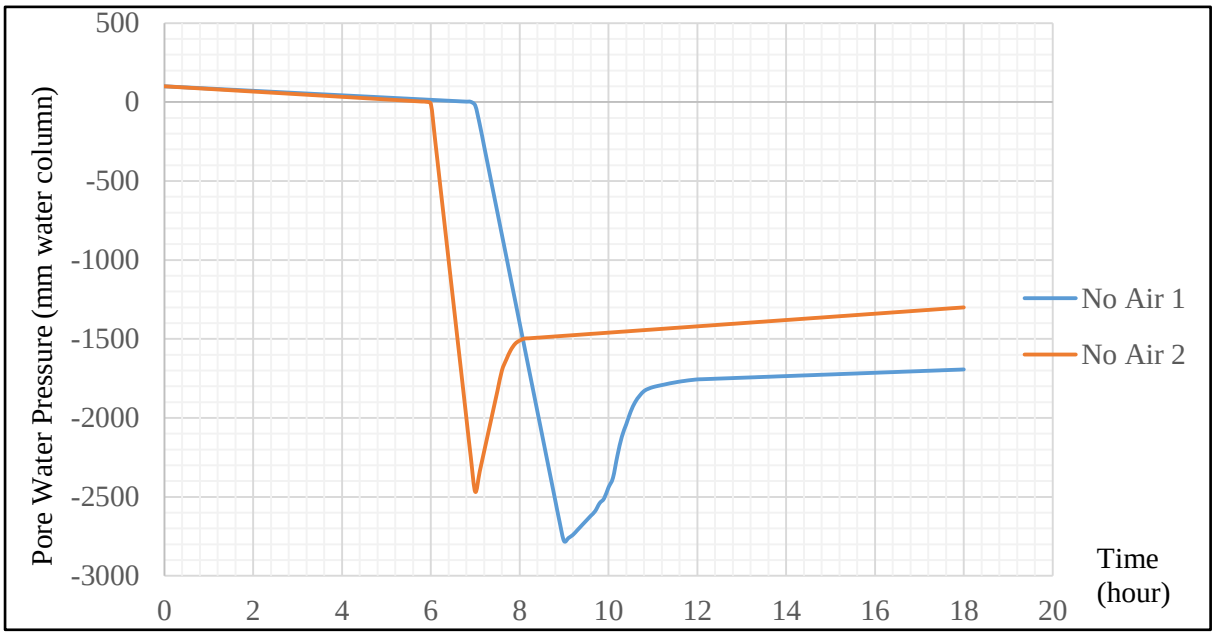

FIGURE 7.16 Pore Water Pressure of Asphalt Binder without Air Entraining Mixture

Pore water pressures of the asphalt binder specimen are measured from simulations. Pore pressure at a given point can be measured by the height of water in a standpipe located at that point. Pore pressures are often indicated in this way on diagrams.

$$h_w = \frac{u}{\gamma_w} \tag{39}$$

where u is the pore water pressure, γ_w is unit weight of water, and the height of the water column is the pressure head (h_w). FIGURE 7.16 shows the results of the tests on specimens without air entraining mixture.

Comparing previous work on asphalt mixture without AEM and with varied air voids, FIGURE 7.17 and FIGURE 7.18 show that the influence of air voids on shrinkage are as follows: higher rate of shrinkage before the "knee point", (i.e. in the few hours before autogenous shrinkage rate becomes significantly lower than later), earlier arrival of the knee-point, and lower rate of shrinkage beyond the knee-point. Since the time of full collapse depends on the stiffness evolution of the asphalt binder, the simple explanation can be that

presence of air voids results in a lower stiffness. This suggestion should be further explored by more systematic and accurate measurements.

Another feature is that shrinkage of the asphalt binder without AEM increases distinctly along with the duration of time beyond the knee-point, while shrinkage of the asphalt binder with AEM does not. This is probably directly caused by the buffer effect of air pores. The vacuum effect drives the PWP downwards, but the air pores will release the pressure through expansion. The result is reduced rate of PWP accompanied with reduced shrinkage rate.

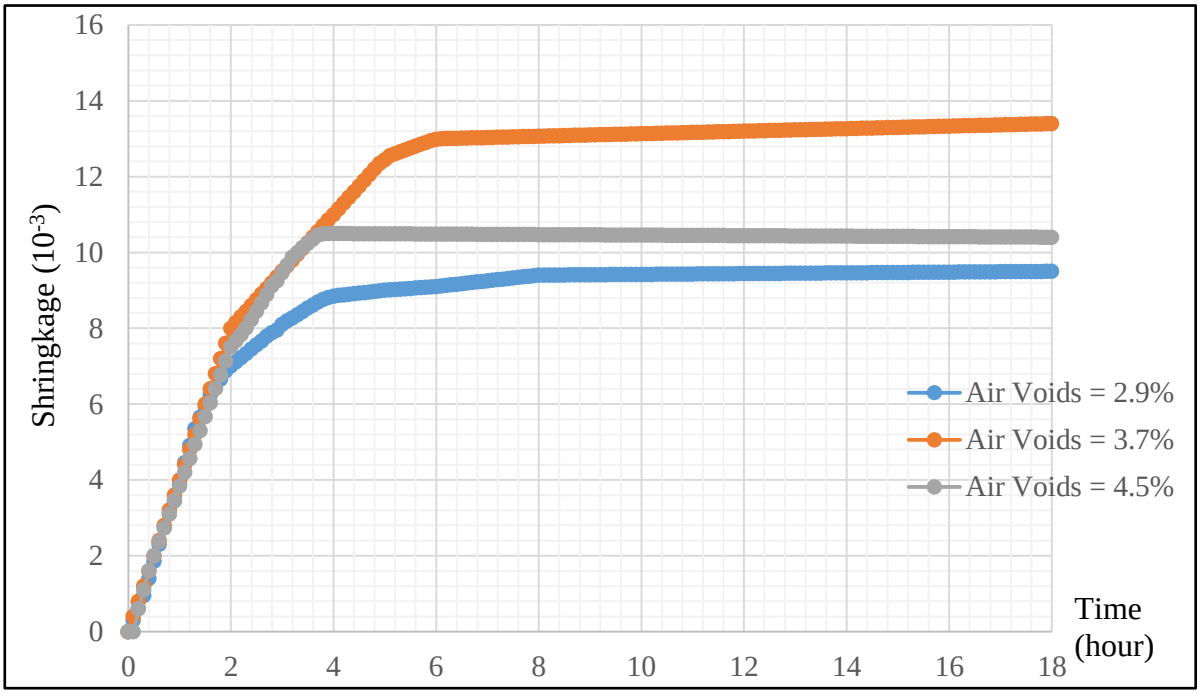

FIGURE 7.17 Shrinkage of Asphalt Binder with Varied Air Voids

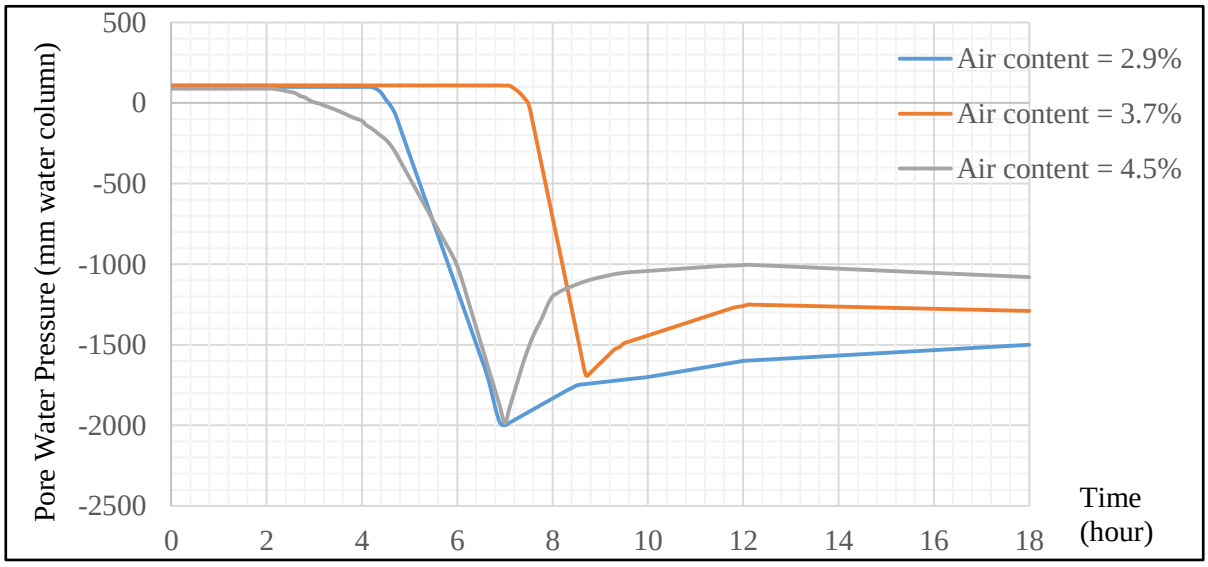

FIGURE 7.18 Pore Water Pressure of Asphalt Binder with Varied Air Voids

Summary

Air voids in asphalt binder seems to contribute to an increased rate of autogenous shrinkage in the time before the "knee-point", and an earlier appearance of the knee-point. Through the period shortly after, air pores alter the pore water pressure evolution in that they act as buffer, and thereby reduce the pressure decrease, and the subsequent autogenous shrinkage as well as the friction against panels in slip forming.

The scatter observed may be related to inaccuracy in measurement, but also to the differences in air content. It can be seen that there is a fairly good coincidence between the knee-point and the point when PWP bends of as expected, which suggests that inaccuracy in measurements does not dominate. This would in turn cause faster hydration, which may explain both earlier bending off of and higher PWP rate.

8 CONCLUSIONS

DEM has been used to simulate the behavior of asphalt mixture with different gradations, different film thicknesses, and different asphalt contents under compressive loads. Optimal gradation and optimum values of asphalt content and film thickness can be determined through DEM simulations.

Gradation is determined based on a simulated packing process. The evaluation of aggregate packing begins with the comparison of two different states of aggregate structures. We assume the newly added aggregates are always equal in size to or smaller than aggregates in a former state. After gravity and loading cycles are applied, the contact force and unbalanced force were recorded. Then finer aggregates were added into the structure. After mixing and compacting the structure into equilibrium, volume and porosity of the new structure were calculated. By comparing five digital models, an optimal model which has the lowest porosity was selected.

The asphalt content was determined using an approach that is based on modeling the inter-aggregate contact with a binder layer. The total surface area is related to the gradation, particle shape, angularity and texture of the aggregates. Once the gradation is determined, the total surface area, asphalt content and the binder film thickness can be calculated. Ten digital mixtures were built in software PFC3d, and the asphalt content ranges from 3.9% to 5.9%. As compressive loading is applied, the number of contacts between aggregates and asphalt binder were recorded. This number was used as a judgment to tell whether the mixtures were damaged due to cracking. The mixture that reached the highest peak strength was considered as optimal. Therefore, optimal asphalt content determined by this process was 5.3%. The

procedure described in this study determines the optimum asphalt content by adding the capability of internal deformation mechanism (breaking of bonds and loss of contacts), eliminating laborious and tedious laboratory experiments.

Based on optimal gradation and optimal asphalt content determined by computational methods, a particular mixture was simulated with sphere aggregates and asphalt binder. A simple visco-elastic model was applied to contacts between aggregates and asphalt binder in PFC3d. The thickness of the asphalt binder layer was calculated to be 9.2 micrometers associated, consistent with data in literature.

The indirect tensile strength of HMA with four different shapes of aggregate was evaluated in simulated test to evaluate the relative quality of materials. The image analyzer was a useful tool for quantifying the morphological characteristics of coarse aggregates. Image evaluation provided quantitative indices, such as geometric measurement and angle rotation of granular materials. Data showed that the morphological characteristics of coarse aggregates correlated well with the results of other indirect tests such as the particle index. Cubical particles possessed the best resistance over the other shapes. The particle index (*PI*) was shown to be an adequate measure of the combined contribution of particle shape, angularity, and surface texture to the stability of an aggregate. The *PI* value correlated well to aggregate geometric characteristics including elongation ratio, flatness ratio, shape factor, and sphericity. The particle shape determined how aggregate was packed into a dense configuration and also determined the internal resistance of a mix. The morphological characteristics of coarse aggregates found from both digital test and image analysis were in good agreement with the engineering properties of HMA mixtures. This study presents a

precise method to evaluate the aggregate characteristics in a HMA mix and demonstrates their effects on pavement performance. The results of this study would provide useful guidelines for highway engineers to construct a long-lasting pavement.

In this study, considering the necessity of preservation of the compaction temperature, the effect of various temperatures on Hot Mix Asphalt (HMA) samples properties has been evaluated. As well, to evaluate the effect of this parameter on different grading, two different grading have been used and samples were compacted at various temperatures.

Based on the results of asphalt mixture without AEM and with varied air voids, one could conclude that the influence of air voids on shrinkage are as follows: higher rate of shrinkage before the knee point, earlier arrival of the knee-point, and lower rate of shrinkage beyond the knee-point. Another feature is that shrinkage of the asphalt binder without AEM increases distinctly along with the duration of time beyond the knee-point, while shrinkage of the asphalt binder with AEM does not. This is probably directly caused by the buffer effect of air pores. The vacuum effect drives the PWP downwards, but the air pores will release the pressure through expansion. The result is reduced rate of PWP accompanied with reduced shrinkage rate.

REFERENCES

1. Roberts, F.L., Prithvi S. Kandhal, E. Ray Brown, D.Y. Lee and Thomas D. Kennedy. *Hot Mix Asphalt Materials, Mixture Design and Construction. First Edition*, NAPA Education Foundation, Maryland, 1991.
2. Cundall, P. A., and Strack, O. D. L. A discrete numerical model for granular assemblies. *Geotechnique*, Vol. 59, 1979, pp. 47-51.
3. Nukunya, B. Aggregate Gradation Characterization Factors and Their Relationships to Fracture Energy and Failure Strain of Asphalt Mixtures. *Journal of the Association of Asphalt Paving Technologist,* Vol. 33, 2002, pp. 56-67
4. Cundall, P.A. and O.D.L. Strack, A Discrete Numerical Model for Granular Assemblies. *Geotechnique*,Vol. 29, 1979, pp. 47-65.
5. Bernardita Lira, Denis Jelagin, "Gradation-based framework for asphalt mixture." *Materials and Structures*, 2012, pp 21-38.
6. Goode, J. E., and Lufsey, L. A. "A New Graphical Chart for Evaluating Aggregate Gradation." *Association of Asphalt Paving Teclmologists,* 1962.
7. American Society of Testing and Materials (ASTM) *C117: Standard Test Method for Materials Finer than 75 µm (No. 200) Sieve in Mineral Aggregates by Washing.* Philadelphia, PA. 1997.
8. American Society of Testing and Materials (ASTM) *C136: Standard Test Method for Sieve Analysis of Fine and Coarse Aggregates.* Philadelphia, PA. 1997.
9. Gradex 2000 Particle Size Analyzer Catalog 229, ROTEX, INC., Cincinnati, OH
10. Sales Literature on the VDG-40, Obtained from EMACO, Ltd., Montreal, Canada

11. Standard for Granulometric Analysis of Aggregate and Determination of Flatness and Elongation of Particles by Video Granulometer, Laboratoire Central des Ponts et Chaussées (the French Public Works Laboratory), 1993.

12. Harlow, R. L., "Design of a Particle Size Analyzer for Gravel Sized Aggregate." Master's Thesis, University of Texas at Austin, 1972.

13. Aljassar, A., and Haas, R., "Toward Automating Size-Grading Analysis of Mineral Aggregate." *Transportation Research Record* 1437 Transportation Research Board, Washington, D.C., 1994, pp. 35-42.

14. Surgrue, S., and Row, G., "True Resolution in Laser Diffraction Particle Sizing: Who needs it and where does it come from?" Technical Monograph, Coulter Corporation.

15. Thomas, T. W. White, T. D., and Kuczek, T., "Siliceous Content Determination of Sands Using Automatic Image Analysis." *Transportation Research Record* 1437 Transportation Research Board, Washington, D.C., 1994, pp. 51-58.

16. Alba, Felix, "Phase I Final Report for Developments of a Prototype for On-Line Real Time Measurement and Control of Aggregate Gradation in Asphalt Plants." Report presented to the SHRP-IDEA Program Manager, May 1992.

17. Alba, Felix, "Phase II (Stage 2) Report for Developments of a Prototype for On-Line Real-Time Measurement and Control of Aggregate Gradation in Asphalt Plants." Report presented to the SHRP-IDEA Program Manager, September 1993.

18. Yu, H., and S. Shen Investigation of aggregate packing using discrete element modeling. *Geotechnical Special Publication*, 2010, pp.33-58

19. Brown, E. R., Murphy N. E., Yu L. and Mager S., "Historical Development of Asphalt Content by the Ignition Method," *Asphalt Paving Technology*, Association of Asphalt Paving Technologists, St. Paul, MN, 1995, pp. 1-35.
20. Behrens, M. L., Dvorak B. I. and Woldt W. E., "Comparison of Asphalt Extraction Procedures: Implications of Hidden Environmental and Liability Costs," *Transportation Research Record* 1661, Transportation Research Board, Washington, DC, 1999, pp. 46-53.
21. Brown, E. R. and Mager S., "Asphalt Content by Ignition Round Robin Study," Report No. 95-3, National Center for Asphalt Technology, Auburn, AL, 1995.
22. McKeen, R. G., "Asphalt Content by Ignition: Round Robin Experiment," New Mexico State Highway and Transportation Department, Santa Fe, NM, December 1997, pp. 13-14.
23. Burati, J.L. and Connell J., "Study of Alternative Procedures for Controlling and Accepting Asphalt Mixtures," FHWA-SC-96-05, Washington, DC, 1996.
24. Howard, C. P. and Burati J. L., "Study of the NCAT Ignition Oven for Control of Asphalt Mixtures," FHWA-SC-96-06, Washington, DC, 1996.
25. Lee, R. E. and Tahmoressi M., "Using Ignition Ovens to Determine Asphalt Content and to Prepare Aggregates for Sieve Analysis," Texas DOT, Austin, TX, 1996.
26. Mallick, R. and Brown E. R., "Limited Round Robin Asphalt Content Test Using Troxler Furnace," Report No. 99-6, National Center for Asphalt Technology, Auburn, AL, 1999.
27. American Society of Testing and Materials (ASTM) *T308: Determining the Asphalt Binder Content of Hot Mix Asphalt (HMA) by the Ignition Method.* Philadelphia, PA. 2013
28. Schroer J., "Asphalt Content of Dolomite Mixtures Using the Troxler NTO," Missouri DOT, August 21, 2002.

29. Prowell B. D. and Schreck R., "Asphalt Content by the Ignition Method: Virginia's Experience," *Eight International Conference on Asphalt Pavements*, University of Washington, Seattle, August 10-14, 1997.

30. "Asphalt Content by the Ignition Method, VTM 102" Orientation School, Virginia DOT, Virginia Transportation Research Council (VTRC), Virginia Asphalt Association (VAA), Virginia, April 1995.

31. Hurley G. C. and Prowell B. D., "Evaluation of Infrared Ignition Furnance for Determination of Asphalt Content," *Transportation Research Record* 1861, Transportation Research Board, Washington, DC, 2003, pp. 44-50.

32. Prowell B. D., "Evaluation of Infrared Ignition Furnace for Determination of Asphalt Content," Report No. 02-05, National Center for Asphalt Technology, Auburn, AL, 2002, pp. 5-10.

33. Williams S. G. and Hall K. D., "A Comparison of Ovens Used in Determination Binder Content by the Ignition Method." *Journal of Association of Asphalt Paving Technologists*, Proceedings of the technical Sessions, Vol. 70, 2002, pp. 712-728.

34. Mallick R., Brown E. R. and McCauley N., "Effect of Ignition Test for Asphalt Concrete on Aggregate Properties." presented at *Transportation Research Board 77th Annual Meeting*, Washington D.C., 1998, pp. 1-15.

35. Prowell B. D. and Carter C. B., "Evaluation of the Effect on Aggregate Properties of Samples Extracted Using the Ignition Furnance." Virginia DOT, Interim Report, VTRC 00-IR1, April 2000, pp. 14-17.

36. Rogers C., Williams D., Gorman B., Sahsuvar H., Greenbury B. and Masliwec T., "Ignition Oven Problems with Quartz Rich Aggregates Materials." *International Center for Aggregates Research*, Twelfth Annual Symposium Proceedings, Denver, CO, April 4-7, 2004.

37. American Society of Testing and Materials (ASTM) *D6307: Standard Test Method for Asphalt Content of Hot-Mix Asphalt by Ignition Method.* Philadelphia, PA. 1998

38. Lavin, P. *"Asphalt Pavements: A Practical Guide to Design, Production and Maintenance for Engineers and Architects".* 2003

39. Van der Poel, C. A "General System Describing the Visco-Elastic Properties of Bitumen and Its Relation to Routine Test Data". *J. Appl. Chem*., Vol.4, May 1954, pp. 221-236

40. Hills, J.F. "The Creep of Asphalt Mixes." *Journal of the Institute of Petroleum*, Vol. 59, 1973.

41. Cheung, C.Y. and Cebon, D. (1997). "Thin Film Deformation Behavior of Power Law Creeping Materials." *Journal of Engineering Mechanics*, Vol. 123-11, pp. 1138-1152.

42. Uddin, W., "A Micromechanical Model for Prediction of Creep Compliance and Viscoelastic Analysis of Asphalt Pavements." *Transportation Research Record* 1596, Transportation Research Board, Washington, DC, 1998, pp. 43-56.

43. Zhong, Xiaoxiong., Chang, Ching S. "Micromechanical Modeling for Behavior of Cementitious Granular Materials". *Journal of Engineering Mechanics*, November, 1999.

44. Levenberg,E., Uzan, J. , "Triaxial Small-Strain Viscoelastic Modeling of Asphalt Aggregate Mixes." *Mechanics of Time-Dependent Materials*, 2004, Vol 8, pp. 365–384.

45. Mazzotti, Claudio and Savoia, Marco. "Nonlinear Creep Damage Model for Concrete under Uniaxial Compression." *Journal of Engineering Mechanics*., September 2003, pp.1065-1075.

46. Huang, Baoshan., Mohammad, Louay N. and G. Wije Wathugala. "Application of a Temperature Dependent Visco-plastic Hierarchical Single Surface Model for Asphalt Mixtures." *Journal of Materials in Civil Engineering*, March/April, 2004, pp.147-154.

47. Ghassan R. Chehab, and Y. Richard Kim. “Viscoelastoplastic Continuum Damage Model Application to Thermal Cracking of Asphalt Concrete.” *Journal of materials in civil engineering,* 2005, pp.384-392

48. Sepehr, K., Svec, O.J., Yue, Z.Q., and El Hussein, H.M. “Finite Element Modelling of Asphalt Concrete Microstructure.” *Computer Aided Assessment and Control of Localized Damage Proceedings of the International Conference,* 1994, p 225.

49. Bahia, H.U., Zhai, H., Bonnetti, K., and Kose, S. “Non-Linear Viscoelastic and Fatigue Properties of Asphalt Binders.” *Journal of the Association of Asphalt Paving Technologists,* AAPT, 1999, Vol. 68, pp. 1-34.

50. Abbas, A., Papagiannakis, A.T. and Masad, E. “Linear and Non-Linear Viscoelastic Analysis of the Microstructure of Asphalt Concretes.” *Journal of Materials in Civil Engineering,* ASCE, 2004, Vol. 16, pp. 133-139.

51. Saadeh, S., Masad, E., Stuart, K., Abbas, A., Papagainnakis, T., and Al-Khateeb, G. “Comparative Analysis of Axial and Shear Viscoelastic Properties of Asphalt Mixes.” *Journal of the Association of Asphalt Paving Technologists,* AAPT, 2003, Vol. 72, pp. 122-153.

52. Rothenburg, L., Bogobowicz, A., Haas, R., Jung, F.W., and Kennepohl, G. “Micromechanical Modelling of Asphalt Concrete in Connection with Pavement Rutting Problems.” *Proceedings of the 7th International Conference on Asphalt Pavements,* 1992, pp. 230-245.

53. Chang, G. k., Meegoda, N. J. “Simulation of the Behaviour of Asphalt Concrete using Discrete Element Method.” In: *2nd International Conference on Discrete Element Methods,* M.I.T 1993

54. Buttlar, W. G., and You, Z. “Discrete element modelling of asphalt concrete: A microfabric approach.” *Transportation Research Record* 1883, Transportation Research Board, Washington, DC, 2001, pp. 13-21.

55. Adhikari, S., and You, Z. “3D microstructural models for asphalt mixtures using X-ray computed tomography images.” *International Journal of Pavement Research and Technology*, 2008, pp. 94–99.

56. Anderson, T. Balakrishnan, H. Parulkar, G. and Peterson, L. “Integrated Open Flow–GMPLS control plane: an overlay model for software defined packet over optical networks.” *Optics Express*, Vol. 19, Issue 26, 2011, pp. B421-B428

57. H Cleland, M Suzuki, N Ito, 2010, “Efficient Implementations of Molecular Dynamics Simulations for Lennard-Jones Systems.” *Progress of Theoretical Physics*, Vol. 126, No. 2, 2011, pp. 203-235.

58. Itasca, PFC3d 4.0 Manual: Background and Theory.

59. Skyscan 1174 X-ray microtomograph – user guides.

60. Kim, Y.R., Shah, K.A, and Khosla, N.P, “Influence of Test Parameters in SHRP P07 Procedure on Resilient Moduli of Asphalt Concrete Field Cores”, *Transportation Research Record* 1353, Transportation Research Board, Washington, DC, 1992, pp.82-89.

61. Shklarsky, E. and Livneh, M. “The use of gravels for bituminous mixtures.” *Proceedings of Association of Asphalt Paving Technologists*, 33, 23-65, 1964.

62. Krutz, N.C., and Sebaaly, P.E. “Effect of aggregate gradation on permanent deformation of asphaltic concrete.” *Proceedings of Association of Asphalt Paving Technologists*, 1993

63. Li, M.C., and Kett, I. “Influence of coarse aggregate shape on the strength of asphalt concrete mixtures.” *Highway Research Record* 178, 93-106, 1967.

64. Huber, G.A., and Heiman, G.H. “Effect of asphalt concrete parameters on rutting performance: a field investigation.” *Proceedings of Association of Asphalt Paving Technologists*, Vol. 56, 1987, pp. 33-61.

65. Stephens, J.E., and Sinha, K.C. “Influence of aggregate shape on bituminous mix character.” *Journal of Association of Asphalt Paving Technologists*, 47, 1978, pp. 434-456.

66. Yue, Z., Bekking, W., and Morin, I. “Application of digital image processing to quantitative study of asphalt concrete microstructure.” *Transportation Research Record* 1492, Transportation Research Board, Washington, DC, 1995, pp. 53-60.

67. Kuo, C.Y., Rollings, R.S., and Lynch, L.N. “Morphological study of coarse aggregates using image analysis.” *Journal of Materials in Civil Engineering*, 10, 1998, pp. 135-142.

68. American Society of Testing and Materials (ASTM) *D4791: Standard Test Method for Flat Particles, Elongated Particles, or Flat and Elongated Particles in Coarse Aggregate*. Philadelphia, PA. 2010

69. American Society of Testing and Materials (ASTM) *D3398: Standard Test Method for Index of Aggregate Particle Shape and Texture*. Philadelphia, PA. 2000

70. American Society of Testing and Materials (ASTM) *D4123: Standard Test Method for Indirect Tension Test for Resilient Modulus of Bituminous Mixtures*. Philadelphia, PA. 1995

71. American Society of Testing and Materials (ASTM) *D6926: Standard Practice for Preparation of Bituminous Specimens Using Marshall Apparatus*. Philadelphia, PA. 2004

72. Bahia, H.U. “Recommendation s for Mixing and Compaction Temperatures of Modified Binders.” National Cooperative Highway Research Program Report 9-10, Transportation Research Council, Washington, D.C., 2000.

73. Huner, M.H., and Brown, E.R. “Effects of Re-heating and Compaction Temperature on Hot Mix Asphalt Volumetric.” National Center for Asphalt Technology Report 01-04, Auburn, Ala, 2001.

74. Azari, H., McCuen, R.H., and Stuart, K.D. “Optimum Compaction Temperature for Modified Binders.” *Journal of Transportation Engineering*, 129(5), 2003, pp. 531-537

75. Kennedy, T. W., Robbert F.L, and Mcgennis R. “effect of compaction temperature and effort on the engineering properties of asphalt concrete mixtures.” *Symposium on placement and compaction of asphalt mixtures*, 1982.

76. “Mix Design Method for Asphalt Concrete and Other Hot Mix Types.” The Asphalt Institute, Manual series No 2 (MS-2), College Park, MD, 1979.

77. Sassa, K. “Motion of landslides and debris flows—prediction of hazard area.” In: Report of Grant-in-Aid for Scientific Research, Japanese Ministry of Education, Science and Culture, 1988

78. Ishihara, K., Okusa, S., Oyagi, N., and Ischuk, A. “Liquefaction-induced flow slide in the collapsible loess deposit in Soviet Tajik.” *Soil Found* Vol. 30, No. 4, 1990, pp. 73–89.

79. Eckersley, J.D., “Flowslides in stockpiled coal.” *Eng Geol*, Vol. 22, 1985, pp. 13–22.

80. Hutchinson, J.N., “A sliding-consolidation model for flow slides.” *Can Geotech*, Vol. J32, 1986, pp. 610–623

81. Okada, Y., Sassa, K., and Fukuoka, H., “Excess pore pressure and grain crushing of sands by means of undrained and naturally drained ring-shear tests.” *Eng Geol*, Vol. 75, 2004, pp. 325–343.

82. Cundall, P.A., Strack, ODL., “A discrete numerical model for granular assemblies.” *Géotechnique*, Vol. 29, No. 1, 1979, pp. 47–65.

83. Hammer, T.A., “On the strain capacity and cracking mechanisms of high strength concrete at very early age.” *Proceedings of the sixth international conference on creep, shrinkage and durability of mechanics of concrete and other quasi-brittle materials*, Cambridge (MA), 2001, pp. 657–662.

84. Fossa, K.T., “Slipforming of Vertical Concrete Structures - Friction between concrete and slipform panel, Dissertation, Department of Structural Engineering, The Norwegian University of technology, 2001.

85. Tazawa, E., Sato, R., Sakai, E., and Miyazawa, S. “Work of JCI committee on autogenous shrinkage.” RILEM Workshop on Shrinkage of Concrete, Paris, 2000, pp. 21-40.

86. Hammer, T.A., Bjøntegaard, Ø., and Sellevold, E.J. “Internal curing – Role of Absorbed Water in Aggregates.” Presented at ACI Fall 2002 Convention, Session High-Performance Structural Lightweight Concrete, Phoenix, AZ, 2002.

87. Pickett, G. “Effect of aggregate on shrinkage of concrete and a hypothesis concerning shrinkage.” *ACI Journal*, Vol. 52, No. 5, 1956, pp. 581-590.

88. Hansen, T.C., Nielsen, K.E.C., “Influence of aggregate properties on concrete shrinkage.” *ACI Journal*, Vol. 62, No. 7, 1965, pp. 783-794.

89. Hobbs, D.W., “Bulk Modulus Shrinkage and Thermal Expansion of a Two Phase Material.” *Nature*, Vol. 222, 1969, pp. 849-851.

90. Hobbs, D.W., “Influence of aggregate restraint on the shrinkage of concrete.” ACI Journal, Vol. 71, 1974, pp. 445-450.

91. Baron, J., and Buil, M. “Comments on the paper ‘Mechanical features of chemical shrinkage of cement pastes’ bySetter, N and Roy, D.M., *Cem Concr Res* Vol. 9, No. 4, 1979, pp. 545-547.

92. Bjontegaard, Ø. “Thermal dilation and autogenous deformation as driving forces to self-induced stresses in high performance concrete.” Dissertation, NTNU Division of Structural Engineering, Trondheim, Norway, 1999.

93. Morioka, M., Hori, A., Hagiwara, H., Sakai, E., and Daimon, M. “Measurement of autogenous length changes by laser sensors equipped with digital computer systems.” Workshop Autoshrink’98, London, 1999, pp. 191-200.

94. Lokhorst, S.J “Deformational behavior of concrete influenced by hydration related changes of the microstructure.” Research Report, Delft University of Technology, Delft, Netherlands, 1998.

95. Holt, E.E, and Leivo, M.T. “Autogenous shrinkage at very early ages.” Workshop Autoshrink’98, London, 1999, pp. 133-140.

96. Hansen, K.K, and Jensen, O.M. “Equipment for Measuring Autogenous RH-Change and Autogenous Deformation in Cement Paste and Concrete.” *Proc. Int. Res. Sem. on Self-desiccation and its Importance in Concrete Technology*, Lund, Sweden, 1997, pp. 27-30.